Title

Neutron Scattering Studies of Nanomagnetism and Artificially Structured Materials

Journal

Journal of Magnetism and Magnetic Materials, 271(1)

Authors

Fitzsimmons, M.R.
Bader, S.D.
Borchers, J.A.
et al.

Publication Date

2003-02-01

Research frontiers in artificially structured magnets and nanomagnetism at neutron scattering facilities

M.R. Fitzsimmons
Los Alamos National Laboratory, Los Alamos, NM 87545

S.D. Bader
Argonne National Laboratory, Argonne, IL 60439

J.A. Borchers
National Institute of Standards and Technology, Gaithersburg, MD 20899

G.P. Felcher
Argonne National Laboratory, Argonne, IL 60439

J.K. Furdyna
University of Notre Dame, Notre Dame, ID 46556

A. Hoffmann
Argonne National Laboratory, Argonne, IL 60439

J.B. Kortright
Lawrence Berkeley National Lab, Berkeley, CA 94720

Ivan K. Schuller
University of California San Diego, La Jolla, CA 92093

T.C. Schulthess
Oak Ridge National Laboratory, Oak Ridge, TN 37831

S.K. Sinha
University of California San Diego, La Jolla, CA 92093 and
Los Alamos National Laboratory, Los Alamos, NM 87545

M.F. Toney
Stanford Synchrotron Radiation Laboratory, Menlo Park, CA 94025

D. Weller
Seagate Technology, Pittsburgh, PA 15203

S. Wolf
Naval Research Laboratory, Washington, DC 20375

Abstract– Nanostructured magnetic materials are intensively investigated due to their unusual properties and promise for possible applications. The key issues in these materials relate to the connection between their physical properties (transport, magnetism, mechanical, *etc.*) and their chemical-physical structure. In principle, a detailed knowledge of the chemical and physical structure allows calculation of their physical properties. Theoretical and computational methods are rapidly evolving so that magnetic properties of nanostructured materials might soon be predicted. Success in this endeavor requires detailed quantitative understanding of magnetic structure and properties.

Neutron scattering is a well-developed technique that can determine magnetic structure at the atomic level. Modern neutron scattering techniques allow measurements of magnetic properties at the atomic length scale in samples of ever diminishing size. This has opened up the use of neutron scattering to nanostructured materials prepared by thin film and lithographic techniques. Many interesting and unexpected results have emerged from the application of elastic neutron scattering to nanostructured magnetic thin films such as superlattices and multilayers. These include, distinguishing between magnetic and chemical boundaries, observing the spatial dependence of the magnetization vector in nonuniform materials, unusual coupling mechanisms across nonmagnetic materials, unexpected magnetic phase diagrams, *etc.* Extension of elastic neutron scattering to nanostructured arrays and three dimensional magnetic composites will allow future determination of magnetic structure with unprecedented resolution.

In this review, we discuss the impact of neutron scattering on the study of magnetic nanostructures, *i.e.,* magnetic materials that are artificially structured on nanometer length scales, such as magnetic thin films, multilayers and nanodot arrays. The basic interactions and different length scales relevant to these systems as well as the basic issues and phenomena of interest are briefly reviewed. We discuss examples where the techniques of magnetic neutron diffraction, small-angle scattering, reflectivity, grazing incidence diffraction and diffuse scattering have helped to elucidate some of these phenomena and also discuss potentially fruitful future applications of such techniques to the field of nanomagnetism. Furthermore, we argue that the development of inelastic neutron scattering techniques useful for the study of small volumes of material would raise neutron scattering to a much higher level of applicability for nanostructured magnetic materials.

1.0 Introduction to nanomagnetism

The past decade has opened new vistas in magnetism research. A definitive example is that of giant magnetoresistance discussed in this article. Giant magnetoresistance evolved from a laboratory curiosity to a major commercial product in the remarkably short time of about ten years. Today, a myriad of techniques exists, *e.g.,* thin film growth, lithography, templating and self-assembly, to modulate the atomic, electronic and chemical structures of materials. Physical properties can be modulated via confinement in one, two or all dimensions to create multilayers, wires or dots that exhibit novel magnetic behavior. The tailored modulation of structure can influence the magnetic properties in ways that cannot be predicted from the averaging of constituent component properties, *e.g.,* giant magnetoresistance in Fe/Cr superlattices. These new nanocomposites are inhomogeneous materials with unique magnetic properties. To understand the magnetism of such artificially structured materials requires an understanding of the interplay between structure and magnetism at the nanometer length scale— an extremely interesting undertaking in basic research.

We are entering an era in which manipulation of charge and spin offers the possibility to replace present-day semiconductor electronics, the way vacuum tube electronics were supplanted in the past. The term coined to embrace the new wave is "spintronics". As we look to the horizon beyond giant magnetoresistance and the related phenomenon of tunneling magnetoresistance, we see the development of magnetic random access memory, and further development of magnetic central processor units.

Ultimately the goal would be to transcend binary logic and move toward quantum computing strategies that can be implemented via electronic or nuclear spin manipulation utilizing quantum-entanglement. Thus, spintronics can converge with the burgeoning field of molecular electronics toward this end. There are many challenges ahead. For example, the opportunity to fabricate new systems on length-scales that compete with those relevant to magnetism, will challenge the fundamental knowledge in magnetism and naïve wisdom that magnetic properties at the nanoscale can be understood in terms of bulk or atomic magnetic properties. And, control of magnetism at the nanoscale offers a pathway to create new devices utilizing systematic principles of nanotechnology, rather than merely relying on the incremental Edisonian approach prevalent in the past. With such opportunities and challenges, it is valuable to examine the field, define our terms and limit the scope of the present document, to describing issues associated with artificially engineered materials and nanomagnetism. This report written in the spirit of the Falicov *et al.* [1] and Kortright *et al.* [2] reports, identifies opportunities and highlights promising approaches in neutron scattering.

The first term to define is "nanomagnetism". Nanomagnetism refers to magnetic phenomena in materials with physical dimensions that are comparable to length-scales relevant to magnetism. By transcending these length-scales, certain aspects of magnetic phenomena can be enhanced or suppressed. Some magnetic phenomena and length-scales of interest are shown in Figure 1 [3], and are discussed presently in the context of nanomagnetism. The present article examines the role neutron scattering plays in addressing problems involving artificially structured magnetic materials, and articulates future uses of neutron scattering for studies of nanomagnetism.

1.1 Terms of interaction

Quoting Aharoni [4]: "There is no way to neglect (in a ferromagnetic system) the three energy terms exchange, anisotropy and magnetostatics, and all three must be taken into account in any realistic theory of the magnetization process." This sentence, which set the stage for the micromagnetic theory of ferromagnetism, is also valid for the treatment of micromagnetic materials with walls or boundaries created artificially. Therefore, we review briefly not only the exchange and the anisotropy energies and how they are affected by reduced dimensionality, but also, on equal footing, the dipolar interaction and their affect on the interaction between domains.

1.2 Exchange interaction and the magnetic exchange length

The coupling between spins, which typically spans a length-scale on the order of a lattice parameter (d_{ex} in Figure 1), is governed by the exchange interaction (related to the exchange integral, J). Exchange coupling is produced by overlap of electronic orbitals, and therefore is necessarily short-ranged. We often refer to the global J of the system, which has been calculated numerically from first principles for many ferromagnetic materials based on the electron structure. The nature of the interaction, *e.g.,* ferromagnetic or antiferromagnetic, depends upon interatomic distances and the detailed arrangement of electron orbitals. In materials with nanometer-scale structure, a significant fraction of atoms reside at or near surfaces, buried interfaces (between materials with different chemistries and magnetic properties) and defects. Such features can provide environments that are in general distinct from the bulk. For example, strain, change in coordination number and symmetry, reconstructions, *etc.,* are ubiquitous features in nanostructured materials. The length scales of these features (*e.g.,* the decay

length of strain from an interface) can be comparable to the exchange interaction, *J,* for a pair of spins across an interface and may differ significantly from that in the bulk. An example of the importance of interface structure on *J* is found in the magnetic heterostructure: Fe-MnF_2. The exchange coupling across nearly ideally smooth Fe-MnF_2 interfaces is antiferromagnetic ($J < 0$), while for a rough interface ferromagnetic coupling is observed ($J > 0$) [5]. The change from antiferromagnetic to ferromagnetic coupling may be attributable to locally dilated (strained) atomic structure at rough interfaces. Dilation of the lattice (*e.g.,* tensile strain) generally produces ferromagnetic coupling in accordance with the Bethe-Slater formalism [6, 7, 8, 9]. *Because of the departure from a bulk topology, the macroscopic magnetic properties of nano-systems are determined, or at least largely influenced, by the broken symmetries associated with reduced dimensionality.* Thus, a detailed understanding of atomic and magnetic structure at the nanoscale is essential.

1.3 The Ruderman-Kittel-Kasuya-Yosida (RKKY) interaction

The polarization of conduction electrons near a magnetic impurity can act as an effective field to influence the polarization of nearby impurities. In like manner, two magnetic layers can interact via polarization of the conduction electron gas of a metallic spacer layer. Oscillations in the polarization of the electron wave functions mediate either ferromagnetic or antiferromagnetic exchange coupling depending upon the separation between impurities in 3D materials or interfaces in layered (quasi-2D) materials (d_{RKKY} in Figure 1). In the case of 2D structures, consisting of ferromagnetic layers and nonmagnetic spacer layers, the spacer layer thickness can be chosen to promote ferromagnetic or antiferromagnetic coupling across the spacer layer.

An understanding of the complex spin structures of rare-earth superlattices, obtained by means of pioneering neutron diffraction studies [10, 11, 12, 13, 14, 15, 16, 17, 18, 19, 20, 21] provided a basis for understanding the anomalous electronic and magnetic behavior of transition-metal multilayers comprised of magnetic and nonmagnetic layers (*e.g.,* Cu/Ni [22] or Cu/Co [23]). Coupling between neighboring thin ferromagnetic films mediated by conduction electrons in a conducting nonmagnetic spacer layer is just one example of an RKKY interaction in transition-metal multilayers. In general the existence of coupling across interfaces between dissimilar materials is of interest. For example, antiferromagnetic coupling of Fe layers separated by semiconducting Si has been claimed [24, 25, 26]. Ferromagnetic coupling between a ferromagnetic metal and ferromagnetic semiconductor may also be possible in spite of the impedance mismatch between the conduction electrons in the two materials. An open question is whether magnetic coupling across a conducting polymer can be realized. Moreover ascertaining whether the coupling is a result of the (short-range) exchange interaction across an interface or a consequence of the dipolar interaction (in the presence of roughness) is important.

1.4 Dipolar interactions at the nanoscale: domains, domain walls and single domain particles

The magnetostatic energy of a magnetized material can be minimized if the spatial extent of the magnetic field outside the material is reduced. This is achieved through formation of domains in the material with oppositely directed magnetization. The interface between the two domains, a domain wall, consists of magnetic spins that point in directions intermediate between those in the domains on either side of the wall. The width of a 180° domain wall is given by $d_w = \sqrt{JS^2\pi^2/Ka}$ (Figure 1), where J is the

exchange coupling parameter, S is the magnitude of the spin, a is the separation between the spins, and K is the anisotropy constant. The values of J, S, and Ka are all influenced by atomic structure, which may be different in nanostructured materials from those in the bulk. For example, the anisotropy constant is a measure of the energy required to change the magnetization axis of an ordered array of electronic moments. The magnetization includes contributions from the spin and orbital moment of the electron. The orbital moment is strongly coupled to the crystal symmetry. The interaction between spin and orbital moment (spin-orbit coupling) can be altered by changes to the atomic structure and site symmetry of the material, *e.g.,* the Jahn-Teller distortion. In nanostructured magnetic materials, the local atomic structure of defects, such as interfaces, are important in determining the magnitude of the orbital moment. Consequently, a detailed understanding of spin-orbit coupling in the context of broken symmetry, lattice expansion/contraction [27] *etc.,* is required in order to make meaningful predictions about the magnetic anisotropy of artificially structured materials. Understanding the anisotropy is fundamental to the explanation of basic magnetic features such as the widths of domain walls.

An example illustrating the importance of dipolar interactions is the suppression of domain wall formation due to spatial confinement in thin films and fine particles. For example, shape anisotropy of a small particle can dominate over its crystalline anisotropy, consequently suppressing the formation of domain walls within the particle. In some cases, single domain particles (with size given by d_p in Figure 1) may in fact be larger than what would be expected based on domain wall formation in bulk materials.

Other factors that can also dominate the magnetic anisotropy in nanoscale materials include surface and interface anisotropy.

1.5 Spin diffusion

Injection or diffusion of spin-polarized electrons (or holes) across an interface into a nominally nonmagnetic material, in particular a semiconductor, is of paramount interest to the development of new materials in which information is conveyed using the spin degree of freedom. Optical pump-probe techniques have measured the decay time constant of electron polarization in a semiconductor. Assuming the electrons travel at their Fermi velocity, length-scales on the order of 10 nm to 1 μm are deduced for spin diffusion (d_{sd} in Figure 1). Of interest is the magnitude and spatial distribution of spin-polarized electrons in the interior of thin film materials. In particular, the dependence of the polarization of the spin current in the ferromagnetic source, the semiconductor in which the spins are injected, and in the interface between the materials is important [28]. The interface plays a critical role in the spin injection process. For example, pinholes across an interface can short-circuit the tunneling process. Furthermore, if the interface is not sharply defined, *e.g.,* interdiffused, a nonmagnetic dead layer may form from which unpolarized spins can be injected into the semiconductor diminishing the polarization of the spin current.

2.0 Neutron scattering and complementary techniques

Neutron scattering may not be an obvious tool for studies of nanostructured materials. However, neutron scattering has already enhanced the general understanding of magnetism in nanostructured materials by providing information that cannot be

obtained using other techniques. Indeed, neutron scattering is a time consuming technique and often requires large samples; however, carefully planned neutron scattering experiments aimed at answering specific questions about magnetism of nanostructured materials have been and continue to be very fruitful. In order to understand the types of questions suitable for exploration with neutron scattering, the technique is briefly described.

Neutrons are scattered from materials due to an interaction between the neutron and nucleus (nuclear scattering), and/or by the magnetic induction due to electron spin and/or orbital moments (magnetic scattering). The nuclear interaction has three characteristics. First, the interaction is weak. Thus, neutrons penetrate materials, and the scattering tends to be "intensity challenged"; however, since the interaction is weak, the scattering process can be easily quantified. Secondly, the nuclear interaction arises from nuclear physics processes (that do not need to be understood in order to obtain quantifiable results), so adjacent elements on the periodic table (or isotopes of the same element) often have very different (even negative) scattering factors. As a consequence, enhancement of scattering from interfaces can be achieved by decorating interfaces using an appropriate selection of elements or isotopes. Isotopic substitution of an element can provide additional neutron contrast to enable detailed studies of inhomogeneous magnetic structures in otherwise structurally homogeneous materials. Thirdly, the amplitude of magnetic scattering of a neutron is comparable to the scattering amplitude from the nuclear interaction. However, the magnetic scattering amplitude has a dependence on the momentum transfer (Q-dependence) quite different from that of nuclear scattering. The nuclear interaction process is nearly point-like; therefore, the (nuclear) scattering

amplitude is Q-independent. On the other hand, magnetic scattering of neutrons is due to the interaction of the neutron spin with magnetic induction, which is often produced by spin and orbital moments of bound electrons. In this instance, the magnetic scattering is finite over a Q-region inversely proportional to the size of their shell [29]. However, if the source of magnetic scattering is more delocalized (in comparison to the ionic radius), *e.g.,* the magnetization is distributed over a nanometer (or larger) sized dot, the form factor decay will be stronger. For example, spin-polarized electrons injected into the conduction band of a semiconductor might be delocalized (*i.e.,* not bound to a particular atom). In this case, the neutron scattering might only be observable in the region very close to the origin of reciprocal space, *i.e.,* in the forward scattering direction. Small-angle neutron scattering and neutron reflectometry are examples of techniques developed for the purpose of measuring neutron scattering close to the origin of reciprocal space.

Table 1 Brief compilation of neutron scattering techniques appropriate for studies of nanomagnetism.

Neutron technique	Typical sample size or mass (exceptions exist!)
Reflectometry	surface area 1 cm^2 and film thickness 1 nm to 1 μm
Small-angle neutron scattering	sample mass 100 mg
Powder diffraction	sample mass > 50 mg
Single crystal diffraction	sample volume 1 mm^3 or sample mass > 100 μg
Inelastic spectroscopy	sample mass >1 g

In the field of "nanomagnetism" many materials have buried interfaces, of unknown magnetic structure. For these materials neutron and hard X-ray scattering, due to their low absorption, are ideally suited to extract information about magnetic structure. Magnetic force microscopy, scanning electron microscopy with polarization analysis and X-ray spectro-microscopy, on the other hand are only surface sensitive.

Antiferromagnets often form important parts of magnetic nanostructures (*e.g.,* as in giant magnetoresistance and tunneling magnetoresistance sensors). Despite their importance, characterization of antiferromagnets is often difficult, since there is usually no net magnet moment. Neutron diffraction is ideally suited to measure properties of these antiferromagnets, including the magnetic coherence length and Néel (ordering) temperature. While much research has been dedicated to the analysis of bulk antiferromagnets, wide-angle neutron diffraction has recently been used to characterize antiferromagnetic films with thicknesses on the order of 30-500 nm. [30, 31, 32]

Microscopy (optical, electron and X-ray) techniques typically resolve local real-space variations in magnetic structure and complement capabilities of statistical probes such as, neutron (and other) scattering techniques, which measure an ensemble average of magnetic structure. Magnetic microscopy techniques such as magnetic force and scanning electron with polarization analysis microscopies have excellent sensitivity to magnetic domain structure. While microscopy techniques provide a real space picture, they typically examine only a small, perhaps non-representative, area. In contrast, both neutron and X-ray scattering statistically average a large area (mm^2 to ~10 cm^2). While sometimes harder to interpret, a statistical average is representative of the complete sample and is relevant for many macroscopic magnetic and magnetotransport properties.

Moreover unlike neutron scattering, which can be used to study magnetic materials in any applied field (in addition to pressure and temperature), many microscopy techniques and those relying on emission of secondary electrons require near zero-field (remanent) conditions.

3.0 Nanomagnetism and the role of neutron scattering

The capability to fabricate structures with confined geometries at the nanoscale using film deposition, lithography and self-assembly offers opportunities to study fundamental physics of nanomagnetism, and to create interesting and technologically important materials that exhibit entirely new functionalities. In addition to the progress made towards fabrication of new magnetic materials, significant advances arise from simulations of increasingly large ensembles.

Neutron scattering is well known for its role in elucidating much of the foundations of traditional bulk magnets. The neutron, with its magnetic moment $\boldsymbol{\mu}$ uniquely interacts with the local values of the magnetic induction **B**. Neutron scattering is used to identify ordered spin structures, to obtain the detailed distribution of spins around each atom, and the magnetic inductance of single impurities in matrices. Temperature dependent measurements of inelastic neutron scattering have determined the magnetic excitation spectra of materials, in the form of spin wave dispersion curves at low temperatures, to magnetic transformations from ordered to disordered paramagnetic states, where excitation levels of single atoms have been observed. With such a wealth of achievements in bulk magnetism, neutron scattering is poised to have a significant role in the study of nanomagnetism.

Neutron scattering probes magnetic structure at many different length scales. Wide-angle diffraction provides information about the atomic and magnetic structures in single-crystal films and multilayers. The magnetic order parameter of ferromagnets, ferrimagnets and antiferromagnets can be measured directly. Average magnetic domain sizes can be extracted from peak widths. Neutron diffraction techniques probe the detailed magnetic structures of spin modulations and dispersion of spin waves in materials. For instance neutron scattering showed that in Fe/Cr(100) superlattices, the incommensurate antiferromagnetic spin density wave of the Cr exhibits nodes near the Fe interfaces in order to minimize the spin frustration at the necessarily atomically rough interfaces [33, 34, 35].

For studies of magnetic phenomena that occur over length scales that are large compared to atomic distances, magnetic small-angle neutron scattering is appropriate. This technique is ideal for the characterization of magnetic domains, ferromagnetic correlations and long-wavelength oscillatory states in superconductors, vortex structures in superconductors, and other spatial variations of the magnetization density on length scales from 1 nm to 1 μm. An important example involves the propagation of ferromagnetic coupling between nanoparticles. Small-angle neutron scattering from nanometer-sized grains of Fe, Co and Ni has shown that ferromagnetic coupling occurs between the grains in a wide variety of materials [36]. The important implication of the neutron study is that control of physical dimensions does not in general assure control of magnetism.

Polarized neutron reflectometry, is used to investigate the magnetization profile near the surface of single crystals, and of thin films and multilayers. Surface sensitivity

derives from working in grazing incidence geometry near the angle for total external reflection. Polarized neutron reflectometry is highly sensitive, having measured the absolute magnetization of a monolayer of iron (~10^{-4} emu) with 10% precision [37] (even better precision is obtainable today), and has excellent depth resolution, on the order of a tenth of a nanometer even for films as thick as several hundred nanometers. Reflectometry has enjoyed dramatic growth during the last decade and has been applied to important problems such as for example, the origin of exchange bias. Exchange bias, the shift of the center of the ferromagnetic hysteresis loop away of zero of applied field, can occur from interactions between ferromagnets and antiferromagnets. The interfacial spin frustration between the ferromagnetic and antiferromagnetic layers adds a staggering level of complexity to the problem, since real interfaces are not atomically smooth, and possess varying degrees and types of roughness, *i.e.,* chemical/structural and magnetic roughness. Neutron scattering has provided insight in the magnetization reversal processes of the ferromagnet [38], and the importance of the detailed spin structure of the antiferromagnet in exchange biased systems [31, 39, 40, 41, 42, 43].

3.1 Fundamental issues in nanomagnetism

Competition between structural length-scales and magnetic length-scales gives rise to a range of new magnetic phenomena. In this section, we highlight the exploration of fundamental questions pertaining to nanomagnetism that are being addressed by basic researchers.

3.1.1 Reduced Dimensionality

The effect of dimensionality on magnetic order in simple models can be rigorously formulated. The dimensionality of a system can be obtained by comparing its spatial dimensions with its exchange length, $d_L = \sqrt{A} / M_S$, where A is the exchange constant (a measure of the force tending to keep adjacent spins parallel) and M_s the saturation magnetization (typically d_L is of order 10 nm in Fe, Ni or Co) [44]. A particle or sample that is much larger than d_L in all three dimensions is considered a bulk material. The Mermin-Wagner theorem [45] states that for the isotropic Heisenberg model there can be no magnetic phase transition in less than three dimensions (3D). In 1D, long-range order is forbidden even in an anisotropic Heisenberg model [46]. Despite these simple theoretical predictions, materials with reduced dimensions can have intriguing and diverse magnetic properties. The discrepancy between idealized theoretical constructs and experimental observations is mainly due to the fact that all real magnetic materials exist in 3D space and have finite size.

In a quasi-2D system, one of the spatial dimensions is less than d_L, *e.g.,* as in an ultra thin film (Figure 2). Magnetic phase transitions in thin films are dominated by two competing mechanisms, magnetocrystalline anisotropy and magnetostatic interactions. The latter gives rise to shape anisotropy and favors in-plane alignment of the moments for thick films. The dominant part of the magnetocrystalline anisotropy is due to the reduction of symmetry at the surface of the film. It typically favors perpendicular alignment of the moments [47, 48, 49], but is essentially independent of film thickness, thus, very thin films tend to exhibit anisotropy perpendicular to the film plane. The

resulting spin reorientation transition of the magnetization as a function of film thickness has been the subject of numerous studies in the past decade [50, 51, 2], and the exact nature of the transition is still a matter of debate [52]. Recently, the spin reorientation transition in Co/Au layered samples was examined with neutron scattering and magneto-optic Kerr effect spectroscopy [53]. The spin reorientation transition was found to be driven by the formation of magnetic domains and is influenced by temperature and magnetic layer thickness. Many spin reorientation transitions occur as expected— the magnetization rotates from out-of-plane to in-plane with increasing film thickness (driven by shape anisotropy). However, there are exceptions, *e.g.,* Ni on Cu(100), which reorient from in-plane to out-of-plane with increasing film thickness (presumably due to strain effects) [54].

Modification of magnetic transition temperatures, *e.g.,* Curie or Néel transition temperatures, is another consequence of reduced dimensionality in artificially layered materials [55, 56]. Neutron diffraction studies of transition-metal oxide multilayers composed of a ferrimagnet and an antiferromagnet, such as Fe_3O_4/CoO [31] and Fe_3O_4/NiO [42, 57] or of alternating antiferromagnets, such as CoO/NiO [58, 59], demonstrated that the magnetic ordering temperatures of the individual layers are strongly perturbed by local coupling at the interfaces. For antiferromagnetic CoO/NiO multilayers with thin bilayers, the CoO and NiO antiferromagnetic structures develop simultaneously at temperatures that scale between their bulk ordering temperatures and relative bilayer composition [60].

Reducing all spatial dimensions below the exchange length, d_L, produces quasi-zero-dimensional particles ("nanodots") (Figure 2). The competition between the

effective anisotropy of the nanodots along with their inter-dot interactions controls their (collective) behavior. The case where the anisotropy dominates has been studied extensively due to its immediate relevance to magnetic recording media and is well described by the Stoner-Wolfarth model for independent particles [61]. At issue is mainly the stability of the net moment of a particle with regard to thermal fluctuations (and also the magnetic interactions between small particles). At low temperatures, when k_BT is much smaller than the energy barrier due to the net anisotropy, the particle moment is locked into the directions of the net anisotropy axis.

In the opposite limit, where interactions between particles become comparable with or dominate the anisotropy energies, the magnetic properties are those of the entire ensemble [36]. It is in this case that neutron scattering studies may be useful. For example, in Figure 3(a) we show single crystal Fe particles, which are partially aligned in one of three orientations (Figure 3(b)) with respect to an yttrium stabilized zirconia (YSZ) single-crystal matrix [62]. The magnetization curves (Figure 3(c)) for this system [63] do not show the dependence on directions of the applied field expected for independent particles. In fact, the magnetization curve is that of a frustrated system (Figure 3(d)) understood in terms of particles that interact magnetostatically [64], *i.e.,* the magnetization and anisotropy axes point in directions given by their orientations in the matrix (Figure 3(b)). Small-angle neutron scattering of such systems helps determine possible short-range order in the magnetic structure.

So far we have discussed the effect of dimensionality on the stability of magnetic order. Dimensionality also affects the magnitude of the magnetic moments. Dimensionality reduction implies a change in coordination that produces a concomitant

change of atomic moments. For example, Fe in the bulk bcc structure has a moment of 2.2 μ_B compared to 4 μ_B for an isolated Fe atom in vacuum. The magnetic moments in film, wire, and particle geometries vary depending on details of the structures and substrates [65]. The moment of a system can be determined from measurements of the saturation magnetization, provided the systems can be saturated and that only one type of magnetic atom, is present. That is certainly not the case for α-Mn, an antiferromagnetic metal with a complex crystalline unit cell composed of four inequivalent Mn atoms, with different magnetic moments. The complexity of Mn carries over to its nanostructured materials. In molecular magnets, *e.g.,* Mn-12 acetate, the magnetic moment depends upon the point symmetry and local atomic environment and does not reflect values found in the bulk (see Figure 4) [66]. For example, the magnetic moment of an isolated Mn^{+2} ion is 5 μ_B, while in Mn-12 acetate the magnetic moments of Mn^{+3} and Mn^{+4} ions range from 2.3 to 3.8 μ_B. Indeed, neutron scattering is one of the few tools capable of measuring moments of individual lattice sites. In other systems that show spin-glass-like behavior, *i.e.,* systems that cannot be fully saturated, atomic moments cannot be rigorously determined with magnetometry, therefore, neutron scattering is again a key tool.

A new class of materials that has a low magnetic moment and a high Curie temperature was prepared recently. These materials, *e.g.,* CaB_6 [67], are mostly formed by alloys of nonmagnetic elements. Most claims of magnetism in these materials are based on global measurements such as magnetometry and some limited superconducting tunneling. These materials might also benefit from polarized neutron scattering to ascertain the origin and location of the magnetism.

Enhanced magnetic moments at surfaces and interfaces have been theoretically predicted. For example, the moment magnitude, direction and type of magnetic order at a surface is expected to differ from that of bulk, as the result of a complex set of circumstances, such as the incomplete quenching of the orbital moments, the stretching (or compressing) of the lattice on the substrate, and electron transfer between magnetic film and substrate. Previously, polarized neutron reflectometry determined the absolute value of the magnetic moment per atom in very thin films (5 atomic planes) sandwiched between Ag on one side and Pd, Ag, Au, Cu on the other side. At this thickness, an average moment per Fe atom has been found of ~2.5 μ_B, compared to a bulk value of 2.2 μ_B [68]. This result is in agreement with the 30% increase of the Fe moment predicted for the surface layer. In contrast, it was found that Ni in Cu/Ni/Cu sandwiches exhibits a decreased magnetization for films as thick as 100 Å, with a residual magnetization of ~0.1 μ_B /Ni at a nickel thickness of 30 Å [69].

Experimental realization of enhanced moments at a single interface, has been elusive, and the experimental detection of enhancement of magnetic moments at a single interface is challenging with magnetometry, since the magnetization of the interface is a minute fraction of the contribution from the substrate (a source of magnetic background). Since polarized neutron reflectometry is inherently interface specific, the magnetization of or near an interface can be measured, in principle, with a great degree of accuracy even in the presence of a magnetic substrate. Two cases in hand include observations of enhanced magnetic moments of Ni atoms at a grain boundary interface [70] and frozen magnetization at the interface between Co and $LaFeO_3$ (an antiferromagnet) [43].

Resonant hard and soft X-ray techniques have also been used to detect enhanced interfacial moments in layered systems [51, 71].

To observe enhanced magnetic moments at interfaces, intimate contact must be present between the adjoining materials, and it is important that the magnetization (*i.e.,* "order parameter") of the ferromagnet survive all the way to the interface and into the adjoining nonmagnetic material. In other words, the uniformity of the ferromagnet must be kept at the length scale of the ferromagnetic exchange length. This length scale is naturally very short (typically about 1 nm). Therefore, structural and chemical issues are important at this length scale. The spatial dependence of the order parameter is determined by the exchange length in the ferromagnet and in the non-ferromagnetic material. Thus it may very well be that the magnitude of the order parameter is substantially reduced at the interface.

3.1.2 Magnetic structure

A starting point for understanding the behavior of any magnetic system is to characterize its structure. In general, knowledge of a magnetic structure is required as a function of temperature, external magnetic field, and other parameters. The magnetic structure can be observed at different length-scales, ranging from domain sizes at macroscopic length-scales down to the spin structure of a magnetic molecule.

In naturally occurring magnetic materials, the moment is affected by the development of electronic bands in a crystal. The bands can be engineered to modify magnetic properties through artificial structuring. For example, by introducing interfaces and surfaces and by perturbing local stresses and strains as well as reducing relevant

dimensionalities, modifications of bulk magnetic structures can be achieved, *e.g.,* by developing new anisotropies. Further, an artificial structure can give rise to new interactions between different magnetic constituents such as separate layers, granular particles, or patterned lateral structures. One example of a new or modified interaction is oscillation of exchange coupling, where the sign and magnitude of the coupling between two ferromagnetic layers is determined by the thickness of a nonmagnetic metallic spacer layer [22, 72, 73, 74, 75] (see Section 1.3). Another example can be the lateral arrangements of magnetic particles or dots, where the geometry of the arrangement may give rise to a frustration of interactions, such as via dipole-dipole interaction [76, 77]. Finally, compounds that do not exist in nature, can be stabilized by means of vapor deposition techniques to create new magnetic materials, as claimed for the ferromagnetic semiconductor (Ga, Mn)As [78].

The magnetic structure on an atomic scale can be important for a variety of interesting materials ranging from geometrically frustrated spin-ice [79,80], to colossal-magnetoresistance materials, to high-T_c superconductors. A recurring question is whether the spin structure at interfaces and surfaces of thin antiferromagnetic layers and small particles is given by the spin structure of the bulk material. In fact, it has been shown that the two structures are generally not the same. For example, the spin-density wave in a Cr layer can be modified or even suppressed as observed with neutron scattering in nanocrystalline Cr (Figure 5) [81, 82, 83], Fe/Cr bilayers [84] and Fe/Cr superlattices (Figure 6) [34, 85], and there are data suggesting that ferromagnetic overlayers can modify the spin-structure of NiO [86, 87, 88] at the interface. The unambiguous determination of the spin structure in thin films and small particles, both at their

interfaces and surfaces as well as in their interior still remains one of the most challenging experimental questions.

3.1.3 Magnetic vs. Structural Roughness

It is by now generally accepted that interfaces play a large (perhaps even dominant) role in the phenomena governing the magnetic and magnetotransport properties of thin films [1]. However, theories that attempt to explain these properties generally assume "perfect" or regular crystalline interfaces. The role of disorder effects, in particular of roughness or interdiffusion across the interface, is still poorly understood and systematic investigations of these effects are lacking. Thus straightforward attempts to correlate important effects such as magnetoresistance, exchange bias and magnetic proximity effects with quantities such as the average roughness appear to show rather contradictory results [89, 90]. In the case of exchange bias, for instance, there has been a steady progression of theoretical models to account for the discrepancies between the experimentally realized values and those expected from the most idealized model of the interface. What is clearly needed is a microscopic picture of the spin and orbital magnetization density at and on both sides of the interface, and how the magnetization density varies systematically with the nature of the interface (*e.g.,* what crystalline structures are involved at the interface, strain and lattice distortion effects, and the effect of film thickness, as well as of magnetic field and temperature). For this purpose, one also needs convenient models to represent such disordered interfaces and to represent the magnetization distribution, which can be fitted to the results of scattering and other experiments and which in turn can be used to calculate quantities such as magnetotransport, coercive fields, exchange bias fields, *etc.* A conceptually simple way

to model such effects is to visualize a "magnetic interface" between the two layers which may be distinct from the actual chemical interface, but may also be highly correlated with the latter (Figure 7). The relevant length scale here may be from 1 nm to microns, which is the range amenable to study with the techniques described here. (Magnetic moments, which are disordered on shorter length scales, will simply appear as a loss of magnetization.) In addition there may be domain formation within the ferromagnetic layers, which can also be studied as described later. The concept of the magnetic interface leads naturally to the concept of "magnetic roughness," which is distinct from the "chemical roughness" and may be specified in terms of the same types of parameters used to describe the latter, namely a root-mean-square value for the height fluctuations about the average, a roughness correlation length and a roughness exponent.

More than 15 years ago, polarized neutron reflectometry was used to measure the chemical and magnetic roughness of interfaces in magnetic (Ni)/nonmagnetic(Mo) superlattices [91]. Figure 8 [91] shows the intensity of various order superlattice peaks measured both by neutron and X-ray scattering. Calculations using the two extreme models for the magnetization distribution (using as an input, the structure obtained from X-ray studies) show that the experimentally measured neutron intensities are higher than the calculated ones. Resolution of this discrepancy requires different values for the magnetic and chemical roughness. In this example, the magnetic roughness of the Ni/Mo interface is smaller than that of the chemical interface. More recently, smoother magnetic than chemical interfaces have been observed in Fe/Cr superlattices via neutron diffraction [92] and via synchrotron radiation in a variety of other magnetic-nonmagnetic interfaces [93, 94].

Since the writing of the Falicov *et al.* [1] report, powerful tools for the analysis of diffuse (non-specular) neutron and X-ray scattering first based on the distorted wave Born approximation [95, 96] and more recently involving the "supermatrix" formalism [97, 98, 99, 100] have been developed. Quantitative analysis of neutron or X-ray diffuse scattering to isolate magnetic roughness of surfaces and buried interfaces from structural and chemical interdiffusion is now possible [101]. For example, in analyzing the intensity, distribution and polarization of diffusely scattered neutrons, the mean square deviation of magnetic spins, σ_m, and the lateral length scale over which deviations of spin are correlated, ξ_m, are obtained (Figure 7).

Magnetic X-ray scattering using circularly polarized synchrotron X-rays on thin films of Co indicates that it is the magnetic roughness parameters (in particular the correlation length) rather than the chemical roughness determines the coercive field in these films [102]. Another example of a case where magnetic roughness and its interplay with chemical roughness is of importance occurs for magnetic multilayers that display giant magnetoresistance, *i.e.,* multilayers with alternate ferromagnetic layers antiferromagnetically aligned across intervening metallic layers. In the absence of field, the ferromagnetic layers are antiferromagnetically aligned, which hinders electron transport across or along the conducting films. These layers are ferromagnetically aligned with the application of magnetic field that creates low resistance paths for electron current to follow (the large change in magnetotransport is the giant magnetoresistance effect). The behavior of electron transport across magnetic layers and in particular spin-dependent transport is clearly sensitive to both the chemical and magnetic roughness at the interfaces, but attempts to correlate the giant

magnetoresistance effect with the chemical roughness alone often show contradictory results [89, 103, 104].

Measurements of diffusely scattered neutrons with or without polarization analysis provide an unprecedented level of insight into the magnetic structures of complicated nanostructured systems. For example, field-dependent magnetic diffuse scattering was observed in transverse measurements through the half-order antiferromagnetic reflection for Fe/Cr multilayers, which are antiferromagnetically coupled [105, 106, 107, 108, 109]. The field dependence of this scattering is directly correlated with the magnetoresistance of these multilayers. While magnetic diffuse scattering may result from either the domains across the sample plane or from rough magnetic interfaces [110], in at least one case, the diffuse scattering for Fe/Cr multilayers was found to originate entirely from the magnetic disorder at the interfaces.

Figure 9 shows a more recent example of the polarization dependence of the diffuse neutron scattering from an Fe/Cr multilayer. From these data, quantitative information about the field-dependent evolution of magnetic roughness along the growth direction, as well as the formation of in-plane magnetic domains, can be obtained. Quantitative measurements of in-plane domain sizes ranging from 1 to 20 μm have been obtained for magnetic multilayers such as Co/Ru [111], $Ni_{80}Fe_{20}$/Ag [112] and Co/Cu [113,114], and also from arrays of periodic magnetic entities [115]. The wealth of information available in measurements of in-plane correlations makes it possible to distinguish between chemical interdiffusion, structural roughness, magnetic roughness and magnetic domain formation. The ability to obtain quantitative information about domains in buried ferromagnetic films is a strength of neutron scattering.

3.1.4 Proximity effects: induced magnetization

Materials with magnetically dissimilar properties can be nanostructured in a manner that influences the magnetic properties of the ensemble. A simple example is the exchange bias of a ferromagnet in proximity with an antiferromagnet. Since many magnetic properties vary on a nanometer length-scale, fabrication of samples with a high degree of structural perfection is important. To achieve perfection is challenging, particularly since interesting effects are often obtained by combining dissimilar materials that may be structurally incompatible, *e.g.,* a transition element ferromagnet with a semiconductor or superconducting oxide. In these and other cases, detailed interface characterization in terms of interface roughness, interface density, broken symmetry, *etc.,* as a function of external parameters such as applied magnetic field magnitude, direction, temperature, *etc.,* are needed in order to understand the influence of interface structure on the magnetic properties of the interface, and the spatial extent of interface magnetism away from the physical interface.

A question germane to the magnetic proximity effect concerns induced magnetic order in nominally nonmagnetic materials when placed in contact (proximity) with a magnetic material [116]. For example, easily polarizable materials, such as Pd (*i.e.,* materials that are almost ferromagnetic), could acquire a magnetic moment if they are in contact with a ferromagnetic material. Giant moments can be induced in Pd when magnetic impurities are incorporated into the matrix. Even for very low concentrations of magnetic impurities, sizable ferromagnetism has been observed in the Pd matrix [117, 118]. Furthermore, in the case of a well-defined thin film interface, a moment of about

0.3 μ_B/ Pd atom has been inferred for the first layer in contact with the ferromagnetic material from electronic structure calculations [119] magnetometry data [120, 121, 122], and X-ray magnetic circular dichroism studies [123]. On the other hand, the magnon spectra show very little effect due to the magnetic proximity effect [124]. Recently, on the basis of magnetometry studies, Pd was claimed to become magnetic when in proximity to an antiferromagnet, NiO [125]; however, neutron reflectometry measurements with enhanced sensitivity to the Pd/NiO interface (achieved through the use of isotopic Ni), did not observe a magnetic moment in the Pd (or NiO) [126].

In contrast to induced magnetization in a normally nonmagnetic material, a ferromagnetic layer may lose its magnetization at the interface to a nonmagnetic material and form a magnetically "dead" layer. This issue can be of paramount concern for spin-injection from a ferromagnet into a semiconductor or across an insulator, as for tunnel junctions, where the spin polarization at the interface is one of the parameters that determines the net spin current across the interface [127]. For example, a magnetically dead metallic layer at the tunnel junction interface can destroy the polarization of the transmitted current by serving as a source of unpolarized spins [128]. Magnetic dead layers have been directly observed in Fe/Si multilayers using polarized neutron reflectivity [129], and in Ni/Pt multilayers via X-ray circular dichroism [130].

A related idea is the growth of "digital" ferromagnetic semiconductors, where magnetic dopants are placed selectively as thin layers throughout the semiconductor to produce a ferromagnetic heterostructure [131]. In this example, determination of the detailed magnetization profile obtained by means of neutron scattering through the semiconductor, or across a magnetic heterostructure, could provide important clues

relating to the formation and injection of spin currents in spintronic materials. Preliminary neutron reflectivity studies of (Ga, Mn)As/GaAs multilayers indicate that thin ferromagnetic layers may interact across the nonmagnetic GaAs [132].

3.1.5 Polarization of conduction electrons, spin transport and injection

The challenge to develop "spintronic" systems, creates interest in the spin polarization of carriers that play a role in transport. This can entail measurements of the density of states at the Fermi level or alternatively, the density of states weighted by the charge velocity (or its square) [133]. Together with the spin structure and larger-scale magnetization structure, the spin polarization of the conduction band controls the "transport" of magnetic information. A key characteristic of the magnetic layers used to produce spin-polarized current is the degree to which the carriers are spin-polarized. Magnetoresistance is a strong function of the spin polarization of the ferromagnet and the properties of the interface across which injection is desired. The spin polarizations of ferromagnetic materials can be measured by spin-polarized electron tunneling methods [134], point contact Andreev reflection from a superconducting tip [135, 136, 137], transmission through a tunnel junction between ferromagnetic layers [138], and spin-resolved photoemission from light emitting diode structures [139]. Since spin-polarized electron tunneling is sensitive to the density of states of the tunneling electrons, the measurement technique on which it is based is particularly sensitive to the quality of the tunnel junction, *e.g.,* the sharpness of the interfaces on either side of the junction. Modern-day fabrication techniques have greatly improved the quality of interfaces in tunnel junctions [138, 140], so reliability of spin polarization determined via tunneling is improving. Point contact Andreev reflection can also be sensitive to the quality of the

interface between the superconducting tip and metal; however, considerable progress has been achieved in understanding the influence of interface quality on the experimental data [141] from which the transparency of the superconducting/metal interface, and spin polarization in the metal can be deduced. Spin-resolved photoemission tends to be sensitive to surface quality. All these methods rely on the properties of the interface (or surface), so experimental determinations of spin polarization are not necessarily characteristic of the bulk.

As interfacial quality, *e.g.,* smoothness, improves with better processing, the spin polarization of currents injected across the interface also increases. The correlation between spin polarization and interfacial quality suggests a spatial dependence of the polarization. Thus, determination of the magnitude and spatial distribution of conduction carrier spin polarization is important. Neutron scattering determination of the magnetization profile (arising from spin polarization) at and near the heterostructure interface may help to resolve discrepancies between spin-polarizations obtained with different techniques- tunneling, point contact Andreev reflection, and photo-emission, for nominally similar systems.

The polarization of conduction electrons in a ferromagnet has been determined in the past by combining neutron diffraction with magnetization measurements. For example, in Gd metal, [142] the magnetization yields an ordered moment of 7.7 μ_B/atom, while the intensities of the Bragg reflections fit the form factor functional behavior characteristic for 4f electrons, and yield a moment of 7.0 μ_B/atom. The difference is attributed to the polarization of the 5d, 6s conduction electrons. It should be possible to extract the conduction electron contribution from an analysis of small-angle neutron

scattering or reflectometry [143] of suitably prepared surfaces, or from measurements of Bragg reflections from superlattices.

3.1.6 Stimulated Collective Excitations

Materials close to instabilities can exhibit interesting phenomena such as collective states introduced by external means. Examples include producing collective states (mostly in superconductors) by light [144] or with pressure [145]. Similar effects have been observed recently in manganites [146] where persistent photoinduced magnetism was produced. Interestingly, the photoinduced magnetism coincides with the metal-insulator transition in these systems. While photoinduced metal-insulator transitions in semiconductors are well known [147], the creation of collective states, such as superconductivity and magnetism, is a recent development, with important implications. Since neutrons are highly penetrating, they are transparent to optical windows. Thus, the influence on skin depth or formation of vortices by light could be investigated using neutron scattering. In general, the materials often used to make sample environment, *e.g.,* high field magnets, or those employed with magnetometry, such as ferromagnetic resonance [148], are often transparent to neutron beams, thus, a wide variety of equipment and many table-top characterization tools can be readily adapted to neutron scattering.

Another form of collective excitation, involves the correlation of magnetic form factors of neighboring dots or antidots in arrays [115, 149, 150, 151]. How is, for example, a thermally activated change in the magnetization of one dot communicated throughout an array (regular or random) of nanodots? If the dots are placed on a weakly

magnetic substrate, would collective excitations be transmitted via spin waves in the substrate?

A related subject involves spin waves in materials of reduced dimensionality. A key ingredient to understand magnetic phenomena is to characterize the magnetic excitations. For example, information about magnetic anisotropies is obtained from magnon dispersion curves. Perhaps even more intriguing is to understand the transition from spin waves found in bulk materials to discrete excitations as Walker modes [152] in arrays of nanodots or Damon-Eshbach modes [153] at interfaces. A grand challenge for inelastic neutron scattering is to characterize dispersion of spin wave excitation spectra in nanostructured materials.

Traditionally, large quantities (grams) of material are required for inelastic neutron scattering, which is not very practical in this case. However, inelastic neutron scattering measured the dispersion of spin waves in superlattices, using tens of milligram-sized samples. In a tour-de-force of sample fabrication, a superlattice consisting of 280 repeats of identical Dy/Y bilayers was studied using a triple-axis neutron spectrometer. The magnon dispersion curves shown in Figure 10 demonstrate that measurements of inelastic excitations in nanostructured materials are feasible [154].

Fabrication of superlattices with many repeat layers poses a practical difficulty. Thus, their use in conventional neutron scattering studies of spin waves in layered systems will probably be uncommon. A solution involves combining neutron reflectometry with inelastic neutron scattering (this approach is suggested in Falicov *et al.* [1]). Bernhoeft *et al.,* [155] using inelastic neutron scattering in forward geometry (the geometry used in reflectometry), observed spin-wave excitations in Ni_3Al. The scattered

intensity from the excitations was one-tenth the magnitude of the elastic energy/incoherent signal (Figure 11 (a)). Note that with neutron reflectometry, the measured elastic signal covers a dynamic range of seven orders of magnitude from samples with masses on the order of 300 μg (Figure 11 (b)). Therefore, a combination of inelastic neutron scattering with reflectometry should succeed in measurements of spin waves in thin films, albeit in a restricted range of momentum transfer compared to conventional inelastic neutron scattering (though large in comparison to light scattering techniques [156, 157]). We note the cross section for magnon scattering remains finite for $Q \rightarrow 0$ (in contrast with phonon scattering). However, scattering within the first Brillouin zone is kinematically restricted to low-energy and -momentum excitations.

Finally, a promising route to obtain information about spin waves at interfaces involves combining magnetic resonance techniques with neutron scattering. In magnetic resonance experiments, a sample is placed inside a microwave (tens of GHz) cavity, and a magnetic field (peak amplitude of order 1-10 G) is applied to the sample. The cavity can be made from Al, which is essentially transparent to neutrons. A static magnetic field is applied to the sample perpendicular to the microwave field and parallel to the sample plane (Figure 12 (left)). By adjusting the static field strength, a resonance condition can be achieved (corresponding to a pronounced power loss in the cavity). During resonance, the magnetic moments in the sample precess in phase about a cone (Figure 12 (right)). We note the projection of the sample magnetization along the applied field is reduced typically by a couple of percent compared to the off-resonance condition. This reduced moment could be detected in a neutron scattering experiment by a reduction in the difference between the intensities of spin-up and spin-down scattered neutrons. A

more significant effect could be observed by measuring the intensity of neutrons whose spins flip. Spin flip scattering is a measure of the mean square component of the sample magnetization perpendicular to the applied field, *e.g.,* the component in the direction of the microwave-field. In this experiment, magnetic resonance would be used to excite spin waves (as described, the uniform mode is excited), and neutron scattering would be used to discern spin waves at interfaces (known as anomalous ferromagnetic resonance modes), from those in the film bulk. In other words, interface specificity of neutron scattering can complement measurements of anisotropies averaged over entire samples as obtained using ferromagnetic magnetic resonance.

3.1.7 Vortices in superconductors

Type-II superconductors in a magnetic field develop a mixed state, through which the magnetic field penetrates the material inhomogeneously. This gives rise to vortices of superconducting currents, with quantized ($\Phi_0 = hc/2e = 20.7$ Gμm^2) magnetic flux lines in their interiors. These vortices have a repulsive interaction, which generally leads to the formation of a regular lattice. The vortex lattice is expected to be hexagonal.

When a sufficiently large electric current is applied to a superconductor in the mixed state, the vortices move, which gives rise to a finite resistance. Vortex motion is typically detrimental for many applications of superconductors, thus, various schemes have been devised to suppress vortex motion using artificial defects to pin them. Besides inhibiting vortex motion, the pinning of vortices gives rise to a rich variety of new static and dynamic phases of vortex matter.

The progress in small scale structuring of materials has enabled new approaches to studies of vortex physics, since it is now possible to carefully place pinning centers at specific locations in the superconductors. For example, holes can be placed in the superconductor [158, 159] or small magnetic dots located on the superconductor [160, 161]. By arranging these artificial pinning centers on regular arrays one can observe striking coherent pinning effects, whenever the vortex lattice becomes commensurable with the artificial pinning array. Especially at fields where multiple vortices exist per pinning center, one can observe rather unusual arrangements of vortices positioned in between the artificial pinning centers [162]. One can even intentionally distort the vortex lattice from its equilibrium lattice, through which new insights into static and dynamic pinning properties [163, 164] can be achieved.

Vortex physics in superconductors provides a rich playground of magnetic structures. These vortex structures have been investigated quite successfully with a variety of neutron scattering techniques. For example, small-angle neutron scattering has been used to map out the vortex lattice phase diagram as a function of magnetic field and temperature [165, 166, 167, 168, 169] for arrays of vortices forming an hexagonal or a square lattice at the surface [170]. For thin films, the vortex distribution parallel to the film has been determined from polarized neutron reflectometry [171, 172, 173, 174]. More complex systems, such as artificially layered superconducting thin films, also exhibit coherent pinning effects [175, 176], and should benefit from study with polarized neutron reflectometry.

3.2 Important issues in nanomagnetism (materials)

Since growth of artificial magnetic materials can be controlled over most relevant magnetic length-scales (see Figure 1), many interesting new properties appear as the structure's dimensions approach a length-scale characteristic of a particular phenomenon. Generally nanostructured magnetic materials can be deposited on a substrate or can be embedded in the bulk of an otherwise nonmagnetic material. On a substrate, nanostructuring can be performed either perpendicular to its surface or in the plane parallel to it.

Perpendicular-structures: Thin films have been used to produce a variety of nanostructured magnetic materials. These structures are produced using a number of growth techniques such as sputtering, molecular beam epitaxy, laser ablation, and metal oxide chemical vapor deposition. In all of these cases structural length-scales can be engineered that are comparable to magnetic length-scales. Issues of interfacial roughness and interdiffusion vary between preparation methods and are strongly dependent upon the details of the preparation conditions. Due to the variability of fabrication processes, there is always a need for quantitative structural, chemical and magnetic characterization of the samples.

Planar Structures: Recently a number of fabrication techniques have emerged that can produce nanostructured magnetic materials within the plane of the substrate, *e.g.,* as in arrays of magnetic dots or antidots. However, some fabrication techniques (*e.g.,* atom manipulation using a scanning tunneling microscopy) usually do not produce sufficiently large samples to benefit from neutron scattering characterizations. As a rule-of-thumb, planar samples should have a cross-sectional area of order 1 cm^2 to be suitable for

neutron scattering studies. We note that suitably sized samples containing arrays of dots [177] and antidots have been produced with electron lithography [115].

Other techniques are available that readily produce large sample volumes. Typical examples include self-assembly methods utilizing di-block copolymers, and electrochemically produced masks through which nanoscaled arrays over macroscopic areas have been produced [178]. The potential advantage of self-assembly is that the length-scales are not limited by lithographic constraints. Self-assembly via vacuum evaporation can entail the same technologies as the growth of films. The difference is that the deposited material does not wet the substrate, but instead forms island structures. If the islands have a suitably narrow size distribution and orientational spread, the resultant material is deemed successfully self-assembled.

Another approach to self-assembly is to guide the formation of low-dimensional features, such as by using corrugated substrates [179]. Step decoration is a method to create striped structures. The stripes can be narrower than are accessible via lithography and can extend down to monatomic widths that decorate atomic steps on nonmagnetic substrates.

One of the great potential achievements of self-assembly is the development of low-cost chemical methods to create small structures that are subsequently spin-coated onto substrates. Remarkable progress is being made toward the creation of future-generation discrete magnetic recording media utilizing this synthetic route. Di-block copolymers self assemble into a rich array of dot, stripe and two-dimensional network structures. The hope is to incorporate magnetic atoms directly into the polymeric building blocks, or to

subsequently attach or decorate the resultant nanostructures with magnetic atoms. In the future, patterned substrates might provide a useful way to control feature placement in self-assembly that is lithographically assisted [178].

Self-assembled structures as described above can be used as masks for the preparation of magnetic arrays in a variety of configurations (see Figure 13). For instance, Figure 14 shows an example of nanostructuring using di-block copolymer lithography for the preparation of nanoholes in an Fe-FeF_2 exchange biased bilayer [180]. Interestingly, these materials exhibit modified magnetic behavior, such as the stabilization of magnetism above their blocking temperature and enhancement of magnetic moments. Of particular interest would be characterization of the detailed magnetization reversal processes at different points along the hysteresis loops, and the collective behavior of the exchange biased dot/network structures for dot/network coverages below and above the percolation limit. Neutron scattering has been used in the past to observe the rotation and nucleation of magnetic domains [38, 181, 182], and such studies would provide information needed to understand collective behavior in this system. We note that anisotropic magnetoresistance measurements have been used to obtain information about magnetization reversal processes in exchange biased materials; however, owing to the discrete nature of laterally structured materials, transport measurements will not be particularly useful in this instance. Furthermore, direct observation of the magnetic correlation between entities in laterally structured samples is an important capability of neutron scattering.

A number of complex structures can be engineered in which a nanostructured magnetic material is embedded in an otherwise nonmagnetic matrix. These types of

structures can be prepared by ordinary metallurgical techniques combined with techniques such as spark erosion [183, 184], or ball milling [185, 186]. These materials can particularly benefit from neutron scattering [187, 188] since the inhomogeneity of magnetism and collective behavior of clusters can be quantified with neutron scattering, and these materials can be prepared in large quantities.

3.2.1 Giant magnetoresistive heterostructures

The discovery of giant magnetoresistance inspired a new era of magnetism and magnetic electronics. The prototype giant magnetoresistance materials Co/Cu and Fe/Cr further demonstrate a plethora of materials opportunities. While there are many magnetic superlattices and heterostructures that have been studied through the years, giant magnetoresistance materials are featured here in order to best illustrate the veritable playground of new magnetic effects. A hallmark of a rich research problem is that it moves the research in new directions while touching on historical issues. In giant magnetoresistance a partial list of the new directions includes not only the remarkable magneto-transport behavior and oscillatory interlayer magnetic coupling, but also:

- The physics of spin-dependent quantum confinement and magnetic quantum-well states in spacer layers [189, 190]

- The wavevector dependence of the oscillatory magnetic-coupling periodicities [23, 73, 74].

- Model superlattice and multilayer structures engineered to highlight the underlying fundamental physics in many research problems. For example, artificial

antiferromagnets of Fe/Cr(211) have uniaxial in-plane easy axes suitable to explore the existence of the surface spin-flop transition [100, 191, 192, 193, 194].

- Giant magnetoresistance of superlattices have been used to examine the interplay between interfacial chemical and magnetic roughness [79, 80, 81, 195, 196]. This is part of the broader problem of characterizing buried solid-solid interfaces and their connection to the magnetotransport.

Through the years, neutron scattering has played an important role in understanding giant magnetoresistance. Initially, light scattering on Fe/Cr multilayers [197] was used to infer that the ferromagnetic Fe layer moments are aligned antiparallel across the intervening Cr layers in small magnetic fields. This was confirmed by the presence of a half-order magnetic reflection in neutron reflectivity and diffraction data for Fe/Cr [198, 199, 200, 201, 202], Co/Cu [203], and Ni/Ag [204] multilayers, which exhibit the giant magnetoresistance effect [205].

The low-field magnetic structure of giant magnetoresistance multilayers can deviate substantially from a simple parallel or antiparallel alignment of the ferromagnetic layers. The observation of non-collinear spin structures in Fe/Cr [202, 206, 207, 208] and $Ni_{80}Fe_{20}$/Ag [209, 210] multilayers was verified by neutron reflectivity techniques. In fact, the angle between the magnetic layers was determined from the relative intensities of the antiferromagnetic and ferromagnetic Bragg reflections. Interlayer coupling in Fe/Cr multilayers is correlated with the antiferromagnetic ordering of the Cr interlayers, which was characterized using wide-angle neutron diffraction techniques [34, 35, 211]. The Cr layers in Fe/Cr multilayers support an incommensurate spin density wave similar to bulk Cr. Neutron reflectivity and magneto-optic Kerr effect spectroscopy

measurements revealed that the Fe layers exhibit non-collinear interlayer coupling above the Néel temperature of the Cr layers in samples with Cr layer thickness >5 nm. The formation of the Cr spin density wave below the Néel temperature destroys this interlayer coupling [34, 35, 212]. Magnetic frustration from interfacial roughness may give rise to the anomalous coupling between the Fe layers [213, 214, 215].

Other research directions for transition-metal multilayers include studies of hydrogen loading in Fe/Nb [216, 217] and Fe/V [218]. Due to differences in the hydrogen solubilities of the component materials, hydrogen goes exclusively into the nonmagnetic interlayers, and the concentration can be reversibly tuned by changing hydrogen pressure. Neutron reflectivity and bulk magnetization measurements of a Fe(2.6 nm)/Nb(1.5 nm) multilayer showed that by increasing the hydrogen concentration to about 25 at. %, interlayer exchange coupling could be tuned to be either antiferromagnetic or ferromagnetic [216]. A change in the sign of the coupling was attributed to modifications of the Fermi surface in the V interlayers [219]. These neutron scattering studies further emphasize the importance of the Fermi surface in determining the nature of the interlayer exchange coupling in giant magnetoresistance multilayers.

3.2.2 Exchange Bias

In exchange-biased systems [220], the exchange interaction between the two magnetic components, typically a ferromagnet and an antiferromagnet, gives rise to a unidirectional anisotropy in the ferromagnet. Present-day magnetic recording technology utilizes read heads that rely upon magnetic pinning of a magnetic reference layer through exchange coupling with an antiferromagnetic layer (thus producing exchange bias). This technological application of exchange biasing has motivated extensive theoretical and

experimental research [221, 222, 223, 224] designed to explain the physical origin of the phenomenon on a nanometer length-scale.

To date, theoretical explanations have focused on the role and structure of the antiferromagnet [223]. In the earliest model [220], it was assumed that the antiferromagnet spin structure freezes during cooling through the ordering temperature of the antiferromagnet. Uncompensated antiferromagnet spins at the ferromagnet/antiferromagnet interface couple to the ferromagnet and set the direction of the unidirectional anisotropy. In general this model is simplistic as it assumes that the interfaces are perfectly flat and that the antiferromagnetic is comprised of a single magnetic domain. For most exchange-biased systems, this model predicts biasing fields that are substantially larger than those experimentally observed. This idealized model of exchange biasing, however, was realized in a double superlattice system comprised of an antiferromagnetic Fe/Cr superlattice grown epitaxially with a ferromagnetic Fe/Cr superlattice. Neutron reflectivity [192] shows that the antiferromagnetic and ferromagnetic superlattices are aligned collinearly as predicted. In contrast with this model, the direction of the unidirectional anisotropy switches at a field that is well below the field where the antiferromagnetic superlattice undergoes a spin-flop transition. The switching of the exchange bias direction suggests that the antiferromagnetic superlattice breaks into domains in large magnetic fields.

For exchange-biased systems with atomic-scale rather than artificially structured antiferromagnetic components, wide-angle neutron diffraction is one of the few techniques available that provides direct information about the magnetic structure, domain size and ordering temperature of the antiferromagnet. (Another technique, X-ray

photoemission electron microscopy [225, 226], provides spatial images of the antiferromagnetic structure, but is sensitive only to the surface region and cannot be performed in a magnetic field.) For example, wide-angle neutron diffraction studies of Fe_3O_4/NiO superlattices reveal that the exchange bias is correlated with a freezing of magnetic domain walls within the antiferromagnetic NiO layers [227] in agreement with a model proposed by Malozemoff [228]. In related investigations of Fe_3O_4/CoO superlattices [39], it was demonstrated that the moments of ferrimagnetic Fe_3O_4 and the antiferromagnetic CoO are not collinear, but are aligned at 90^o relative to each other due to magnetic frustration at the interfaces, as predicted by several theorists [229, 230]. The onset of the perpendicular alignment is coincident with the onset of the exchange biasing and may be responsible for the biasing in this system [231].

Observations of enhanced magnetization in exchange bias systems upon field cooling [232] and shifts of the magnetization loop about the zero of magnetization [233] suggest the development of a net magnetization in the antiferromagnetic layer or more precisely at the antiferromagnetic/ferromagnetic interface. Furthermore, it has been recently shown by polarized neutron reflectometry that the antiferromagnet in an exchange bias system can acquire a net magnetic moment, which is confined close to the ferromagnetic/antiferromagnetic interface [43]. Recent computer simulations attributing exchange bias to exchange anisotropy produced by alignment of uncompensated spins at the antiferromagnetic/ferromagnetic interface [232] or the antiferromagnetic interior [234] have yielded predictions for exchange bias that are in good agreement with experiment.

Neutron diffraction studies also demonstrated that the "blocking" temperature marking the onset of biasing, T_B, is not necessarily equal to the ordering temperature of the antiferromagnet, T_N, [31, 235] as was previously assumed. In this experiment, the magnetic order parameter of the CoO was measured for several Fe_3O_4/CoO superlattices with variable CoO thickness (Figure 15(a) and (b)). As the CoO thickness decreases, T_N increases above the ordering temperature of bulk CoO (290 K) and approaches the ordering temperature of Fe_3O_4 (858 K). In contrast, the biasing temperature T_B decreases with the CoO thickness and is unrelated to T_N (Figure 15(c)).

Polarized neutron reflectivity studies of exchange-biased Fe/MnF_2 bilayers [38] and Fe/FeF_2 [236] bilayers focus on the ferromagnetic layer and demonstrate that the magnetic reversal process of the ferromagnetic Fe layer can be asymmetric. Specifically, the appearance of spin-flip scattering on the left-hand side of the magnetic hysteresis loop indicates that the magnetization reversal proceeds via rotation of the magnetization. The absence of spin-flip scattering on the right hand side of the hysteresis loop indicates that the reversal proceeds instead via domain nucleation. Notably, the hysteresis loops of Fe/FeF_2 and Fe/MnF_2 bilayers are generally symmetric in appearance, thus magnetometry measurements are unable to discern differences in the reversal processes. In contrast, a distinction was observed with neutron scattering and magnetic-optic microscopy [237]. Additional neutron reflectivity studies [238] indicate that exchange-biased systems with an asymmetric reversal process exhibit large exchange bias, while those with a symmetric magnetization reversal process exhibit a smaller bias.

3.2.3 Exchange Spring Magnets

Exchange spring coupled magnets [239, 240], "spring" magnets, are heterostructures that consist of hard ferromagnetic (*i.e.,* permanent magnet) and soft ferromagnetic (*i.e.,* Fe or permalloy) layers. The two layers are expected to align parallel to each other at the interface and for this reason are predicted to be forgiving of interfacial spin frustration. These exchange-spring systems are of potential importance as ultrastrong permanent magnets. As such, they possess high values of the maximum energy product, $(BH)_{max}$, (*i.e.,* the inflection point in the second quadrant of the hysteresis loop)– the relevant engineering figure of merit. The key is to limit the spatial extent of the soft ferromagnet below magnetic domain wall thickness. The soft magnet is then expected to have its magnetization pinned to that of the hard magnet. This should endow the composite with a higher magnetization per unit volume than hard magnets ordinarily possess. On the other hand, hard magnets have high magnetic anisotropies because they include heavy elements, such as rare earths that have low-symmetry *f*-electron orbitals, and strong spin-orbit interactions producing high magnetocrystalline anisotropy. The magnetocrystalline anisotropy of the rare-earth portion of the nanocomposite is expected to provide the high anisotropy desired for a hard magnet. The spring magnet composite should possess a wide and tall hysteresis loop, so that the stored energy (the area contained in the loop) is high, yielding an ultrastrong magnetic composite material.

When the thickness of the soft component exceeds a domain wall thickness, a twist structure is created upon application of a reverse field (Figure 16). Once the magnetization of the composite is initially set, the soft layer is pinned at the interface, but

the twist fans out with increasing rotation away from the initial magnetization. Recent polarized neutron reflectivity studies [241] of ferromagnetic FePt/FeNi bilayers provide a depth-dependent profile of the magnetic structure of this exchange-spring magnet and elucidate the field evolution of the "twist" (*i.e.,* planar domain wall) that is induced in the soft layer (Figure 17) [242, 243]. These measurements demonstrate that the spiral extends across the interface into the hard magnetic layer, contrary to simple mean-field predictions. This measurement highlights the ability of neutrons to probe complex magnetic structures in buried layers.

3.2.4 Artificial Magnetic Materials— IV-VI and II-VI Semiconductors

Magnetic semiconductors investigated over several decades include three main classes of materials: rare-earth chalcogenides (*e.g.,* EuS and EuSe), IV-VI semiconductor alloys involving Mn (*e.g.,* PbMnTe and PbSnMnTe), and II-VI semiconductor alloys in which a part of the group-II sublattice has been replaced by substitutional transition metal elements [244]. The study of II-Mn-VI magnetic semiconductors provided important insights into the role of spin in semiconductors, which is believed to be key to harnessing the spin degree of freedom for use in electronics [245]. The emergence of epitaxial techniques of crystal growth has led to major new advances in the area of magnetic semiconductors. In the area of II-Mn-VI materials, molecular beam epitaxy provides the ability to form new phases, such as Mn-VI binary compounds in the zinc blende phase [246] (*e.g.,* MnTe, which in the bulk exists only in the NiAs form; and MnSe, whose bulk structure is NaCl). Thick MnTe films have been grown epitaxially along the (001) direction of their fcc lattice [247]. Their

antiferromagnetic structure is of the Type III [248] with its propagation axis (see Figure 18(a)) along any of the edges of the cubic structure.

Epitaxy has also opened the possibility of growing magnetic-semiconductor-based multilayer structures (*e.g.,* MnSe/ZnSe superlattices), introducing strain as a degree of freedom with which to "tune" the type of antiferromagnetic order. Thus, when the magnetic semiconductor remains under compressive strain in the layer plane as in the case of MnTe/ZnTe multilayers, the resulting tetragonal distortion produces type-III antiferromagnetic order with the propagation axis along the growth direction (Figure 18(b)). But tensile strain in the layer plane (as in the case of MnSe/ZnTe or MnTe/CdTe multilayers), produces a new incommensurate form of helimagnetic antiferromagnetic ordering [249, 250]. "Strain engineering" of semiconductor multilayers offers the opportunity to couple the magnetic environment of a device into the electronic environment of semiconductor chips.

Finally, superlattices offer a framework to study interlayer coupling between magnetic layers across nonmagnetic layers [251, 252, 253] as was done for metallic superlattices. Coupling has been observed to take place for nonmagnetic layer thicknesses not exceeding six to seven atomic planes. The correlation lengths observed via neutron scattering in these superlattices are surprisingly long for systems governed by indirect superexchange. Correlation lengths as long as 30 nm were reported for MnTe/ZnTe multilayers [254]; and these lengths are even longer (in excess of 60 nm) when deep electronic levels are introduced into the superlattices by doping [255]. Similarly, neutron scattering was used to determine the magnetic structure and interlayer coupling parameters IV-Eu-VI-based multilayers (*e.g.,* PbSe/EuSe superlattices).

3.2.5 Artificial Magnetic Materials— III-V Semiconductors

II-VI semiconductors are dominated by antiferromagnetic interactions, consequently, their novel magnetic properties (such as the giant Zeeman splitting) are significant only at low temperature. Recently, great interest arose by the emergence of ferromagnetic semiconductors, obtained by alloying III-V materials with Mn. The most widely investigated system of this type is (Ga, Mn)As [78], although ferromagnetic InMnAs [256] and GaMnSb [257] and InMnSb alloys have been formed. The ferromagnetic character of (Ga, Mn)As (Figure 19) is characterized by a hysteresis loop, and by the temperature dependence of the remanent magnetization (inset Figure 19). These ferromagnetic semiconductors could only be produced in thin film form, by non-equilibrium epitaxial methods such as molecular beam epitaxy. Furthermore, epitaxy can only be achieved in a narrow temperature window, at temperatures that are considerably lower than those used to grow the corresponding "parent" III-V compounds. [(Ga, Mn)As is grown at ~280 ^{0}C, while the optimal temperature for GaAs bulk growth is ~600 ^{0}C.] The goal is to prevent precipitation of MnAs in its natural NiAs form. Typical Mn concentrations in epitaxially grown (Ga, Mn)As do not exceed 9%, beyond which precipitation of MnAs cannot be avoided [258].

The origin of the ferromagnetic order in these III-Mn-V alloys arises from the fact that divalent Mn^{+2} replaces trivalent Ga in the cation sublattice. Mn thus plays a dual role: it brings into the system a magnetic moment of 5 μ_B, while it simultaneously acts as an acceptor, *i.e.,* a source of holes in the valence band. The system is thus automatically doped heavily p-type. It is the presence of holes that provides the mechanism for ferromagnetic interactions between Mn ions [259], over-riding their well-known natural

tendency to align antiferromagnetically via the superexchange interaction. While this is universally accepted, it is not yet fully understood whether the holes act as free carriers in the valence band (thus forming the basis for an RKKY interaction between Mn ions), form an impurity band, or conduct via hopping. In any case, it is established that the Curie temperature scales both with the Mn concentration and with the hole concentration.

Two additional comments on the ferromagnetic properties of the III-Mn-V semiconductors merit attention. First, the easy axis is determined by the magnetic anisotropy, which in these layered materials arises from tetragonal strain distortion of the originally zinc-blende lattice. For example, when a (Ga, Mn)As film is grown on a GaAs buffer (which has a smaller lattice parameter than (Ga, Mn)As), the ferromagnetic film is under compressive strain in the layer plane. In this case the easy axis of (Ga, Mn)As is in the plane of the film. If, on the other hand, (Ga, Mn)As is grown on a buffer which subjects it to tensile strain in the plane (*e.g.,* a GaInAs buffer with some 15% In content), the easy axis of magnetization is normal to the film. These two cases are illustrated in Figure 20.

Secondly, it has recently been discovered that post-growth annealing can be used to change the Curie temperature of the as-grown (Ga, Mn)As. In particular, in specimens with relatively high Mn content (typically above 7%) the Curie temperature can be increased by annealing at approximately the same temperature as the molecular beam epitaxy growth (*e.g.,* 280 ^{0}C) [260]. Experiments involving channeled Rutherford back scattering and particle-induced X-ray emission have shown that the population of interstitial Mn atoms, which is present in as-grown (Ga, Mn)As alongside the substitutional Mn ions, drops markedly in the annealing process. Mn interstitials are

detrimental to the magnetic properties of (Ga, Mn)As because they act as donors, thus reducing the concentration of holes which are needed for mediating the ferromagnetic ordering between magnetic moments localized on the substitutional Mn ions.

Neutron reflectivity promises to be an important tool in the characterization of these materials. Preliminary neutron reflectivity studies show long-range ferromagnetic order in (Ga, Mn)As layers across nonmagnetic GaAs spacer layers [132]. The multilayer samples exhibit distinct magnetic Bragg reflections despite the fact that the Mn content in the sample is of trace amount. Long-range ferromagnetic order in multilayer samples may arise from exchange coupling across nonmagnetic spacer layers (thus indicating spin splitting of electronic bands states in the nonmagnetic layer), but may also be attributed to defects in the multilayer structure, such as pinholes across the nonmagnetic layers or steps or roughness of interfaces which can produce dipolar coupling of ferromagnetic layers.

The exciting development of III-V-based ferromagnetic semiconductors brings with it a series of physical issues, the understanding of which is not only scientifically important, but which must ultimately be resolved to optimize these materials for device applications. In a development parallel to that of metals, novel magnetic configurations are being created in semiconductors that are not structurally homogeneous. More novel, and intrinsic of semiconductors, is the possibility of inducing magnetism by external means (such as electrical or optical hole injection).

3.2.6 Magnetic topology of inhomogeneous semiconductors

In the fabrication of semiconductor layer structures one sometimes resorts to the growth of so-called “digital alloys”, where one uses “atomic layer epitaxy” to deposit

alternating anions and cations layer-by-layer, in a desired sequence. Using this approach one can deposit, for example, a single layer of MnAs followed by n monolayers of GaAs, repeated over and over to form an "atomic" superlattice [261, 262]. As an example Figure 21 shows a transmission electron micrograph of a GaSb/MnSb/GaSb digital alloy, formed by "insertion" of Mn layers (of approximately 50% surface coverage) into GaSb [263]. In the case illustrated, the Mn-containing layers are separated by 6 monolayers of GaSb (*i.e.,* ~1.8 nm). This approach holds the promise of increasing the average Mn content of epitaxially-grown III-Mn-V systems beyond the 7 or 8% that presently appears to be the limit for random alloys.

The idea of digital alloys (which involve magnetically-ordered atomic planes) is rather powerful for extending our understanding of two-dimensional magnetism generally. Consider, for example, a digital system comprised of repeated sequences of Ga-As-Ga-As-Mn-As, which is simultaneously doped heavily p-type by an independent dopant (*e.g.,* Be). It is a fundamental question whether one can dope the system to such a level that a multiple of Friedel wavelengths will be in resonance with the separation between the "digital" planes. If that situation were achieved, one could use it to control the spin orientation in successive ferromagnetic-ordered Mn planes *relative to each other* (*i.e.,* the coupling between the planes could be made ferromagnetic or antiferromagnetic). While consequences of such ferromagnetic or antiferromagnetic interplanar correlations can probably affect many physical phenomena, the relative orientations of the individual magnetic layers in such correlated systems could be observed neutron scattering.

III-Mn-V materials grown at high temperature form Mn-based precipitates, such as MnAs or MnSb. These precipitates are of considerable interest in their own right: they

remain ferromagnetic above room temperature, and their dimensions are typically about 30 nm in diameter [264]. An example of such a nanocrystallite precipitated in a (Ga, Mn)As matrix, imaged by TEM, is shown in Figure 22. Neutron scattering from such ferromagnetic inclusions provides an ideal probe for studying the magnetic structures of such nanomagnets. Metal-organic vapor phase deposition has produced inclusions in the form of elongated MnAs nanomagnets, with the long axis along the [111] direction. These nanomagnets gravitate to the surface of the specimen [265], and if growth takes place on the (111) planes, only MnAs ellipsoids oriented along the growth direction form and migrate to the surface. Such systems are attractive for possible nanomagnet-based devices, since both their size and location can be controlled through growth conditions.

3.2.8 Induced magnetism in semiconductors

The ferromagnetic order in the III-Mn-V alloys depends on the presence of holes. This provides a means to switch the ferromagnetic order on and off. It has been demonstrated that the magnetization in InMnAs/AlGaSb heterostructures can be controlled by light [266, 267]. Similarly, in a related system involving InMnAs and AlGaSb, a field-effect transistor structure has been constructed that allows injection of holes into the InMnAs layer [268]. It was observed that the ferromagnetic order in InMnAs can be switched on or off, depending on the hole concentration injected by the applied voltage to the field-effect transistor structure. Apart from the physical interest implicit in these phenomena, such options present a means to ascertain if the neutron scattering signal arises from the magnetism of a given layer, by simply switching its ferromagnetic properties on and off.

3.3 Important issues in nanomagnetism (technology)

Data storage technology has been advancing rapidly for several decades. Magnetic recording in particular has accelerated its rate of advancement several times in the past decade. With annual compound growth rates of areal density (number of "bits" per unit area on the recording medium's surface) rising above 100% [269], research and development to maintain or increase evolution or recording technology is being undertaken, spurring renewed interest in perpendicular recording, and more recently drawing attention to novel approaches of patterned media, hybrid recording and self-organized magnetic arrays.

Periodic arrays of holes or "antidots" in continuous magnetic films have recently received attention because of their potential advantages for high-density data storage [270]. The periodic modulation of the in-plane magnetic shape anisotropy due to the holes produces an ordered domain structure (Figure 23**),** which can be used to store data. Potential advantages include no superparamagnetic lower limit to the bit size and preservation of the properties of the continuous magnetic film. This domain structure can be calculated numerically using the results of micromagnetics calculations, and has also been studied using imaging techniques based on magnetic force microscopy [271], magneto-optic Kerr effect spectroscopy [272], and spin-polarized photoemission electron microscopy [273]. There are, however, advantages to using neutron scattering techniques such as small-angle scattering or grazing incidence diffraction. Unlike magnetic force microscopy, scattering techniques directly measure the spatial distribution of the magnetization rather than the magnetic field arising from the latter, and are insensitive to applied magnetic fields. Also, unlike optical imaging methods (*e.g.,* magneto-optic Kerr

effect spectroscopy), scattering methods can probe magnetization in buried layers, and its depth dependence. Recent grazing incidence polarized neutron diffraction experiments of an array of antidots of 2 micron spacing in a permalloy film [115] were in good quantitative agreement with the results of micromagnetics calculations.

3.3.1 Recording Media Noise and Scaling Limitations

The achievable areal density in magnetic recording is primarily determined by the read-back signal-to-noise ratio. To a large extent, signal-to-noise ratio is determined by the sensitivity of the read-back transducer that generates an electrical signal from the stray fields emanating from recorded transitions. The key-limiting factor today, however, is media noise, generated by magnetic dispersions and magnetic correlations in the medium due to its granular make-up and random placement and orientation of the magnetic grains.

Reducing media noise generally implies reducing grain size, which inevitably leads to thermal instability. When the size dependent reversal energy falls below a certain multiple of the thermal energy, the grains become thermally unstable. Figure 24 illustrates recent developments in grain size and grain size distributions. At achieved densities of 45 Gbit/in^2 the mean grain diameter is about 9 nm. At this diameter the estimated ratio of anisotropy energy to thermal energy, K_uV/k_BT, is only about 70-80, which is close to the estimated requirement of K_uV/k_BT >60 for stability over a ten year period [269, 274].

Today's recording materials are based on hexagonal Co-alloys with an approximate maximum anisotropy constant of $K_u \sim 4.5 \cdot 10^6$ erg/cm^3 for pure Co. The smallest

thermally stable grain diameter is estimated using the equation $d_p = (60\ k_B T/K_u)^{1/3}$, which assumes a ten year storage time at T ~ 300 K. For hexagonal Co one obtains d_p = 8 nm. Representative CoPtCrB recording alloys have d_p = 9.1 nm. Grain sizes of these magnitudes are already achieved today. The path forward towards higher density magnetic recording media involve narrowing grain size distributions, followed by reducing grain sizes and using high K_u materials (provided the anisotropy of the magnetic bit is small enough that the write-field can switch its magnetization).

Table 2 Compilation of relevant materials and magnetic properties from Refs. [269, 275, 276 277, 278]. All materials are capable of sustaining d_p <10 nm grain sizes over storage times of ten years.
Definitions of parameters:
anisotropy field: $H_K = 2K_1/M_S$
domain wall width: $d_w = \pi(A/K_1)$, where exchange coupling constant $A=10^{-6}$ erg/cm
domain wall energy: $\gamma \cong 4\ (A \cdot K_1)$
particle domain size: $d_c = 1.4\gamma_W / M_S^2$
minimal stable grain size: $d_p = (60\ k_B T/K_1)^{1/3}$

alloy system	material	K_1 (10^7erg/ cm^3)	M_S (emu/ cm^3)	H_K (kOe)	T_C(K)	d_w (Å)	γ (erg/cm^3)	d_c (μm)	d_p (nm)
Co-alloys	CoPtCr	0.20	298	13.7	--	222	5.7	.89	10.4
	Co	0.45	1400	6.4	1404	148	8.5	.06	8.0
	Co_3Pt	2.0	1100	36	--	70	18	.21	4.8
$L1_0$ phases	FePd	1.8	1100	33	760	75	17	.20	5.0
	FePt	6.6-10	1140	116	750	39	32	.34	3.3-2.8
	CoPt	4.9	800	123	840	45	28	.61	3.6
	MnAl	1.7	560	69	650	77	16	.71	5.1
rare-earth	$Fe_{14}Nd_2B$	4.6	1270	73	585	46	27	.23	3.7
transition metals	$SmCo_5$	11-20	910	240-400	1000	22-30	42-57	.71-.96	2.7-2.2

A common assumption is that the crystalline grain size of the media is the same as the magnetic cluster size (regions of the media that are magnetically coupled together, which may be larger than individual grains). Since the length-scales of the clusters are typically smaller than those accessible by standard microscopy techniques such as

magnetic force microscopy, the assumption is being examined with magnetic small-angle neutron scattering [36]. In order to isolate the magnetic cluster with small-angle neutron scattering, it is necessary to separate the scattering caused by physical and magnetic inhomogeneities. This is achieved with two separate small-angle neutron scattering measurements. Data were first taken with no applied magnetic field, where the small-angle neutron scattering contains contributions from small-angle scattering of the physical thin film structure (*e.g.,* grains) and of the magnetic film structure (magnetic clusters). Following the measurement, data were obtained in a strong magnetic field that orients the magnetic moments, hence, minimizes the magnetic scattering in the Q-range of interest. Figure 25(a) shows typical data obtained at both fields. Subtracting these two spectra leaves the desired magnetic small-angle neutron scattering from which magnetic correlation lengths can be determined (see Figure 25(b)). These experiments began with a study of 500 nm thick Co-Cr media [279], but now include investigations of Co-Pt-Cr-X media with technologically-relevant film thickness [280]. These studies show that while the cluster size is larger than the grain size, the difference is small for media presently in use. Similar measurements have been reported on a variety of nanostructured and nanoscale magnetic systems [36, 281, 282, 283].

3.3.2 Antiferromagnetically coupled media

Increases in magnetic recording areal density have traditionally been accomplished by decreasing the media grain size and remanent areal moment density. However, this approach is limited, since if the magnetic grains are too small, the media will become superparamagnetic. A novel solution to this dilemma was recently implemented through the use of media comprised of antiferromagnetically coupled recording layers [284, 285],

which are being used to extend longitudinal recording schemes to higher recording densities (Figure 26(a)). In this strategy the bit is reduced in lateral size, but is anchored to another magnetic layer across a spacer in order to stabilize it thermally.

A typical hysteresis loop for an antiferromagnetically coupled media is shown in Figure 26(b). In these trilayer structured media, the antiferromagnetic coupling is overcome with large applied fields, which force the magnetization of each ferromagnetic layer parallel to the field. As the field is reduced, the magnetization of the thinner, bottom layer reverses first to become antiparallel to that of the top layer. As the field is further reversed, the magnetization of the thick layer switches and the magnetizations of both layers are again parallel to the field. While this explanation of the magnetic reversal behavior is qualitatively correct, the details are not completely understood. In particular, it is desirable to obtain a clearer picture of the lower-layer reversal mechanisms, *e.g.,* whether reversal occurs via coherent rotation of the magnetization vector or through domain nucleation and wall motion, at remanence, and near coercivity. In addition, a better understanding of the importance of thermal activation in the magnetization process is important. Polarized neutron reflectometry has been used to identify magnetization reversal processes in buried films previously [38, 286, 287] and is now being applied to antiferromagnetically coupled media. Preliminary measurements indicate that the reversal of the layer moments occurs via domain nucleation rather than coherent rotation. In addition, the top layer does not appear to be fully magnetized in remanence [288].

3.3.3 Magnetic recording heads, present and future directions

Presently, fabrication of head structures utilizes lithography to produce features with sizes on the order of 400 nm. While this feature size is larger than that used in the

semiconductor industry, the dimensions will become ~100 nm within a few years [289]. Similarly, typical film thicknesses, ~20 nm to 1 μm, are comparable to those used in the semiconductor industry. Hence, the physical dimensions of head structures are now approaching nanoscopic dimensions, and the manufacture of recording heads will involve nanoscale preparation techniques, such as e-beam lithography. Large scale, reproducible fabrication of the nanoscale features will be difficult, but should be achievable owing to the small number of devices on a head wafer.

In order to write high-K_u media (desired for thermal stability of small bits), the write head must produce larger fields than possible. Since the maximum field is limited by the saturation field of the write head material, there is need for new thin films with high saturation magnetization. These materials must also be corrosion resistant and have low magnetostriction. Successful development of such materials would reduce the effect of superparamagnetism (since higher high K_u media could be written) [290, 291, 292, 293]. Possible candidates include FeCoNi alloys and FeN_x compounds (such as the controversial giant moment α''-$Fe_{16}N_2$ phase). These materials could be understood better if their magnetic spin structures were known, which could be achieved with neutron scattering.

All present-day read heads are spin-valve field sensors. These sensors consist of several layers of magnetic alloy films. The antiferromagnetic layer pins the direction of the reference ferromagnetic layer through exchange biasing, while the unpinned ferromagnetic layer is free to rotate with the magnetic field of the disk. There are several challenges associated with spin valve heads that neutron scattering can address. One of

the most important of these is the need for thinner antiferromagnets for exchange biasing in the head. For future devices, the gap spacing betweens the shields in the read sensor must decrease in order to improve the bit resolution of the sensor, and hence the total spin valve thickness must decrease. Since the antiferromagnetic layer is, by far, the thickest film in the spin valve stack, reducing this thickness (while maintaining exchange bias) is essential. Current thin film antiferromagnets do not provide exchange bias when the film thickness falls below ~10 nm [294, 295]. A better fundamental understanding of exchange biasing could provide guidance needed to fabricate novel thin antiferromagnetic films. To date, neutron scattering has been used extensively to investigate exchange-biased systems. These measurements provide insight into the magnetization reversal processes of the ferromagnet [38, 296] and the spin structure of the antiferromagnet [31, 39, 227]. Neutron diffraction has also been used to identify and characterize new antiferromagnetic materials, such as MnN [30, 297] and MnPd [40] that may exhibit better performance in spin-valve structures. Since the spin structure at the interface between the ferromagnet and antiferromagnet is important in exchange bias, it is important to extend these neutron measurements to technologically relevant materials of appropriate film thickness.

4.0 Conclusions

Neutron scattering has been seminal to the modern understanding of bulk magnetism and the characterization of ferromagnets, ferrimagnets and antiferromagnets. The outlook for the future is that neutron scattering will continue to be an important probe of magnetism on the nanoscale. In the area of molecular magnets, neutron

scattering might be expected to be the primary probe of the magnetic structure. More generally, the novelty of magnetic properties of artificially structured materials is a consequence of the competition between the physical dimensions imposed upon the structures and the length scales relevant to magnetism. The common feature shared by artificially structured materials is that the magnetism is inherently inhomogeneous; therefore, bulk probes, such as magnetometry, are ill-suited to provide information about the spatial variation of magnetization in non-homogeneous materials (and antiferromagnets). One important strength of neutron scattering is its ability to measure the individual components of the vector magnetization. Thus, neutron scattering naturally provides information directly relevant to studies of inhomogeneous materials.

For example, polarized neutron reflectometry is a technique that can measure the depth dependent magnetization in thin films. Since polarized neutron reflectometry is inherently interface specific, the magnetization of the interfacial region can be measured with a great degree of accuracy even in the presence of a strongly magnetic substrate. Even though a magnetometer can be ~100 times more sensitive to magnetic induction than neutron scattering, the ability of the latter to discriminate the magnetization of an interface against the film bulk or substrate offers obvious advantages.

Much interest in ferromagnetic semiconductors is motivated by the prospect of spin-injection devices that *automatically imply the existence of buried interfaces* in the structures of interest. Characterization and understanding of interface quality is therefore a key issue for such devices to succeed. Here, polarized neutron reflectometry is expected to play an important role.

The ability to study nanostructures under a variety of environmental conditions (*e.g.,* extremes of field, temperature and pressure) is important in understanding complex materials. As a result of the low neutron absorption for most materials, neutron scattering is compatible with a wide range of sample environments. For example, sample environments that provide extreme conditions of temperature (10 mK to 2000 K), pressure (ultrahigh vacuum to 1.4 GPa below room temperature, or 10 GPa above room temperature), and magnetic field (11+ T continuous, or 30+ T pulsed) are available at neutron scattering facilities.

Presently, sufficient computational capability and theoretical skill exist to calculate and predict magnetic phenomena for the same nanoscale structures that are being assembled in the laboratory. Thus, an opportunity exists to test theories of fundamental magnetic phenomena, and to develop a detailed understanding and predictive capability of nanomagnetism. Theoreticians are not limited to calculations of magnetic properties for bulk materials, but can predict the magnetic properties of composites that go beyond averaging properties of constituent components. Thus, theoretical models and our understanding of nanomagnetism can be tested provided we are able to experimentally measure magnetic structures at the nanoscale. Neutron scattering is ideally suited to this task. For example, the structural and magnetic roughness of interfaces, all of which can be characterized by neutron scattering, is an important ingredient in theoretical studies of physical properties such as magnetotransport, magneto-optics and magnetism. An important challenge before us is to integrate research activities of experimentalists and theoreticians to achieve new insights in magnetism that are now possible with artificially structured materials.

Arguably a central issue in magnetism is the understanding of the magnetization cycle. Hysteresis loops of hard magnetic materials are interpreted in terms of the uniform rotation of the magnetization or else as due to a breakdown into domains. Here, each stage of the magnetization is considered quasi-static. On the other hand, for many magnetic materials, the interesting issue is the response of the system to a time-dependent (*i.e.,* high frequency) magnetic field, its kinetics or possibly its dynamics. Modern magnets and magnetic materials are not uniform bodies, but often composites at the mesoscopic scale, precisely the same scale which often is that of magnetic domains. The sizes and shapes of the (buried) inhomogeneities can be determined by neutron scattering, while the magnetic relaxation processes can be monitored by neutron inelastic scattering. With such a detailed knowledge of static and dynamic magnetic properties, optimal sizes, shapes and arrangements of nanometer-sized constituents in a magnetic composite material can be identified to engineer materials with desirable and unique magnetic properties. It is fortunate that these materials developments are taking place at the same time that the technology of neutron scattering undergoes a rapid development; first, because more efficient ways are being devised to control neutron spin; and second, because a new generation of neutron sources promise fluxes exceeding anything hitherto available. The future looks exciting indeed.

Acknowledgments

This workshop was funded by Institutional Program Development funds obtained from the Los Alamos National Laboratory. The Los Alamos National Laboratory is operated by the University of California for the U.S. Department of Energy under

contract No. W-6405-Eng-36, and Argonne National Laboratory under contract W-31-109-Eng-38. The authors thank E.E. Fullerton, K.V. O'Donovan, J.A. Dura, C.F. Majkrzak and H. Zabel for contributions of figures, P. Montano for discussions, and K. O'Brien for assistance with graphics.

Figure Captions

Figure 1 Length-scales relevant to different magnetic phenomena are shown in purple. In recent years, a number of nanofabrication techniques (shown in blue) have been developed that are capable of making structures whose physical dimensions compete with fundamental magnetic length-scales. Important, also, is the ability to probe magnetism with nanometer sensitivity. Tools suitable for probing magnetic structures across the thin dimension of a film (Z-structures) are shown in orange, those that are applicable to studies of lateral inhomogeneities are shown in green. Theoretical tools (red) are also available that can predict magnetic properties of nanometer-scale structures. Adapted from Ref. [3].

Figure 2 Examples of structures with reduced dimensionality.

Figure 3 (a) TEM image of α-Fe particles embedded in yttria-stabilized zirconia (YSZ); diffraction spots in the inset show that the α-Fe lattice is coherent with the YSZ matrix; (b) Three possible and approximately equally populated orientations of α-Fe in the YSZ matrix; (c) Measured magnetization curves with orientations of the field normal (closed symbols) and parallel (open symbols) to the substrate surface; (d) Calculated hysteresis loops for film of oriented Fe cubes with field applied normal (solid line) and parallel (dotted lines) to film plane.

Figure 4 A spin density map of Mn12-acetate obtained using polarized neutron diffraction. Spin down density is shown as dashed lines, spin up as solid. Mn^{4+} ions are

located on "Mn1" sites (μ=–2.34 μ_B), and Mn^{3+} ions are on sites "Mn2" (μ=+3.7 μ_B) and "Mn3" (μ=+3.8 μ_B). Adapted from Ref. [66].

Figure 5 (a) The magnetic moment of nanocrystalline Cr is observed to decrease with decreasing grain size. (b) The Néel point of nanocrystalline Cr with grain size of 73 nm is suppressed below T_N=311 K observed for bulk (coarse grained) Cr. Adapted from Ref. [82].

Figure 6 (a) Temperature dependence of the antiferromagnetic Bragg reflection from thin layers of Cr in an Fe/Cr superlattice, with Fe layer thickness of 1.4 nm. From left to right in the figure, the Cr layer thicknesses, t_{Cr}, for the samples were 5.1, 6.3 11.5 and 19 nm. Inset: The measured Néel temperatures for the Cr layers in the superlattice samples. (b) Variation of magnetic moment in the Fe and Cr layers for multilayer samples with different Cr layer thickness as deduced from neutron scattering. Adapted from Ref. [34].

Figure 7 Schematic diagram showing parameters of correlation functions that separately described chemical/structural roughness and magnetic roughness, *i.e.,* deviations of spin directions. The root-mean-square displacement of a moment or atom above the average position of the interface plane is given by σ_m and σ_c, respectively. The displacements are correlated across the plane with dimension given by ξ_m and ξ_c, respectively.

Figure 8 Measured ratio of spin-up neutron intensity to spin-down intensity (•) plotted as a function of modulation period in the Ni/Mo superlattice. The experimental measurements are consistently larger than those calculated for a wide variety of model structures in which the magnetic roughness was constrained to be the same as the

chemical roughness (as determined from X-ray scattering), indicating that the magnetic Ni/Mo interface is smoother than the chemical Ni/Mo interface. Adapted from Ref. [91].

Figure 9 Intensity map of scattering of polarized neutrons [polarization state antiparallel (-) or parallel (+) to the applied field] shown as a function of momentum transfer parallel to the sample surface (Q_x) and normal to the sample surface (Q_z). The Bragg reflection from the chemical periodicity of the superlattice ($Q_z \sim 1.2$ nm^{-1}) is observed for both polarization states in (near) remanence (upper panels, B=10 G). The half-order reflection ($Q_z \sim 0.6$ nm^{-1}), indicative of long-range antiferromagnetic order of the Fe layer magnetization, is also observed. In saturation (B=215 G, lower panels), spin-dependent scattering is observed for the superlattice reflection (indicative of ferromagnetic order). Separate values for magnetic and chemical roughness can be determined from the off-specular scattering (the streak of intensity parallel to the Q_x-axis). (Figure courtesy of H. Zabel.)

Figure 10 Spin wave dispersion curves measured for a superlattice of Dy and Y. Adapted from Ref. [154].

Figure 11 (a) Thermally activated spin waves appear as satellite peaks about the main elastic peak. The integrated intensity of a satellite peak is about 20 times weaker than the central peak. These data were obtained using a conventional triple axis spectrometer, transmission geometry, and in the small-angle regime ($Q \sim 0.1$ nm^{-1}). Adapted from Ref. [155]. (b) Reflectivity measurement of a thin oxide layer on Si demonstrating a range in useful neutron signal collected over eight orders of magnitude (courtesy of J.A. Dura and C.F. Majkrzak).

Figure 12 (left) Illustration of a neutron scattering experiment employing ferromagnetic resonance. The sample (orange block) is housed inside an Al microwave cavity. Microwaves are introduced into the cavity producing an oscillating magnetic field that is perpendicular to the static magnetic field. The polarized neutron beam (blue arrows) is scattered by the sample. (right) During resonance (achieved by selecting an appropriate strength for the static field), the magnetization of the sample rotates about the static field. The depth dependence of the component of the sample magnetization parallel to the static field is obtained from splitting of the spin-up and spin-down (non-spin-flip) neutron cross-sections. The root mean square value of the component of the magnetization perpendicular to the static field is deduced from the spin-flip scattering of the neutron beam polarization, *i.e.,* the intensity of scattering that changes polarization after reflection from the sample.

Figure 13 Schematic diagram of an inorganic process for fabricating large areas of nanodots. An alumina mask with holes is placed on a substrate. Material is deposited through the holes, then the mask is removed, leaving ~ 60 nm diameter dots on the substrate.

Figure 14 Schematic diagram (left) showing a three-step process used in the fabrication of networked islands of iron metal (atomic force microscope image at upper right). The network exhibits unusual magnetic hysteresis, including exchange bias, and multiple magnetization reversal processes. Figure adapted from Ref. [180].

Figure 15 The intensity of the (111) Bragg reflection as a function of temperature for a (a) (10 nm Fe_3O_4/10 nm $CoO)_{x50}$ and (b) (10 nm Fe_3O_4/3 nm $CoO)_{x50}$ multilayer. The

ordering temperatures, T_N, for the CoO films deduced from data in (a) and (b) are shown in (c) as a function of film thickness. Also shown are the temperatures at which non-zero exchange bias is observed, *i.e.,* the blocking temperatures, T_B, as determined from magnetometry.

Figure 16 The magnetization depth profile of the soft (hard) ferromagnet is shown by the blue (red) arrows. (Left) The magnetizations of soft and hard ferromagnets are aligned. As the applied field is reversed and its strength increased (right), the magnetization of the soft ferromagnet begins to reverse (rotate, thus creating a "fan" magnetic structure). For the situation shown on the right, the magnetic field is not strong enough to overcome the pinning of the soft ferromagnetic layer to the hard layer (nor is the field strong enough to reverse the magnetization of the hard layer). (Figure courtesy of K. O'Donovan.)

Figure 17 (upper panel) Neutron reflectivity data taken from an exchange spring magnet. (lower panel) Schematic diagram showing the evolution of the magnetization in the soft layer at the coercive field, as deduced from neutron scattering data. Adapted from Ref. [241].

Figure 18 (a) Schematic diagram illustrating the Type III antiferromagnetic structure. (b) Schematic diagram showing how the antiferromagnetic planes of the Type III structure are arranged in a superlattice.

Figure 19 Hysteresis loops for (Ga, Mn)As (5.5 atomic % Mn) observed at several temperatures. The inset shows remanent magnetization as a function of temperature, indicating a Curie temperature of 65 K for this specimen. The sample growth and measurements were carried out by Y. Sasaki and X. Liu at Notre Dame University.

Figure 20 Hysteresis loops for samples under compressive and tensile strain in the layer plane (upper and lower panels, respectively) at 5 K. The open and full symbols are taken with the applied magnetic field normal and parallel to the layer, respectively. Note that the easy axis is in the layer plane for compressively-strained layers, and is normal to the plane for tensile strain [298].

Figure 21 A TEM micrograph of a $(MnSb)_{x1}(GaSb)_{x6}$ digital superlattice ("digital alloy") grown by atomic layer epitaxy. The Mn-containing "digital" layers are much thinner than the image indicates, because TEM is significantly more sensitive to the strain produced by the inserted atomic species than to its atomic number. Adapted from Ref. [263].

Figure 22 High-resolution TEM image of a single-crystalline MnAs particle formed in the GaAs matrix. Adapted from Ref. [264].

Figure 23 A micromagnetic simulation of the spin configuration of magnetic induction in a bit constrained at the corners by four antidotes (holes). Adapted from Ref. [115].

Figure 24 Trends in grain size distributions [mean (standard deviation)] for different recording densities.

Figure 25 Small-angle neutron scattering data from magnetic recording disk. (a) Intensity at zero applied magnetic field and 6 kOe field. (b) Magnetic small-angle neutron scattering, which is the difference of the curves in (a). A fit to these data is shown by the line using a log-normal distribution of magnetic cluster sizes [280].

Figure 26 (a) Schematic representation of antiferromagnetically coupled media showing the two magnetic layers coupled parallel at a bit transition. (b) Magnetic hysteresis loop

of an antiferromagnetically coupled media. Blue circles are the major loop and the red squares are the remanent loop. The arrows indicate the magnetization of the layers at different places on the hysteresis loop. (Figure courtesy of E.E. Fullerton, IBM).

---

[1] L.M. Falicov, D.T. Pierce, S.D. Bader, R. Gronsky, K.B. Hathaway, H.J. Hopster, D.N. Lambeth, S.S.P. Parkin, G. Prinz, M. Salamon, I.K. Schuller, and R.H. Victora, J. Mater. Res., **5**, 1299 (1990).
[2] J.B. Kortright, D.D. Awschalom, J. Stohr, S.D. Bader, Y.U. Idzerda, S.S.P. Parkin, I.K. Schuller, H.C. Siegmann, J. Magn. Magn. Mater., **207**, 7, (1999).
[3] I.K. Schuller, S. Kim and C. Leighton, J. Magn. Magn. Mater., 200, 571 (1999).
[4] A. Aharoni, Introduction to the theory of ferromagnetism, Oxford 1996, p. 133.
[5] J. Nogués, C. Leighton, I.K. Schuller, Phys. Rev. B, **61**, 1315 (2000).
[6] R. M. Bozorth, "Ferromagnetism", Van Nostrand, New York 1955.
[7] R. C. O'Handley, "Modern Magnetic Materials: Principles and Applications", Wiley, New York 2000
[8] J. C. Slater, Phys. Rev. **36**, 57 (1930).
[9] H. Bethe, Handbuch der Physik **24**, pt. 2, 595 (1933).
[10] C.F. Majkrzak, J.W. Cable, J. Kwo, M. Hong, D.B. McWhan, Y. Yafet, J.V. Waszczak and C. Vettier, Phys. Rev. Lett. **56**, 2700 (1986).
[11] M.B. Salamon, Shantanu Sinha, J.J. Rhyne, J.E. Cunningham, R.W. Erwin, J. Borchers and C.P. Flynn, Phys. Rev. Lett. **56**, 259 (1986).
[12] R.W. Erwin, J.J. Rhyne, M.B. Salamon, J. Borchers, Shantanu Sinha, R. Du, J.E. Cunningham and C.P. Flynn, Phys. Rev. B **35**, 6808 (1987).
[13] Y. Yafet, J. Kwo, M. Hong, C.F. Majkrzak and T. O'Brien, J. Appl. Phys. **63**, 3453 (1988).
[14] R.S. Beach, J.A. Borchers, A. Matheny, R.W. Erwin, M.B. Salamon, B. Everitt, K. Pettit, J.J. Rhyne and C.P. Flynn, Phys. Rev. Lett. **70**, 3502 (1993).
[15] J.J. Rhyne, R.W. Erwin, J. Borchers, M.B. Salamon, R. Du and C.P. Flynn, Physica B **159**, 111 (1989).
[16] B.A. Everitt, M.B. Salamon, B.J. Park, C.P. Flynn, T. Thurston and D. Gibbs, Phys Rev. Lett., **75**, 3182 (1995).
[17] J. Bohr, D. Gibbs, J.D. Axe, D.E. Moncton, K.L. D'Amico, C.F. Majkrzak, J. Kwo, M. Hong, C.L. Chien and J. Jensen, Physica B **159**, 93 (1989).
[18] D.A. Jehan, D.F. McMorrow, R.A. Cowley, R.C.C. Ward, M.R. Wells, N. Hagmann and K.N. Clausen, Phys. Rev. B **48**, 5594 (1993).
[19] B.A. Everitt, M.B. Salamon, J.A. Borchers, R.W. Erwin, J.J. Rhyne, B.J. Park, K.V. O'Donovan, D.F. McMorrow and C.P. Flynn, Phys. Rev. B **56**, 5452 (1997).
[20] J.P. Goff, C. Bryn-Jacobsen, R.A. Cowley, D.F. McMorrow, R.C.C. Ward and M.R. Wells, J. Magn. Magn. Mater. **156**, 263 (1996).
[21] D.F. McMorrow, Neutron News 7, 16 (1996).
[22] For a first claim of RKKY coupling see W.-S. Zhou, H.K. Wong, J.R. Owers-Bradley, and W.P. Halperin, Physica B **108**, 953 (1981).
[23] S. S. P. Parkin, N. More and K. P. Roche, Phys. Rev. Lett. **64**, 2304 (1990).

[24] E.E. Fullerton, J.E. Mattson, S.R. Lee, C.H. Sowers, Y.Y. Huang, G. Felcher, S.D. Bader, F.T. Parker, J. Appl. Phys. **73**, 6335 (1993).
[25] P. Walser, M. Hunziker, and M. Landolt, J. Magn. Magn. Mater. **200**, 95 (1999).
[26] R.W.E. van de Kruijs, M.Th. Rekveldt, H. Fredrikze, J.T. Kohlhepp, J.K. Ha, and W.J.M. de Jonge, Phys. Rev. B **65**, 4440 (2002).
[27] For a first look at a quantitative approach towards this problem see I.K. Schuller, Phys. Rev. Lett. **44**, 1597 (1980).
[28] D.L. Smith, and R. N. Silver, Phys. Rev. B **64**, 5323 (2001).
[29] K.H. Oh, B.N. Harmon, S.H. Liu and S.K. Sinha, Phys. Rev. B **14**, 1283 (1976).
[30] H. Yang, H. Al-Brithen, A. R. Smith, J.A. Borchers, R. L. Cappelletti, and M. D. Vaudin, Appl. Phys. Lett. **78**, 3860 (2001).
[31] P.J. van der Zaag, Y. Ijiri, J.A. Borchers, L.F. Feiner, R.M. Wolf, J.M. Gaines, R.W. Erwin and M.A. Verheijen, Phys. Rev. Lett. **84**, 6102 (2000).
[32] J.A. Borchers, Y. Ijiri, S-H. Lee, C.F. Majkrzak, G.P. Felcher, K. Takano, R.H. Kodama and A.E. Berkowitz, J. Appl. Phys. **83**, 7219 (1998).
[33] E.E. Fullerton, K.T. Riggs, C.H. Sowers, S.D. Bader, and A. Berger, Phys. Rev. Lett. **75**, 330 (1995).
[34] E.E. Fullerton, S. D. Bader, and J. L. Robertson, Phys. Rev. Lett. **77**, 1382 (1996).
[35] E. E. Fullerton, S. Adenwalla, G.P. Felcher, K.T. Riggs, C.H. Sowers, S.D. Bader and J.L. Robertson, Physica B **221**, 370 (1996).
[36] J.F. Löffler, H.-B. Braun, and W. Wagner, Phys. Rev. Lett. **85**, 1990 (2000).
[37] Y. Y. Huang, C. Liu, and G. P. Felcher, Phys. Rev. B **47**, 183 (1993).
[38] M.R. Fitzsimmons, P. Yashar, C. Leighton, I.K. Schuller, J. Nogués, C.F. Majkrzak, and J. A. Dura, Phys. Rev. Lett. **84**, 3986 (2000).
[39] Y. Ijiri, J.A. Borchers, R.W. Erwin, P.J. van der Zaag and R.M. Wolf, Phys. Rev. Lett. **80**, 608 (1998).
[40] R.F.C. Farrow, R. F. Marks, M. F. Toney, S. David, A. J. Kellock, J. A. Borchers, K. V. O'Donovan, and D.J. Smith, Appl. Phys. Lett. **80**, 808 (2002).
[41] W.-T. Lee, S. G. E. te Velthuis, G. P. Felcher, F. Klose, T. Gredig, and E. D. Dahlberg, Phys. Rev. B. **65**, 4417 (2002).
[42] J.A. Borchers, R.W. Erwin, S.D. Berry, D.M. Lind, J.F. Ankner, E. Lochner, K.A. Shaw and D. Hilton, Phys. Rev. B **51**, 8276 (1995).
[43] A. Hoffmann, J.W. Seo, M.R. Fitzsimmons, H. Siegwart, J. Fompeyrine, J.-P. Locquet, J.A. Dura and C.F. Majkrzak, Phys. Rev. B **66**, 220406(R) (2002).
[44] B.D. Cullity, **Introduction to Magnetic Materials**, (Addison-Wesley Publishing Co., 1972), pp. 395-398.
[45] N.D. Mermin, and H. Wagner, Phys. Rev. Lett. **17**, 1133 (1966).
[46] L.D. Landau, and E.M. Lifshitz "Statistical Physics", 3rd edition pt. I, Butterworth and Heinemann (1980)., p. 537.
[47] L.J. Néel, J. Phys. Radium **15**, 225 (1954).
[48] J.G. Gay, and R. Richter, Phys. Rev. Lett. **56**, 2728 (1986).
[49] L. Szunyogh, B. Ujfalussy, and P. Weinberger, Phys. Rev. B **51**, 9552 (1995).
[50] D. Pescia, and V.L. Pokrovsky, Phys. Rev. Lett. **65**, 2599 (1990).
[51] D. Weller, J. Stohr, R. Nakajima, A. Carl, M.G. Samant, C. Chappert, R. Megy, P. Beauvillain, P. Veillet, and G. A. Held, Phys. Rev. Lett., **75**, 3725 (1995).

[52] E.Y. Vedmedenko, H.P. Oepen, A. Ghazali, J.C.S. Levy, and J. Kirschner, Phys. Rev. Lett. **84**, 5884 (2000).
[53] R. Sellmann, H. Fritzsche, H. Maletta, V. Leiner and R. Siebrecht, Phys. Rev. B **64**, 4418 (2001).
[54] R. Jungblut, M.T. Johnson, J.A. Destegge, A. Reinders, and F.J.A. Denbroeder, J. Appl. Phys. **75**, 6424 (1994).
[55] For an early report see, for instance J.Q. Zheng, C.M. Falco, J.B. Ketterson and I.K. Schuller, Appl. Phys. Lett. **38**, 424 (1981).
[56] C. Liu and S.D. Bader, Phys. Rev. B **44**, 2205 (1991).
[57] J.A. Borchers, R.W. Erwin, S.D. Berry, D.M. Lind, E. Lochner and K.A. Shaw, Appl. Phys. Lett. **64**, 381 (1994).
[58] M. Takano, T. Terashima, Y. Bando and H. Ikeda, Appl. Phys. Lett. **51**, 205 (1987).
[59] Y. Bando, M. Takano, T. Terashima and Z. Hiroi, in *Multilayers*, ed. by M. Doyama, S. Somiya, R.P.H. Chang, R. Yamamoto, and T. Ohno, Proc. of the MRS Inter. Meeting on Adv. Mater., Vol. 10, (Materials Research Society, Pittsburgh, 1989). p. 83.
[60] J.A. Borchers, M.J. Carey, R.W. Erwin, C.F. Majkrzak and A.E. Berkowitz, Phys. Rev. Lett. **70**, 1878 (1993).
[61] E. C. Stoner and E. P. Wohlfarth, Trans. Roy. Soc. **A240**, 74 (1949).
[62] S. Honda, F.A. Modine, A. Meldrum, J.D. Budai, T.E. Hayne, and L.A. Boatner, Appl. Phys. Lett. **77**, 711 (2000).
[63] K.D. Sorge, J.R. Thompson, T.C. Schulthess, F.A. Modine, T.E. Haynes, S. Honda, A. Meldrum, J.D. Budai, C.W. White, and L.A. Boatner, IEEE Trans. Magn. **37**, 2197 (2001).
[64] T.C. Schulthess, M. Benakli, P.B. Vischer, K.D. Sorge, J.R. Thompson, F.A. Modine, T.E. Haynes, L.A. Boatner, G.M. Stocks, and W.H. Butler, J. Appl. Phys. **89**, 7594 (2001).
[65] C. Li, A.J. Freeman, H.J.F. Jansen and C.L. Fu, Phys. Rev. B **42**, 5433 (1990).
[66] R.A. Robinson, P.J. Brown, D.N. Argyriou, D.N. Hendrickson, and S.M.J. Aubin, J. Phys.-Cond. Matter **12**, 2805 (2000).
[67] D.P. Young, D. Hall, M.E. Torelli, Z. Fisk, J.l. Sarrao, J.D. Thompson, M.-R. Ott, S.B. Oseroff, R.G. Goodrich, and R. Zysler, Nature **377**, 4121 (1999).
[68] J.A.C. Bland, C. Daboo, B. Heinrich, Z. Celinski, and R.D. Bateson, Phys. Rev. B **51**, 258 (1995).
[69] S. Hope, J. Lee, P. Rosdenbusch, G. Lauhoff, J.A.C. Bland, A. Ercole, D. Bucknall, J. Penfold, H.J. Lauter, V. Lauter, and R. Cubitt, Phys. Rev. B **55**, 11422 (1997).
[70] M.R. Fitzsimmons, A. Röll, E. Burkel, K.E. Sickafus, M.A. Nastasi, G.S. Smith, and R. Pynn, J. Appl. Phys., **76**, 6295 (1994).
[71] Sang-Koog Kim and J.B. Kortright, Phys. Rev. Lett., **86**, 1347 (2001).
[72] A. Cebollada, J.L. Martinez, J.M. Gallego, J.J. de Miguel, R. Miranda, S. Ferrer, E. Batallan, G. Filliou, and J.P. Reboullat, Phys. Rev. B **39**, 9726 (1989).
[73] J. Kwo, M. Hong, F.J. DiSalvo, J.V. Waszczak and C.F. Majkrzak, Phys. Rev. B **35**, 7295 (1987).
[74] S.S.P. Parkin, R. Bhadra and K.P. Roach, Phys. Rev. Lett. **66**, 2152 (1991).
[75] J. Unguris, R. J. Celotta, and D. T. Pierce, Phys. Rev. Lett. **67**, 140 (1991).

[76] D. Altbir, M. Kiwi, R. Ramirez and I.K. Schuller, J. Magn. Magn. Mater. **149**, L246 (1995).
[77] S. Demokritov, E. Tsymbal, P. Grunberg, W. Zinn and I.K. Schuller, Phys. Rev. B **49**, 720 (1994).
[78] H. Ohno, Science **281**, 951 (1998).
[79] A.P. Ramirez, Czech. J. Phys. **46**, 3247 (1996).
[80] A.P. Ramirez, A. Hayashi, R.J. Cava, R. Siddharthan, and B.S. Shastry, Nature **399**, 333 (1999).
[81] M.R. Fitzsimmons, J.A. Eastman, R.A. Robinson, A.C. Lawson, J.D. Thompson, and R. Movshovich, J. Satti, Phys. Rev. B **48**, 8245 (1993).
[82] M.R. Fitzsimmons, J.A. Eastman, R.A. Robinson, and J.W. Lynn, J. Appl. Phys. **78**, 1364 (1995).
[83] M.R. Fitzsimmons, J.A. Eastman, R.A. Robinson and J.W. Lynn, NanoStructured Materials **7**, 179 (1996).
[84] P. Bödeker, A. Hucht, A. Schreyer, J. Borchers, F. Güthoff, and H. Zabel, Phys. Rev. Lett. **81**, 914 (1998).
[85] A. Schreyer, C.F. Majkrzak, Th. Zeidler, T. Schmitte, P. Bödeker, K. Theis-Bröhl, A. Abromeit, J. Dura and T. Watanabe, Phys. Rev. Lett. **79**, 4914 (1997).
[86] H. Matsuyama, C. Haginoya, and K. Koike, Phys. Rev. Lett. **85**, 646 (2000).
[87] H. Ohldag, A. Scholl, F. Nolting, S. Anders, F. U. Hillebrecht, and J. Stöhr, Phys. Rev. Lett. **86**, 2878 (2001).
[88] W. Zhu, L. Seve, R. Sears, B. Sinkovic, and S. S. P. Parkin, Phys. Rev. Lett. **86**, 5389 (2001).
[89] E. E. Fullerton, D.M. Kelly, J. Guimpel, I.K. Schuller, and Y. Bruynseraede, Phys. Rev. Lett. **68**, 859 (1992).
[90] N.M. Rensing, A.P. Payne, B.M. Clemens, J. Magn. Magn. Mater. **121**, 436 (1993).
[91] J.W. Cable, M.R. Khan, G.P. Felcher and I.K. Schuller, Phys. Rev. B **34**, 1643 (1986).
[92] M.J. Pechan, J.F. Ankner, C.F. Majkrzak, D.M. Kelly and I.K. Schuller, J. Appl. Phys. **75**, 6178 (1994).
[93] J.F. MacKay, C. Teichert, D.E. Savage and M.G. Lagally, Phys. Rev. Lett. **77**, 3925 (1996).
[94] C.S. Nelson, G. Srajer, J.C. Lang, C.T. Venkataraman, S.K. Sinha, H. Hashizama, N. Ioshimatsu and N. Norito, Phys. Rev. B **60**, 12234 (1999).
[95] S.K. Sinha, E.B. Sirota, S. Garoff, and H.B. Stanley, Phys. Rev. B **38**, 2297 (1988).
[96] R. Pynn, Phys. Rev. B **45**, 602 (1992).
[97] B.P. Toperverg, Physica B **297**, 160 (2001).
[98] B. Toperverg, O. Nikonov, V. Lauter-Pasyuk, and H.J. Lauter, Physica B **297**, 169 (2001).
[99] A. Rühm, B. P. Toperverg, and H. Dosch, Phys. Rev. B **60**, 16073 (1999).
[100] V. Lauter-Pasyuk, H.J. Lauter, B.P. Toperverg, L. Romashev and V. Ustinov, Phys. Rev. Lett. **89**, 167203 (2002).
[101] R.M. Osgood, S.K. Sinha, J.W. Freeland, Y.U. Idzerda and S.D. Bader, J. Appl. Phys. **85**, 4619 (1999).
[102] J. W. Freeland, K. Bussmann, and Y. U. Idzerda, Appl. Phys. Lett. **76**, 2603 (2000).

[103] R. Schad et al., Phys. Rev. B **57**, 13692 (1998).
[104] Z.-P. Shi, P. M. Levy and J. L. Fry, Phys. Rev. B **49**, 15159 (1994).
[105] S. Langridge, Jörg Schmalian, C.H. Marrows, D.T. Dekadjevi and B.J. Hickey, Phys. Rev. Lett. **85**, 4964 (2000).
[106] M. Takeda, Y. Endoh, H. Yasuda, K. Yamada, A. Kamijo and J. Mizuki, J. Phys. Soc. Jap. **62**, 3015 (1993).
[107] M. Takeda, H. Yasuda, T. Watanabe, K. Yamada, Y. Endoh, A. Kamijo and J. Mizuki, J. Magn. Magn. Mater. **126**, 355 (1993).
[108] M. Takeda, Y. Endoh, A. Kamijo and J. Mizuki, Physica B **213**, 248 (1995).
[109] W. Hahn, M. Loewenhaupt, G.P. Felcher, Y.Y. Huang and S.S.P. Parkin, J. Appl. Phys. **75**, 3564 (1994).
[110] S.K. Sinha, in *Neutron Scattering in Materials Science II*, edited by Dan A. Neumann, Thomas P. Russell and B.J. Wuensch, Materials Research Society Symposia Proceedings (Materials Research Society, Pittsburgh, 1995)., Vol. 376, p. 175.
[111] Y.Y. Huang, G.P. Felcher and S.S.P. Parkin, J. Magn. Magn. Mater. **99**, L31 (1991).
[112] J.A. Borchers, P.M. Gehring, R.W. Erwin, J.F. Ankner, C.F. Majkrzak, T.L. Hylton, K.R. Coffey, M.A. Parker and J.K. Howard, Phys. Rev. B **54**, 9870 (1996).
[113] J.A. Borchers, J.A. Dura, J. Unguris, D. Tulchinsky, M.H. Kelley, C.F. Majkrzak, S.Y. Hsu, R. Loloee, W.P. Pratt, Jr. and J. Bass, Phys. Rev. Lett. **82**, 2796 (1999).
[114] S. Langridge, J. Schmalian, C.H. Marrows, D.T. Dekadjevi, and B.J. Hickey, Phys. Rev. Lett. **85**, 4964 (2000).
[115] D. R. Lee, G. Srajer, M. R. Fitzsimmons, V. Metlushko, S. K. Sinha**,** Appl. Phys. Lett., **82**, 82 (2003).
[116] M. Kiwi, Proceedings of the 2002 MRS Symposium on Magnetoelectronics, (To be published).
[117] J. Crangle and W.R. Scott, J. Appl. Phys., **36**, 921 (1965).
[118] J. W. Cable, E. O. Wollan, and W. C. Koehler, Phys. Rev. **138**, A 755 (1965).
[119] M Weinert, and R.E. Watson, Phys. Rev. B **51**, 17168 (1995).
[120] O. Rader, E. Vescovo, J. Redinger, S. Blügel, C. Carbone, W. Eberhardt, and W. Gudat, Phys. Rev. Lett. **72**, 2247 (1994).
[121] E.E. Fullerton, D. Stoeffler, K. Ounadjela, B. Heinrich, Z. Celinski, and J.A.C. Bland, Phys. Rev. B **51**, 6364 (1995).
[122] J. Vogel, A. Fontaine, V. Cros, F. Petroff, J.P. Kappler, G. Krill, and A. Rogalev, and J. Goulon, Phys. Rev. B **55**, 3663 (1997).
[123] V. Cros, F. Petroff, J. Vogel, A. Fontaine, J.L. Menendez, J.L., A. Cebollada, W. Grange, J.P. Kappler, M. Finazzi, and N. Brookes, Europhysics Letters **49**, 807 (2000).
[124] J.J. Åkerman, I. Guedes, C. Leighton, M. Grimsditch and I. K. Schuller Phys. Rev. B **65**, 104432 (2002).
[125] T. Manago, T. Ono, H. Miyajima, K. Kawaguchi and M. Sohma, J. Phys. Soc. Jap., **68**, 334 (1999).
[126] A. Hoffmann, M.R. Fitzsimmons, J.A. Dura and C.F. Majkrzak, Phys. Rev. B **65**, 4428 (2002).

[127] J. S. Moodera, J. Nowak, L. R. Kinder, P. M. Tedrow, R. J. M. van de Veerdonk, B. A. Smits, M. van Kampen, H. J. M. Swagten, and W. J. M. de Jonge, Phys. Rev. Lett. **83**, 3029 (1999).
[128] J.S. Moodera, J. Nassar, and G. Mathon, Annual Review of Materials Science **29**, 381 (1999).
[129] J.F. Ankner, C.F. Majkrzak, and H. Homma, J. Appl. Phys. **73**, 6436 (1993).
[130] Sang-Koog Kim, Jong-Ryul Jeong, J. B. Kortright, and Sung-Chul Shin, Rev. B **64**, 052406 (2001).
[131] R.K. Kawakami, E. Johnston-Halperin , L.F. Chen, M. Hanson, N. Guebels, J.S. Speck, A.C. Gossard, and D.D. Awschalom, Appl. Phys. Lett. **77**, 3665 (2000).
[132] H. Kepa, J. Kutner-Pielaszek, A. Twardowski, C. F. Majkrzak, J. Sadowski, T. Story, and T. M. Giebultowicz, Phys. Rev. B **64**, 1302 (2001).
[133] I.I. Mazin, Phys. Rev. Lett. **83**, 1427 (1999).
[134] R. Meservey, and P.M. Tedrow, Phys. Reports **238**, 173 (1994).
[135] M.J.M. de Jong and C.W.J. Beenakker, Phys. Rev. Lett. **74**, 1657 (1995).
[136] S.K. Upadhyay, A. Palanisami, R.N. Louie and R.A. Buhrman, Phys. Rev. Lett. **81**, 3247 (1998).
[137] R.J. Soulen, J.M. Byers, M.S. Osofsky, B. Nadgorny, T. Ambrose, S.F. Cheng, P.R. Broussard, C.T. Tanaka, J. Nowak, J.S. Moodera, A. Barry and J.M.D. Coey, Science **282**, 85 (1998).
[138] D.J. Monsma and S.S.P. Parkin, Appl. Phys. Lett. 77, 883 (2000).
[139]A.T. Hanbicki, B.T. Jonker, G. Itskos, G. Kioseoglou and A. Petrou, Appl. Phys. Lett. **80**, 1240 (2002).
[140] F.J. Jedema, H.B. Heersche, A.T. Filip, J.J.A. Baselmans and B.J. van Wees, Nature **416**, 713 (2002).
[141] G.J. Strijkers, Y. Ji, F.Y. Yang, C.L. Chien and J.M. Byers, Phys. Rev. B **63**, 104510 (2001).
[142] G.E. Bacon, Neutron Diffraction, Clarendon Press, Oxford (1975).
[143] With small-angle neutron scattering and reflectometry, the scattering of neutrons is measured in the forward direction near the origin of reciprocal space. Consequently, the form factor decay is less severe than for wide-angle neutron diffraction.
[144] A. Gilabert, A. Hoffmann, M.G. Medici, and I.K. Schuller, Jour. Supercond. **13**, 1 (2000).
[145] K. Shimizu, H. Ishikawa, D. Takao, T. Yagi, and K. Amaya, Nature **419**, 597 (2002).
[146] R. Cauro, A. Gilabert, J.P. Contour, R. Lyonnet, M.-G. Medici, J.C. Grenet, C. Leighton, and I.K. Schuller, Phys. Rev. B **63**, 174423 (2001).
[147] P. M. Mooney, J. Appl. Phys. **67**, R1 (1990).
[148] R.R. Mett, W. Froncisz, and J.S. Hyde, Rev. Sci. Instr. **72**, 4188 (2001).
[149] A. Yu. Toporov, R.M. Langfor and A.K. Petford-Long, Appl. Phys. Lett. **77**, 3063 (2000).
[150] U. Welp, V.K. Vlasko-Vlasov, G.W. Crabtree, C. Thompson, V. Metlushko, and B. Llic, Appl. Phys. Lett. **79**, 1315 (2001).
[151] C.T. Yu, H. Jiang, L. Shen, P.J. Flanders and G.J. Mankey, J. Appl. Phys. **87**, 6322 (2000).

[152] L. R. Walker, Phys. Rev. **105**, 390 (1957).
[153] R. W. Damon and J. R. Eshbach, J. Phys. Chem. Solids **19**, 308 (1961).
[154] A. Schreyer, T. Schmitte, R. Siebrecht, P. Bodeker, H. Zabel, S.H. Lee, R.W. Erwin, C.F. Majkrzak, J. Kwo, and M. Hong, J. Appl. Phys. **87**, 5443 (2000).
[155] N.R. Bernhoeft, G.G. Lonzarich, P.W. Mitchell, and D.M. Paul, Phys. Rev. B **28**, 422 (1983).
[156] M. Grimsditch, M. Khan, A. Kueny and I. K. Schuller , Phys. Rev. Lett. **51**, 498 (1983)
[157] A. Kueny, M. Khan, I. K. Schuller and M. Grimsditch, Phys. Rev. B **29**, 2879 (1984).
[158] A. T. Fiory, A. F. Hebard, and S. Somekh, Appl. Phys. Lett. **32**, 73 (1978).
[159] M. Baert, V. V. Metlushko, R. Jonckheere, V. V. Moshchalkov, and Y. Bruynseraede, Phys. Rev. Lett. **74**, 3269 (1995).
[160] O. Geoffroy, D. Givord, Y. Otani, B. Pannetier, and F. Ossart, J. Magn. Magn. Mater. **121**, 223 (1993).
[161] J. I. Martín, M. Vélez, J. Nogués, and I. K. Schuller, Phys. Rev. Lett. **79**, 1929 (1997).
[162] K. Harada, O. Kaminimura, H. Kasai, T. Matsuda, A. Tonomura, and V. V. Moshchalkov, Science **274**, 1167 (1996).
[163] J. I. Martín, M. Vélez, A. Hoffmann, I. K. Schuller, and J. L. Vicent, Phys. Rev. Lett. **83**, 1022 (1999).
[164] O. M. Stoll, M. I. Montero, J. Guimpel, J. J. Åkerman, and I. K. Schuller, Phys. Rev. B **65**, 104518 (2002).
[165] D. K. Christen, F. Tasset, S. Spooner, and H. A. Mook, Phys. Rev. B **15**, 4506 (1977).
[166] E. M. Forgan, D. McK. Paul, H. A. Mook, P. A. Timmins, H. Keller, S. Sulton, and J. S. Abell, Nature **343**, 735 (1990).
[167] P. L. Gammel, U. Yaron, A. P. Ramirez, D. J. Bishop, A. M. Chang, R. Ruel, L. N. Pfeiffer, E. Bucher, G. D'Anna, D. A. Huse, K. Mortensen, M. R. Eskildsen, and P. H. Kes, Phys. Rev. Lett. **80**, 833 (1998).
[168] J.W. Lynn, N. Rosov, T.E. Grigereit, H. Zhang, T.W. Clinton, Phys. Rev. Lett. **72**, 3413 (1994).
[169] B. Keimer, W.Y. Shih, R.W. Erwin, J.W. Lynn, F. Dogan, I.A. Aksa, Phys. Rev. Lett. **73**, 3459 (1994).
[170] R. Ghilardi, J. Mesot, A. Drew, U. Divakar, S.L. Lee, E.M. Forgan, O. Zaharko, K. Conder, V.K. Aswal, C.D. Dewhurst, R. Cubitt, N. Momono and M. Oda, Phys. Rev. Lett. **88**, 217003 (2002).
[171] V. Lauter-Pasyuk, H.J. Lauter, M. Lorenz, V.L. Aksenov and P. Leiderer, Physica B **267**, 149 (1999).
[172] S.W. Han, J. F. Ankner, H. Kaiser, P. F. Micelli, E. Paraoanu, and L. H. Greene, Phys. Rev. B **59**, 14692 (1999).
[173] S.W. Han, J. Farmer, P.F. Miceli, I.R. Roshchin and L.H. Greene, Phys. Rev. B **62**, 9784 (2000).
[174] S.M. Yusuf, E.E. Fullerton, R.M. Osgood and G.P. Felcher, J. Appl. Phys. **83**, 6801 (1998).

[175] J. Guimpel, L. Civale, F. de la Cruz, J. M. Murduck, and I. K. Schuller, Phys. Rev. B **38**, 2342 (1988).
[176] S. H. Brongserma, E. Verweij, N. J. Koeman, D. G. de Groot, R. Griessen, and B. I. Ivlev, Phys. Rev. Lett. **71**, 2319 (1993).
[177] K. Temst, M.J. Van Bael and H. Fritzsche, Appl. Phys. Lett. **79**, 991 (2001).
[178] C.T. Black, K.W. Guarini, K.R.Milkove, S.M. Baker, T.P. Russell, and M.T. Tuominen, Appl. Phys. Lett. **79**, 409 (2001).
[179] G. Koller, F.P. Netzer, and M.G. Ramsey, Surf. Science **421**, 353 (1999).
[180] K. Liu, S.M. Baker, M. Tuominen, T.P. Russell, and I.K. Schuller, Phys. Rev. B **63**, 403 (2001).
[181] S. Langridge, J. Schmalian, C.H. Marrows, D.T. Dekadjevi, and B.J. Hickey, J. Appl. Phys. **87**, 5750 (2000).
[182] A. Michels, J. Weissmuller, A. Wiedenmann , and J.G. Barker, J. Appl. Phys. **87**, 5953 (2000).
[183] S.B. Slade, A.E. Berkowitz, and F.T. Parker, J. Appl. Phys. **69**, 5127 (1991).
[184] F.T. Parker, F.E. Spada, A.E. Berkowitz, K.S. Vecchio, E.J. Lavernia, and R. Rodriguez, Mater. Lett. **48**, 184 (2001).
[185] P.R. Ruuskanen, R.B. Schwarz, and J.D. Thompson, Philos. Mag. B **69**, 47 (1994).
[186] R.D. Shull, J.P. Cline, I. Baker, and F. Liu, J. Appl. Phys. **79**, 6028 (1996).
[187] A.C. Nunes, C.F. Majkrzak, and A.E. Berkowitz, J. Magn. Magn. Mater. **39**, 59 (1983).
[188] D. Lin, A.C. Nunes, C.F. Majkrzak, and A.E. Berkowitz, J. Magn. Magn. Mater. **145**, 343 (1995).
[189] W. Weber, D.A. Wesner, G. Güntherodt and U. Linke, Phys. Rev. Lett. **66**, 942 (1991).
[190] N.B. Brookes, Y. Chang and P.D. Johnson, Phys. Rev. Lett. **67**, 354 (1991).
[191] J.S. Jiang, G.P. Felcher, A. Inomata, R. Goyette, C. Nelson, and S.D. Bader, Phys. Rev. B **61**, 9653 (2000).
[192] S.G.E. te Velthuis, J.S. Jiang, S.D. Bader, and G.P. Felcher, Phys. Rev. Lett. **89**, 7203 (2002).
[193] S.G.E. te Velthuis, J.S. Jiang, and G.P. Felcher, Appl. Phys. Lett. **77**, 2222 (2000).
[194] J.S. Jiang, G.P. Felcher, A. Drienata, R. Goyette, C. Nelson, and S.D. Bader, Phys. Rev. B **61**, 9653 (2000).
[195] M.C. Cyrille, S. Kim, M.E. Gomez, J. Santamaria, C. Leighton, K.M. Krishnan, and I.K. Schuller, Phys. Rev. B **62**, 15079 (2000).
[196] J. Santamaria, M.E. Gomez, M.-C. Cyrille, C. Leighton, Kannan K. Krishnan, and I.K. Schuller, Phys. Rev. B **65**, 2412 (2002).
[197] P. Grünberg, R. Schreiber, Y. Pang, M.B. Brodsky and H. Sowers, Phys. Rev. Lett. **57**, 2442 (1986).
[198] A. Barthélémy, A. Fert, M.N. Baibich, S. Hadjoudj, F. Petroff, P. Etienne, R. Cabanel, S. Lequien, F. Nguyen Van Dau and G. Creuzet, J. Appl. Phys. **67**, 5908 (1990).
[199] N. Hosoito, S. Araki, K. Mibu and T. Shinjo, J. Phys. Soc. Jap. **59**, 1925 (1990).
[200] T. Shinjo, S. Araki and N. Hosoito, J. Magn. Magn. Mater. **90**, 753 (1990).
[201] S.S.P. Parkin, A. Mansour and G.P. Felcher, Appl. Phys. Lett. **58**, 1473 (1991).

[202]A. Schreyer, J.F. Ankner, Th. Zeidler, H. Zabel, M. Schäfer, J.A. Wolf, P. Grünberg and C.F. Majkrzak, Phys. Rev. B **52**, 16066 (1995).
[203] A. Cebollada, J.L. Martínez, J.M. Gallego, J.J. de Miguel, R. Miranda, S. Ferrer, F. Batallan, G. Fillion and J.P. Rebouillat, Phys. Rev. B **39**, 9726 (1989).
[204] B. Rodmacq, Ph. Mangin and Chr. Vettier, Europhys. Lett. **15**, 503 (1991).
[205]M.N. Baibich, J.M. Broto, A. Fert, F.N. Vandau, F. Petroff, P. Etienne, G. Creuzet, A. Friederich and J. Chazelas, Phys. Rev. Lett. **61**, 2472 (1988).
[206] A. Schreyer, J.F. Ankner, Th. Zeidler, H. Zabel, C.F. Majkrzak, M. Schäfer and P. Grünberg, Europhys. Lett. **32**, 595 (1995).
[207] J.A.C. Bland, H.T. Leung, S.J. Blundell, V.S. Speriosu, S. Metin, B.A. Gurney and J. Penfold, J. Appl. Phys. **79**, 6295 (1996).
[208] S. Adenwalla, C.P. Felcher, E.E. Fullerton and S.D. Bader, Phys. Rev. B **53**, 2474 (1996).
[209] B. Rodmacq, K. Dumesnil, Ph. Mangin and M. Hennion, Phys. Rev. B **48**, 3556 (1993).
[210] K. Dumesnil, M. Hennion, B. Rodmacq and Ph. Mangin, Physica B **213-214**, 245 (1995).
[211] A. Schreyer, C.F. Majkrzak, Th. Zeidler, T. Schmitte, P. Bödeker, K. Theis-Bröhl, A. Abromeit, J.A. Dura and T. Watanabe, Phys. Rev. Lett. **79**, 4914 (1997).
[212] J.F. Ankner, H. Kaiser, K. Hamacher, A. Schreyer, Th. Zeidler, H. Zabel, C.F. Majkrzak, M. Schäfer and P. Grünberg, J. Appl. Phys. **79**, 4782 (1996).
[213] S. Demokritov. E. Tsymbal, P. Grünberg, W. Zinn and I.K. Schuller, Phys Rev. B **49**, 720 (1994).
[214] J.C. Slonczewski, Phys. Rev. Lett. **67**, 3172 (1991).
[215] J.C. Slonczewski, J.Appl. Phys. **73**, 5957 (1993).
[216] Ch. Rehm, F. Klose, D. Nagengast, B. Pietzak, H. Maletta and A. Weidinger, Physica B **221**, 377 (1996).
[217] F. Klose, Ch. Rehm, D. Nagengast, H. Maletta and A. Weidinger, Phys. Rev. Lett. **78**, 1150 (1997).
[218] B. Hjörvarsson, J.A. Dura, P. Isberg, T. Watanabe, T.J. Udovic, G. Andersson and C.F. Majkrzak, Phys. Rev. Lett. **79**, 901 (1997).
[219] J.A. Dura, P. Isberg, T. Watanabe, T.J. Udovic, G. Andersson, and C.F. Majkrzak, Phys. Rev. Lett. **79**, 901 (1997).
[220] W.H. Meiklejohn and C.P. Bean, Phys. Rev. **105**, 904 (1957).
[221] J. Nogués, and I.K. Schuller, J. Magn. Magn. Mater. **192**, 203 (1999).
[222] A.E. Berkowitz, and K.Takano, J. Magn. Magn. Mater. **200**, 552 (1999).
[223] R.L. Stamps, J. Phys D-Applied Physics **33**, R247 (2000).
[224] M. Kiwi, J. Magn. Magn. Mater. **234**, 584 (2001).
[225] F. Nolting, A. Scholl, J. Stohr, J.W. Seo, J. Fompeyrine, H. Siegwart, J.P. Locquet, S. Anders, J. Luning, E.E. Fullerton, M.F. Toney, M.R. Scheinfein, and H.A. Padmore, Nature **405**, 767 (2000).
[226] H. Ohldag, A. Scholl, F. Nolting, S. Anders, F.U. Hillebrecht, and J. Stöhr, Phys. Rev. Lett. **86**, 2878 (2001).
[227] J.A. Borchers, Y. Ijiri, D.M. Lind, P.G. Ivanov, R.W. Erwin, A. Qasba, S.H. Lee, K.V. O'Donovan and D.C. Dender, Appl. Phys. Lett. **77**, 4187 (2000).

[228] A.P. Malozemoff, J. Appl. Phys. **63**, 3874 (1988). .
[229] L.L. Hinchey and D.L. Mills, Phys. Rev. B **34**, 1689 (1986).
[230] N.C. Koon, Phys. Rev. Lett. **78**, 4865 (1997).
[231] Y. Ijiri and T.C. Schulthess, private communication.
[232] K. Takano, R.H. Kodama, A.E. Berkowitz, W. Cao, G. Thomas, Phys. Rev. Lett. **79**, 1130 (1997).
[233] J. Nogués, C. Leighton, I.K. Schuller, Phys. Rev. B **61**, 1315 (2000).
[234] U. Nowak, A. Misra, K.D. Usadel, J. Magn. Magn. Mater. **240**, 243 (2002).
[235] K. Takano, A.E. Berkowitz, W. Cao, G. Thomas, J. Appl. Phys. **79**, 4932 (1996).
[236] M.R. Fitzsimmons, C. Leighton, J. Nogués, A. Hoffmann, K. Liu, C.F. Majkrzak, J.A. Dura, J.R. Groves, R.W. Springer, P.N. Arendt, V. Leiner, H. Lauter, and I.K. Schuller, Phys. Rev. B **65**, 4436 (2002).
[237] V.I. Nikitenko, V.S. Gornakov, A.J. Shapiro, R.D. Shull, K. Liu, S.M. Zhou, and C.L. Chien, Phys. Rev. Lett. **84**, 765 (2000).
[238] M.R. Fitzsimmons, C. Leighton, A. Hoffmann, P.C. Yashar, J. Nogués, I. K. Schuller, C.F. Majkrzak, J.A. Dura and H. Fritzsche, Phys. Rev. B **64**, 4415 (2001).
[239] E. F. Kneller and R. Hawig, IEEE Trans. Magn. **27**, 3588 (1991).
[240] E.E. Fullerton, J.S. Jiang, M. Grimsditch, C.H. Sowers, and S.D. Bader, Phys. Rev. B **58**, 12193 (1998).
[241] K. V. O'Donovan, J.A. Borchers, C. F. Majkrzak, O. Hellwig, and E.E. Fullerton, Phys. Rev. Lett. **88**, 7201 (2002).
[242] C. Dufour, K. Cherifi, G. Marchal, P. Mangin, and M. Hennion, Phys. Rev. B **47**, 14572 (1993).
[243] W. Hahn, M. Loewenhaupt, Y.Y. Huang, G.P. Felcher, and S.S.P. Parkin, Phys. Rev. B **52**, 16041 (1995).
[244] Diluted Magnetic (Semimagnetic). Semiconductors, edited by R. L. Aggarwal, J. K. Furdyna, and S. von Molnar (Vol. 89, Materials Research Society Symposia Proceedings, Pittsburgh, PA, 1987). p. 97.
[245] G.A. Prinz, Science **282**, 1660 (1998).
[246] P. Klosowski, T. Giebultowicz, J. J. Rhyne, N. Samarth, H. Luo, and J. K. Furdyna, J. Appl. Phys. **70**, 6221 (1991).
[247]J.K. Furdyna, J. Appl. Phys., **64**, R29 (1988).
[248] J.S. Smart, Phys. Rev. **86**, 968 (1952).
[249] T. M. Giebultowicz, N. Samarth, H. Luo, J. K. Furdyna, P. Klosowski, and J. J. Rhyne, Phys. Rev. B **46**, 12076 (1992).
[250] T. M. Giebultowicz, H. Luo, N. Samarth, J. K. Furdyna, and J. J. Rhyne, IEEE Trans. Magn. **29**, 3382 (1993).
[251] T. M. Giebultowicz, W. Faschinger, V. Nunez, P. Klosowski, G. Bauer, H. Sitter, and J. K. Furdyna, J. Crys. Gr. **138**, 877 (1994).
[252] T. M. Giebultowicz, V. Nunez, G. Springholz, G. Bauer, J. Chen, M. S. Dresselhaus, and J. K. Furdyna, J. Magn. Magn. Mater. **140**, 635 (1995).
[253] J. Lin, J. J. Rhyne, J. K. Furdyna, and T. M. Giebultowicz, J. Appl. Phys. **83**, 6554 (1998).
[254] L. E. Stumpe, J. J. Rhyne, H. Kaiser, S. Lee, U. Bindley, and J. K. Furdyna, J. Appl. Phys. **87**, 6460 (2000).

[255] J. J. Rhyne, J. Lin, J. K. Furdyna, and T. M. Giebultowicz, J. Magn. Magn. Mater., **177/181**, 1195 (1998).
[256] H. Ohno, H. Munekata, T. Penny, S. von Molnár, and L. L. Chang, Phys. Rev. Lett. **68**, 2664 (1992).
[257] F. Matsukura, E. Abe, and H. Ohno, J. Appl. Phys. **87**, 6442 (2000).
[258] H. Ohno, J. Magn. Magn. Mater. **200**, 110 (1999).
[259] T. Dietl, H. Ohno, F. Matsukura, J. Cibert and D. Ferrand, Science **287**, 1019 (2000).
[260] S. J. Potashnik, K. C. Ku, S. H. Chun, J. J. Berry, N. Samarth, and P. Schiffer, Appl. Phys. Lett. **79**, 1495 (2001).
[261] R. K. Kawakami, E. Johnston-Halperin, L. F. Chen, M. Hanson, N. Guébels, J. S. Speck, A. C. Gossard, and D. D. Awschalom, Appl. Phys. Lett. **77**, 2379 (2001).
[262] H. Luo, B. D. McCombe, M. H. Na, K. Mooney, F. Lehmann, X. Chen, M. Cheon, S.M. Wang, Y. Sasaki, X. Liu, and J.K. Furdyna, Proceedings of the 14th Int'l Conference on the Electronic Properties of 2D Systems, Prague, The Czech Republic, July 30 - August 3, 2001 (accepted for publication in Physica E).
[263] H. Luo, (private communication).
[264] J. De Boeck, R. Oesterholt, A. Van Esch, H. Bender, C. Bruynseraede, C. Van Hoof, and G. Borghs, Appl. Phys. Lett. **68**, 2744 (1996).
[265] T. Hartmann, M. Lampalzer, P.J. Klar, W. Stolz, W. Heimbrodt, H.A.K. von Nidda, A. Loidl, L. Svistov, Physica E **13**, 572 (2002).
[266] S. Koshihara, A. Oiwa, M. Hirasawa, D. Katsumoto, Y. Iye, C. Urano, H. Takagi, and H. Munekata, Phys. Rev. Lett. **78**, 4617 (1999).
[267] A. Oiwa, T. Slupinski, and H. Munekata, Appl. Phys. Lett. **78**, 518 (2001).
[268] H. Ohno, D. Chiba, F. Matsukura, T. Omiya, E. Abe, T. Dietl, Y. Ohno, and K. Ohtani, Nature **408**, 944 (2000).
[269] D. Weller and A. Moser, IEEE Trans. Magn. **35**, 4423 (1999).
[270] R.P. Cowburn, A.O.Adeyeye, and J.C. Bland, Appl. Phys. Lett. **70**, 2309 (1997)
[271] R. Ferre, M. Hehn and K.Ounadjela, J.Magn.Mag. Matls. **165**, 5 (1997)
[272] N. Bardou, B. Bartenlian , F. Rousseaux , D. Decanini , F. Carcenac, E. Cambril, M.F. Ravet, C. Chappert, P. Veillet, and P. Beauvillain, J. Magn. Magn. Mater. **156**, 139 (1996)
[273] J. Bansmann, V. Senz, L. Lu, A. Bettac, K.H. Meiwes-Broer, J.Elec. Spectroscopy and Related Phenomena **106**, 221 (2000).
[274] S.H. Charap, P.-L. Lu, and Y. He, IEEE Trans. Magn. **33**, 978 (1997).
[275] T. Klemmer, D. Hoydick, H. Okumura, B. Zhang and W.A. Soffa, Scripta Metall. **33**, 1793 (1995).
[276] H. Zhou and H.N. Bertam, IEEE Trans. Magn. **35**, 2712 (1999).
[277] see for example, Y. Yamada, T. Suzuki, H. Kanazawa, and J.C. Österman, J. Appl. Phys. **85**, 5094 (1999) and references therein.
[278] Y. Kubota, L. Folks and E.E. Marinero, J. Appl., Phys. **84**, 6202 (1998).
[279] J. Suzuki, K Takei, Y Maeda, and Y Morii, J. Magn. Magn. Mater. **184**, 116 (1998).
[280] M.F. Toney, K.A. Rubin, S.M. Choi, and C.J. Glinka, submitted to Appl. Phys. Lett.

[281] R. Przenioslo, R. Winter, H. Natter, M. Schmelzer, R. Hempelmann, and W. Wagner, Phys Rev. B **63**, 54408 (2001).
[282] A Wiedenmann, J. Appl. Crystal. **33**, 428 (2000).
[283] J.R. Childress, C.L. Chien, J.J. Rhyne, and R.W. Erwin, J Magn. Magn. Mater., **104**, 1585 (1992).
[284] E.E. Fullerton, D.T. Margulies, M.E. Schabes, M. Carey, B. Gurney, A. Moser, M. Best, G. Zeltzer, K. Rubin, H. Rosen and M. Doerner, Appl. Phys. Lett. **77**, 3806 (2000).
[285] E.N. Abarra, A. Inomata, H. Sato, I. Okamoto and Y. Mizoshita, Appl. Phys. Lett. **77**, 2581 (2000).
[286] C.F. Majkrzak, Physica B **221**, 342 (1996).
[287] J.F. Ankner and G.P. Felcher, J. Magn. Magn. Mater. **200**, 741 (1999).
[288] M.F. Toney, K. O'Donovan, J.A. Borchers, E.E. Fullerton and D. Margulies, unpublished.
[289] K.S. Moon, R.E. Fontana, and S.S.P. Parkin, Appl. Phys. Lett. **74**, 3690 (1999).
[290] Z.M. Chen, H. Okumura, G.C. Hadjipanayis, and Q. Chen, J. Appl. Phys. **89**, 2299 (2001).
[291] M. Takahhashi, and H. Shoji, J. Magn. Magn. Mater. **208**, 145 (2000).
[292] P.C. Andricacos, and N. Robertson, IBM J. Res. Devl. **42**, 671 (1998).
[293] T Osaka, M. Takai, K. Hayashi, K. Ohashi, M. Saito, and K. Yamada, Nature **392**, 796 (1998).
[294] K. Nishioka, S. Shigematsu, T. Imagawa, and S. Narishige, J. Appl. Phys. **83**, 3233 (1998).
[295] Y. Ozaki, K. Shimoyama, S. Iwata, and S. Tsunashima, IEEE Trans. Magn. **36**, 2888 (2000).
[296] C. Leighton, M. R. Fitzsimmons, P. Yashar, A. Hoffmann, J. Nogués, J. Dura, C. F. Majkrzak, and I.K. Schuller, Phys. Rev. Lett. **86**, 4394 (2001).
[297] K. Suzuki, Y. Yamaguchi, T. Kaneko, H. Yoshida, Y. Obi, H. Fujimori, H. Morita, J. of the Phys. Soc. of Japan **70**, 1084 (2001).
[298] X. Liu and Y. Sasaki, private communication.

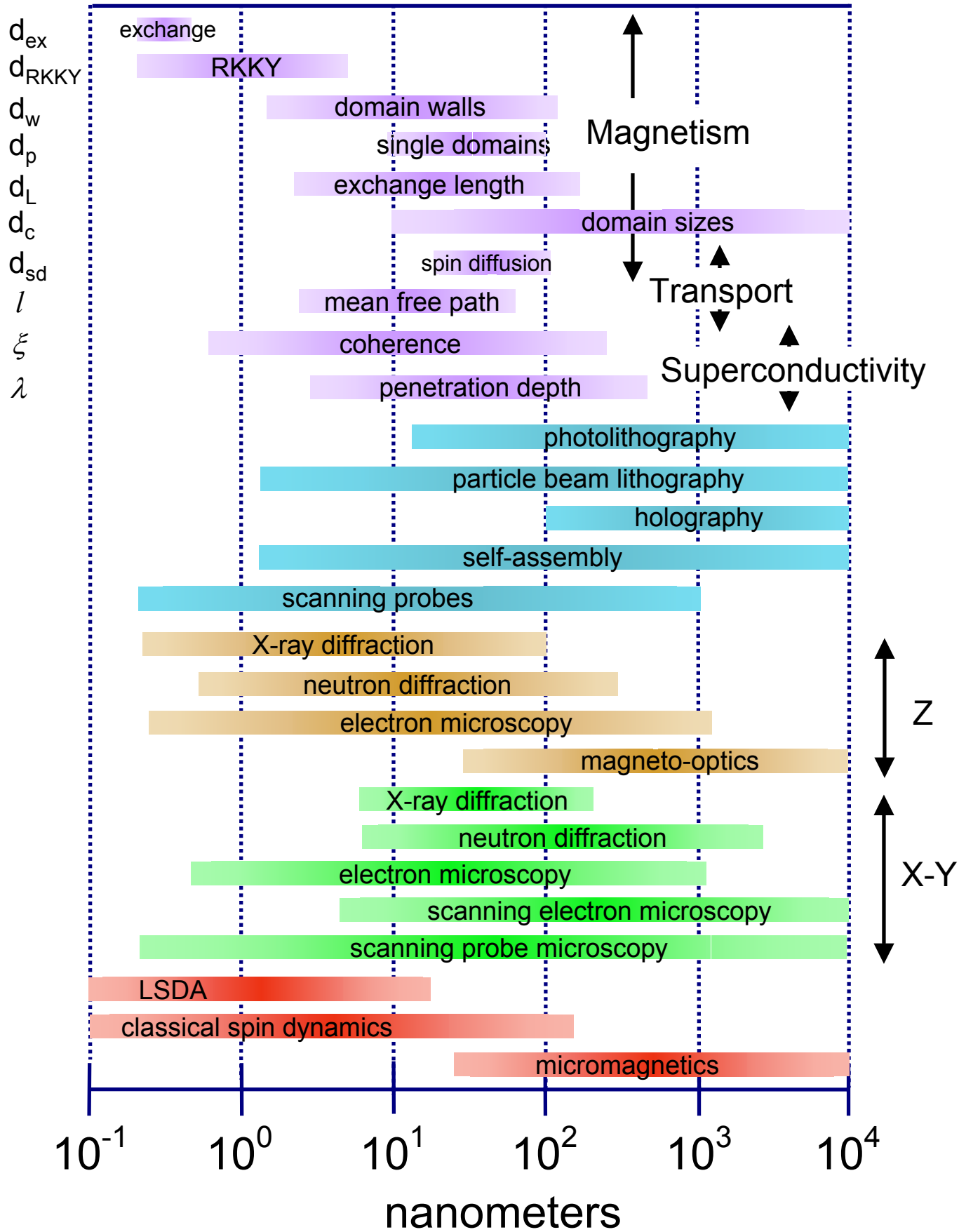
d_{ex}
d_{RKKY}
d_w
d_p
d_L
d_c
d_{sd}
l
ξ
λ
exchange
RKKY
domain walls
single domains
exchange length
domain sizes
spin diffusion
mean free path
coherence
penetration depth
Magnetism
Transport
Superconductivity
photolithography
particle beam lithography
holography
self-assembly
scanning probes
X-ray diffraction
neutron diffraction
electron microscopy
magneto-optics
Z
X-ray diffraction
neutron diffraction
electron microscopy
scanning electron microscopy
scanning probe microscopy
X-Y
LSDA
classical spin dynamics
micromagnetics
10^{-1}
10^{0}
10^{1}
10^{2}
10^{3}
10^{4}
nanometers

Figure 1

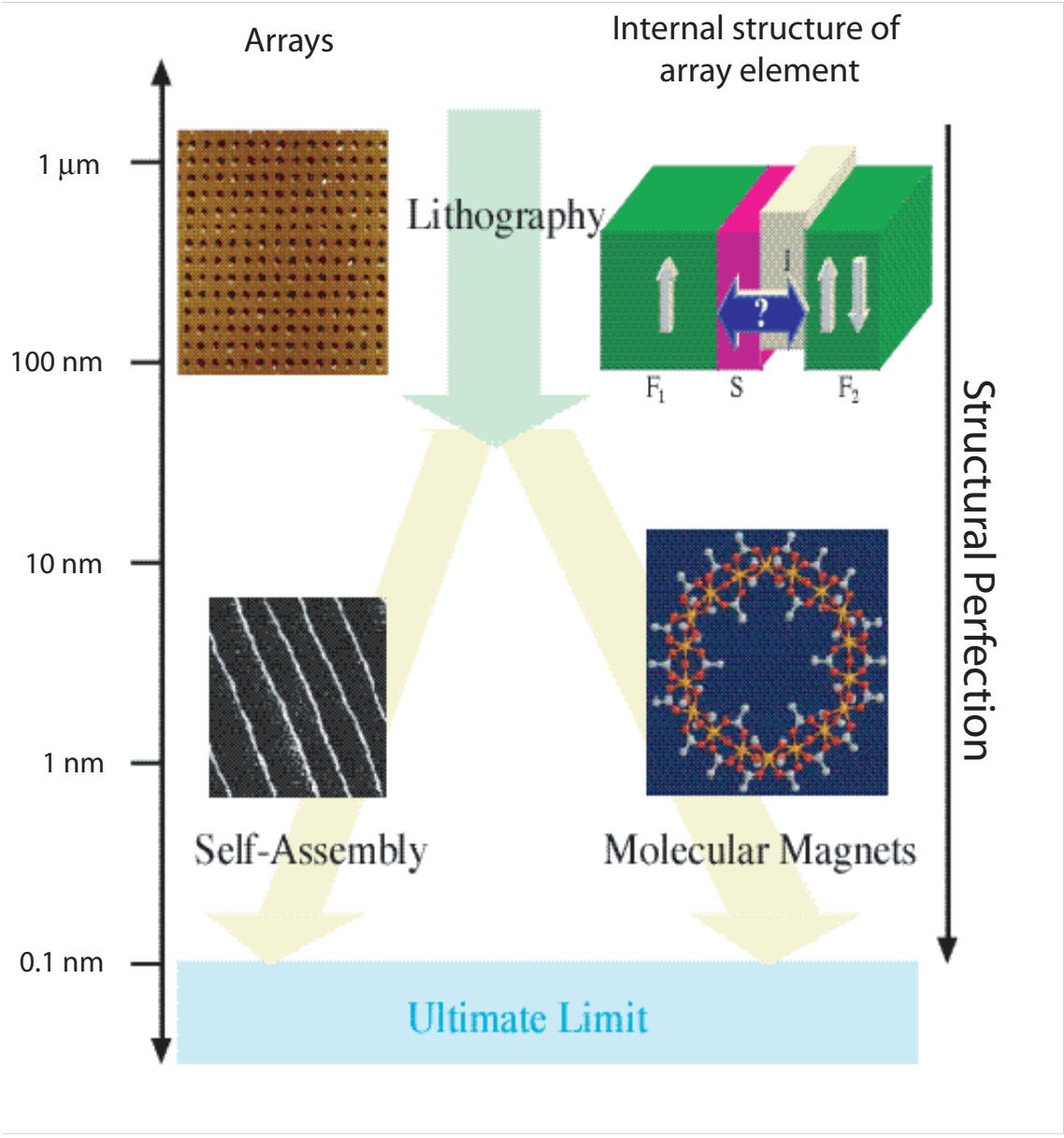
Arrays
Internal structure of array element
1 µm
100 nm
10 nm
1 nm
0.1 nm
Lithography
F1
S
F2
Structural Perfection
Self-Assembly
Molecular Magnets
Ultimate Limit

Figure 2

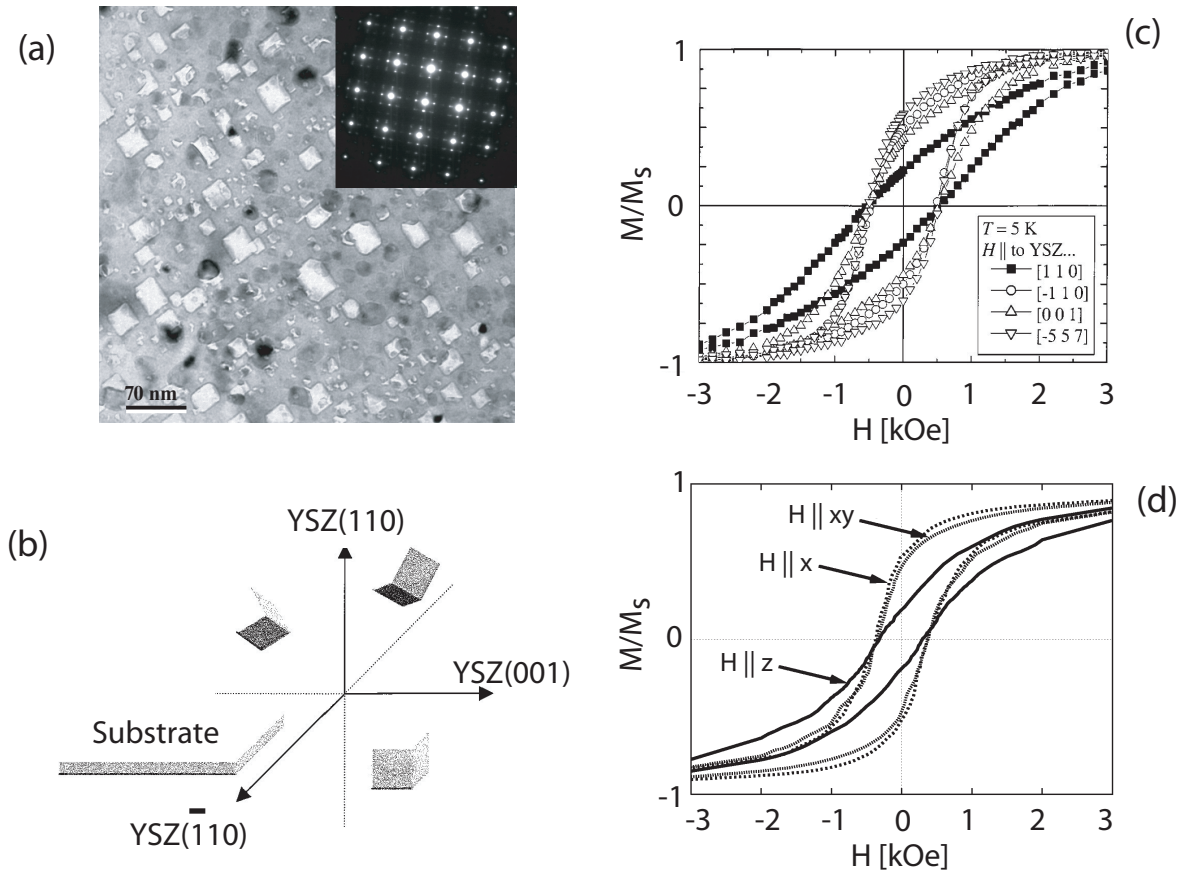
(a)
70 nm
(b)
YSZ(110)
YSZ(001)
Substrate
YSZ(1̄10)
(c)
M/M_S
H [kOe]
T = 5 K
H || to YSZ...
[1 1 0]
[-1 1 0]
[0 0 1]
[-5 5 7]
(d)
H || xy
H || x
H || z
M/M_S
H [kOe]

Figure 3

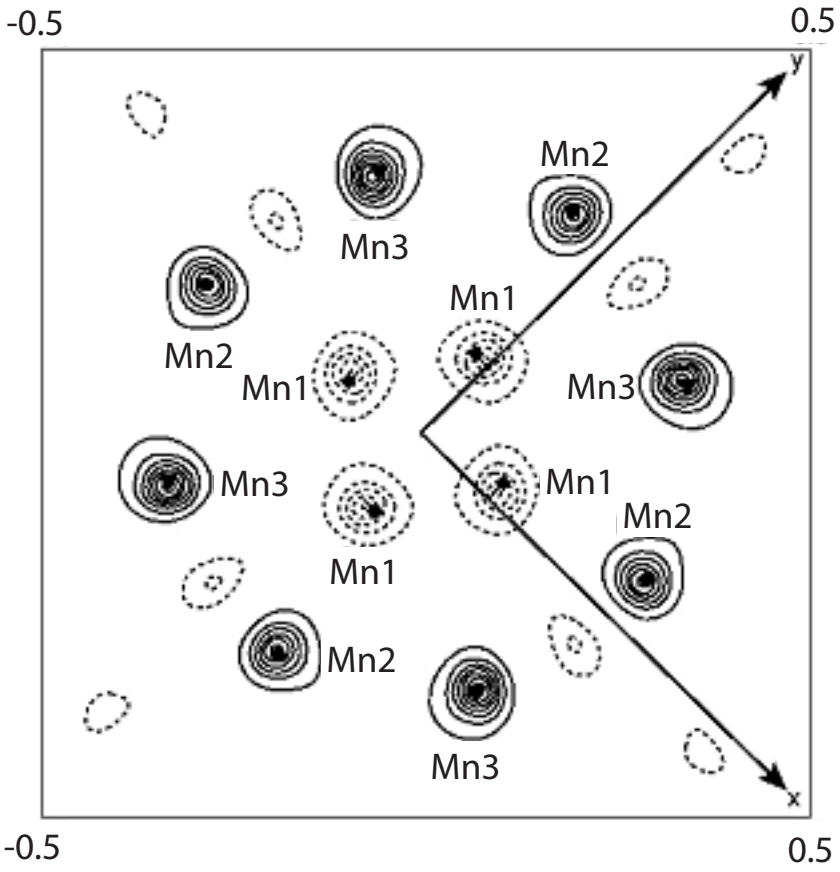

Figure 4

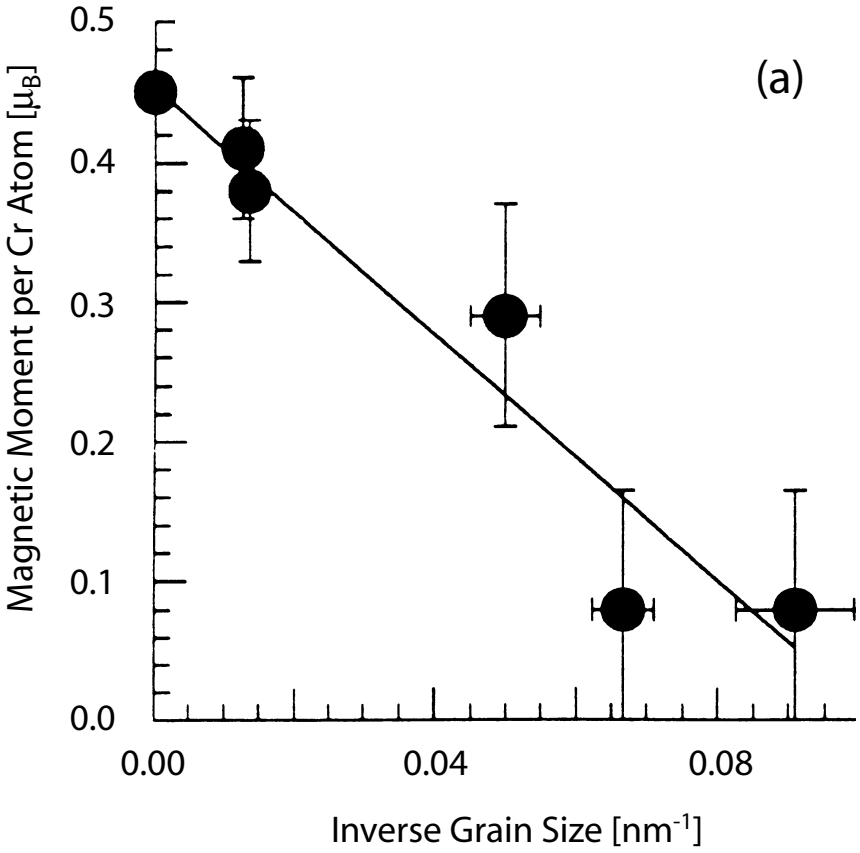
(a)
0.5
0.4
0.3
0.2
0.1
0.0
Magnetic Moment per Cr Atom [μ_B]
0.00
0.04
0.08
Inverse Grain Size [nm^{-1}]

Figure 5(a)

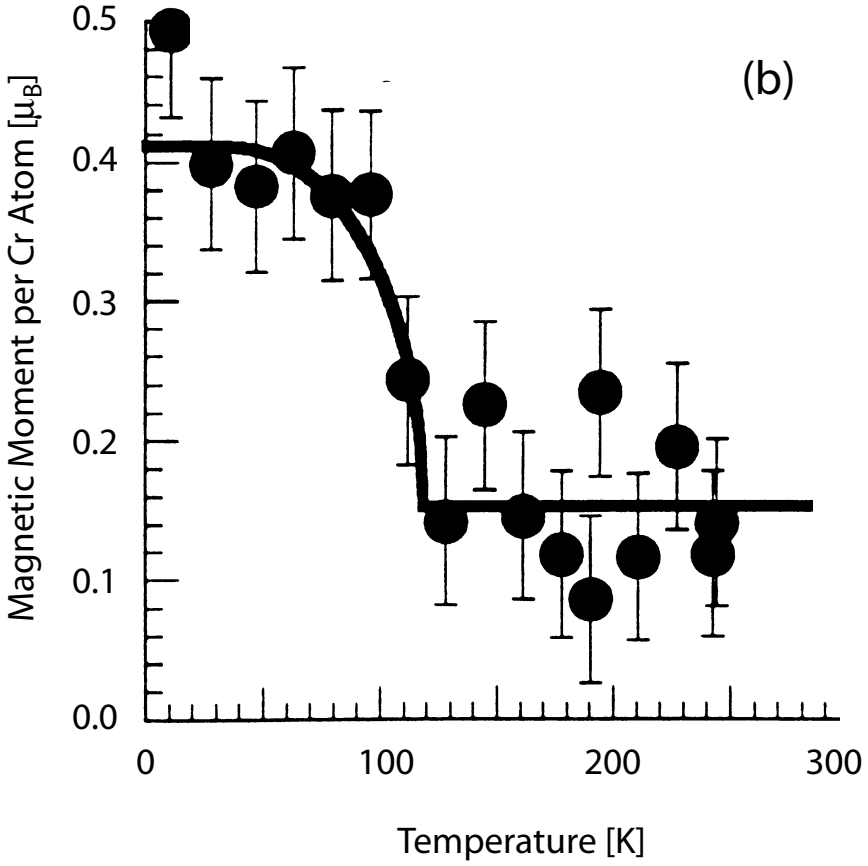
(b)
Magnetic Moment per Cr Atom [μ_B]
0.5
0.4
0.3
0.2
0.1
0.0
0
100
200
300
Temperature [K]

Figure 5(b)

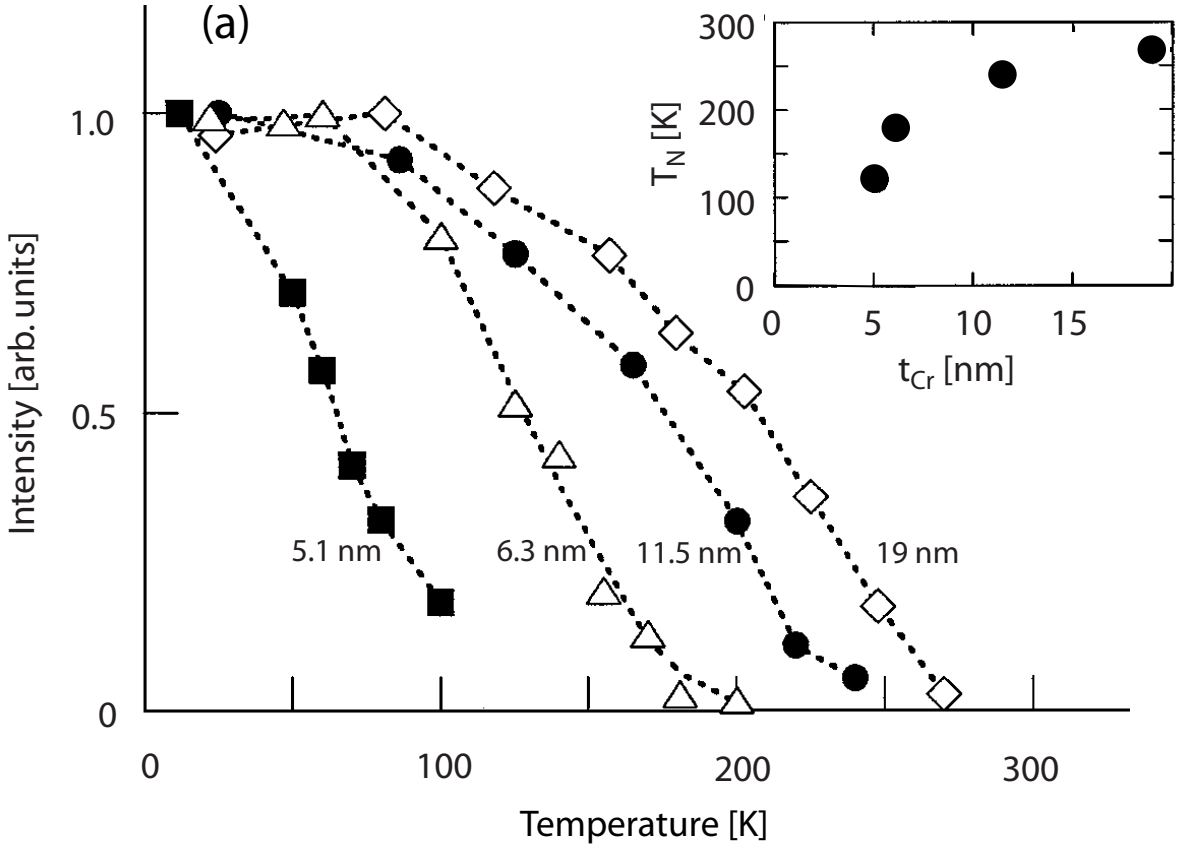
(a)
Intensity [arb. units]
1.0
0.5
0
0
100
200
300
Temperature [K]
5.1 nm
6.3 nm
11.5 nm
19 nm
T_N [K]
300
200
100
0
0
5
10
15
t_{Cr} [nm]

Figure 6(a)

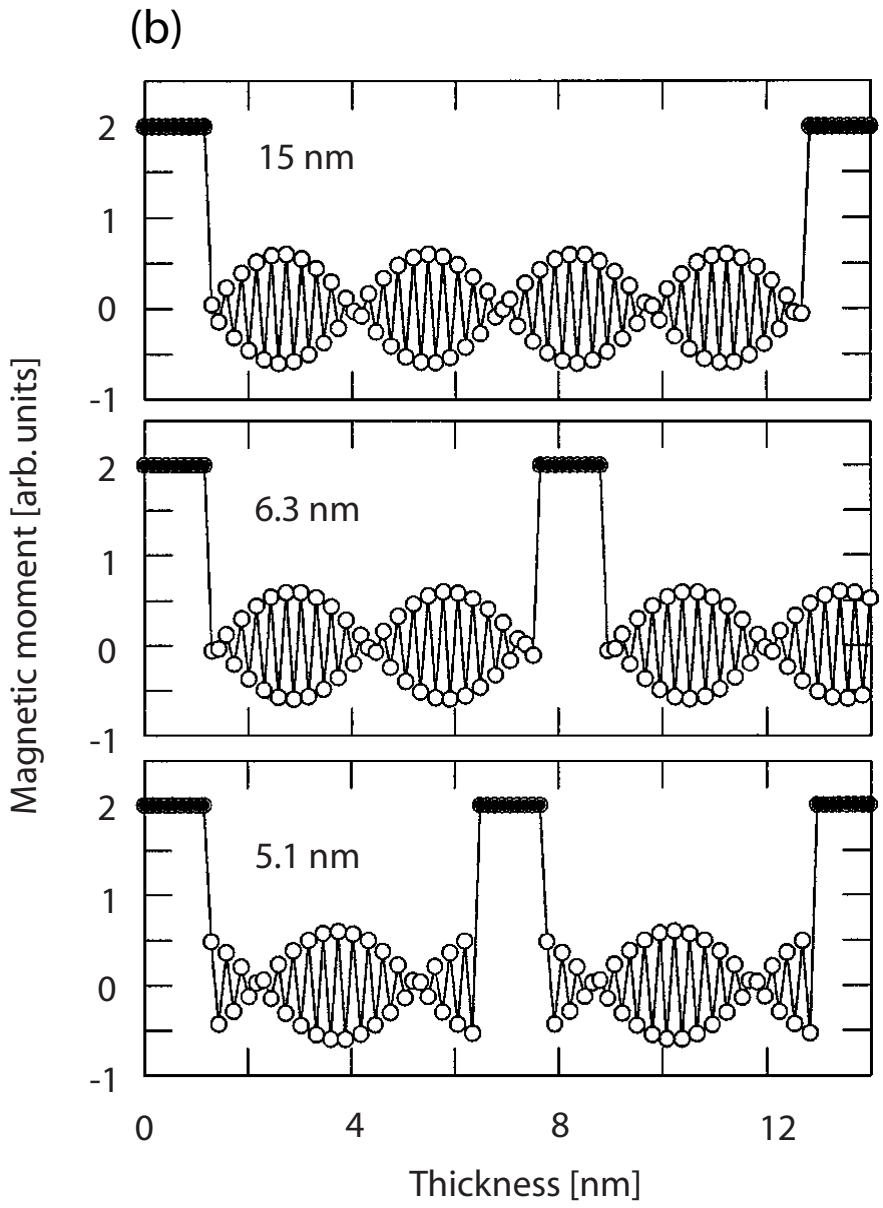
(b)
15 nm
6.3 nm
5.1 nm
Magnetic moment [arb. units]
Thickness [nm]
2
1
0
-1
0
4
8
12

Figure 6(b)

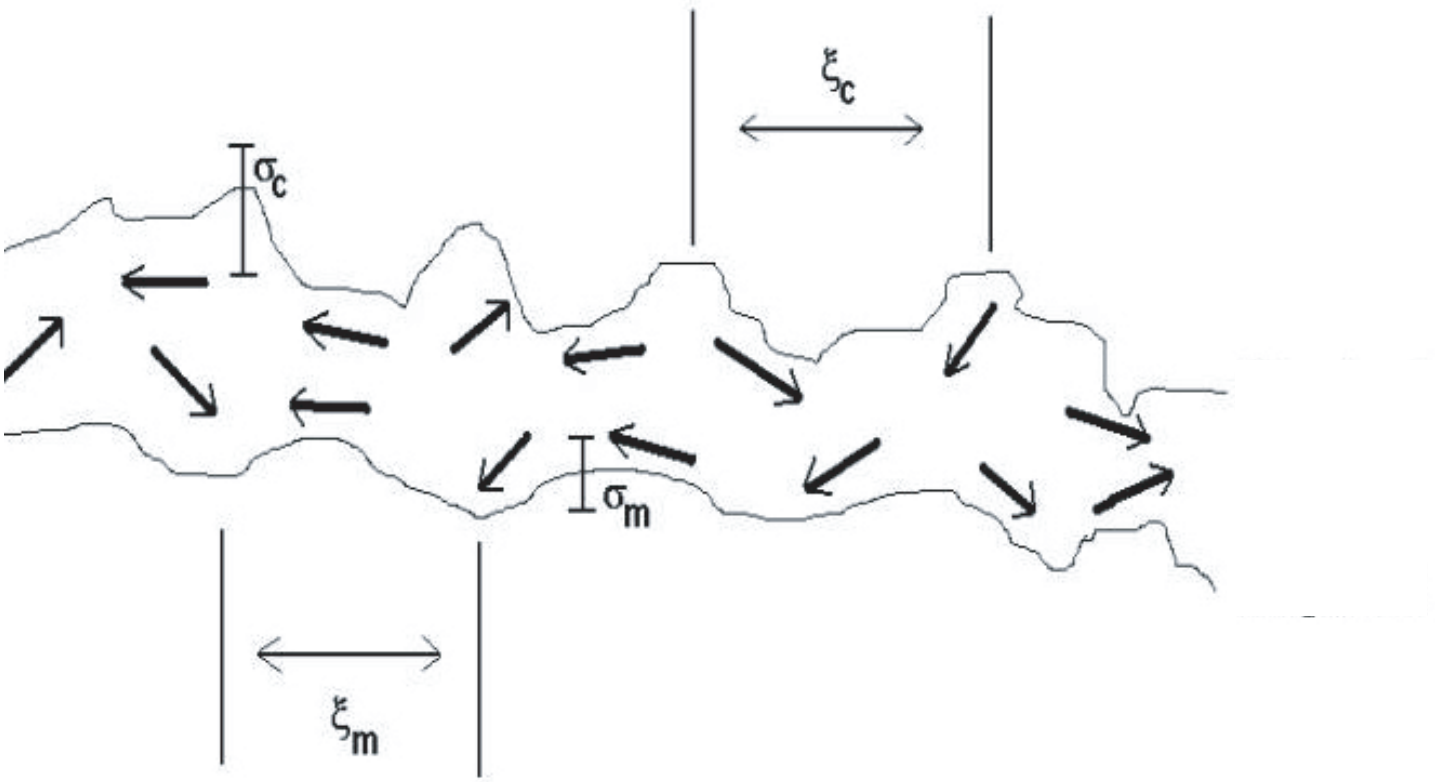

Figure 7

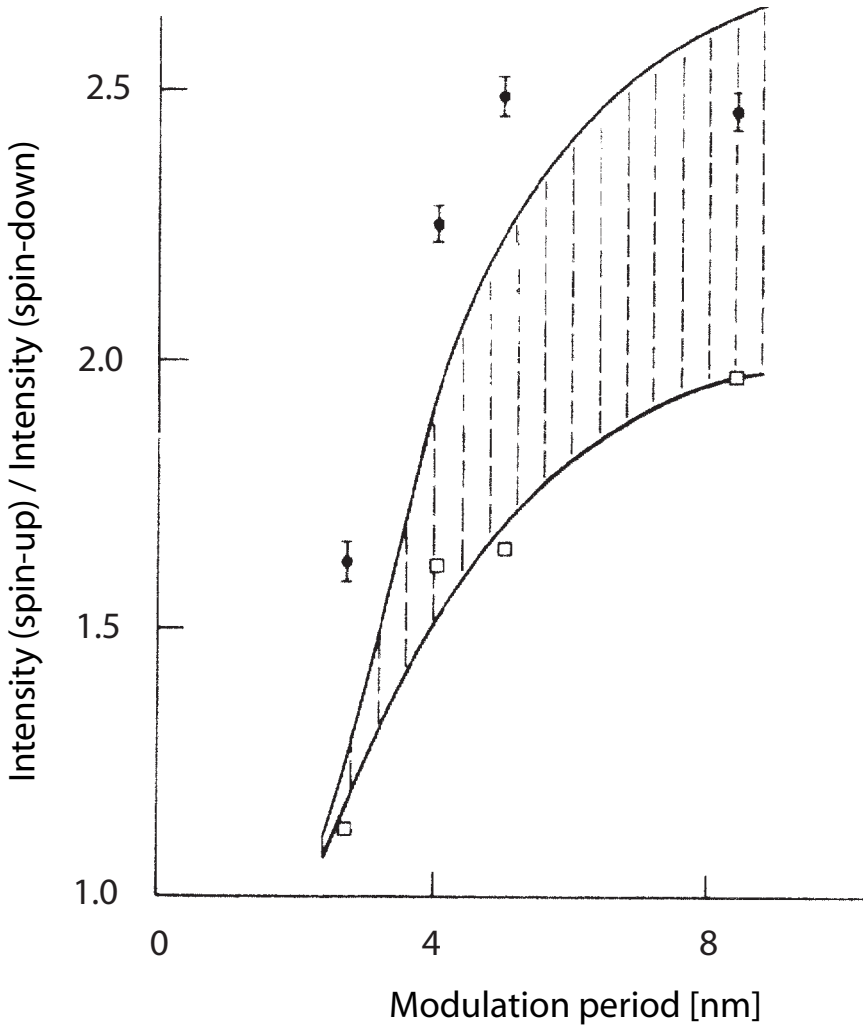
2.5
2.0
1.5
1.0
0
4
8
Intensity (spin-up) / Intensity (spin-down)
Modulation period [nm]

Figure 8

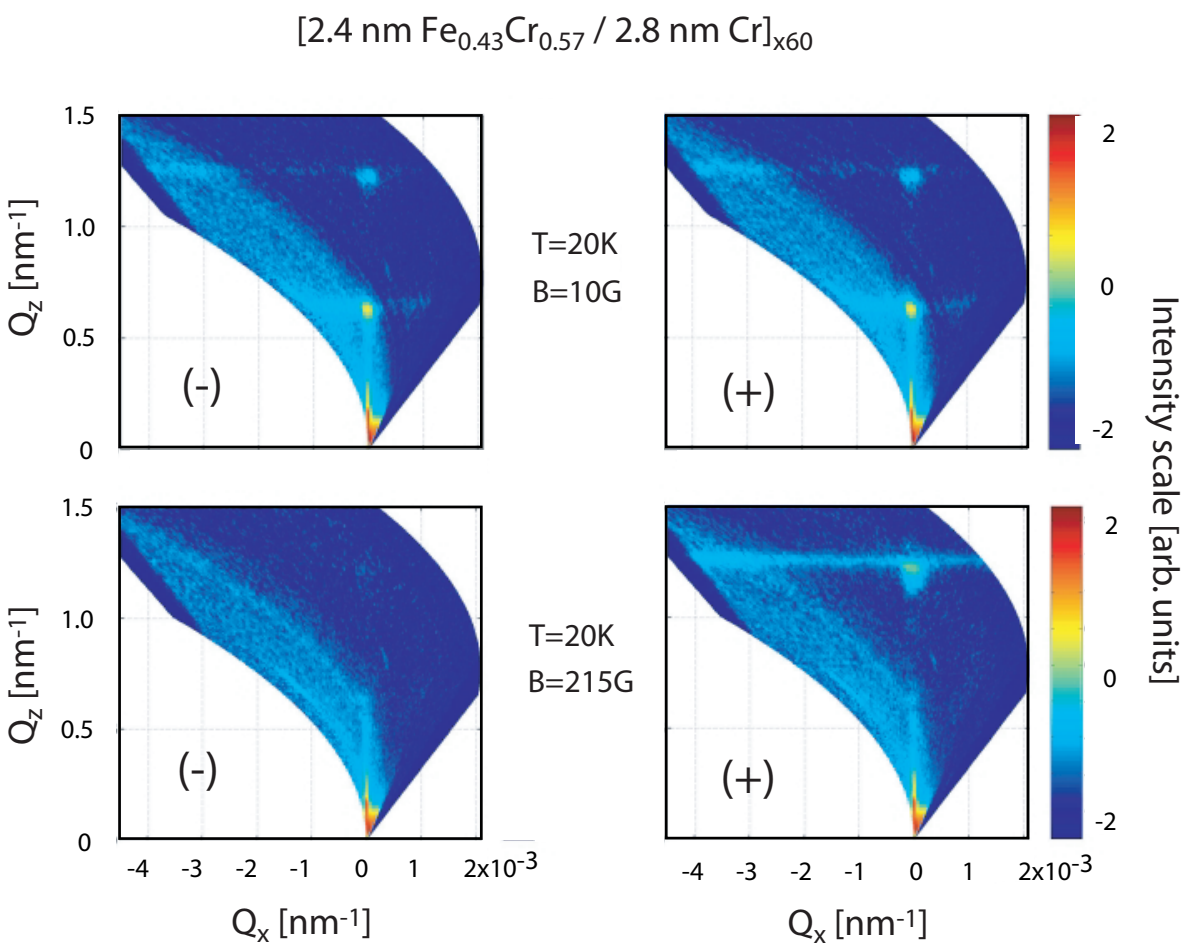
[2.4 nm Fe0.43Cr0.57 / 2.8 nm Cr]x60
Qz [nm-1]
1.5
1.0
0.5
0
(-)
(+)
T=20K
B=10G
T=20K
B=215G
2
0
-2
Intensity scale [arb. units]
-4
-3
-2
-1
0
1
2x10-3
Qx [nm-1]

Figure 9

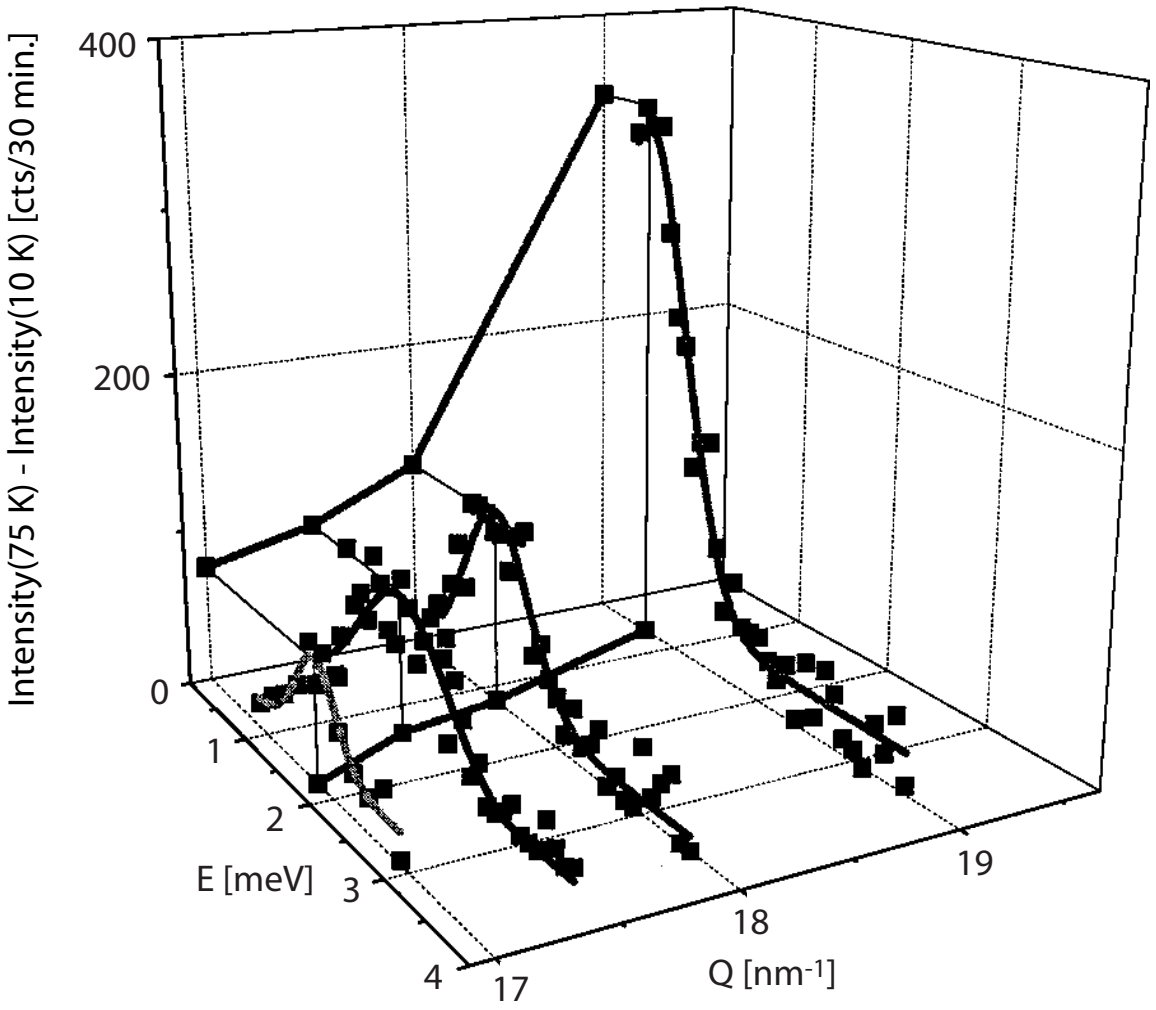
Intensity(75 K) - Intensity(10 K) [cts/30 min.]
400
200
0
1
2
E [meV]
3
4
17
18
19
Q [nm-1]

Figure 10

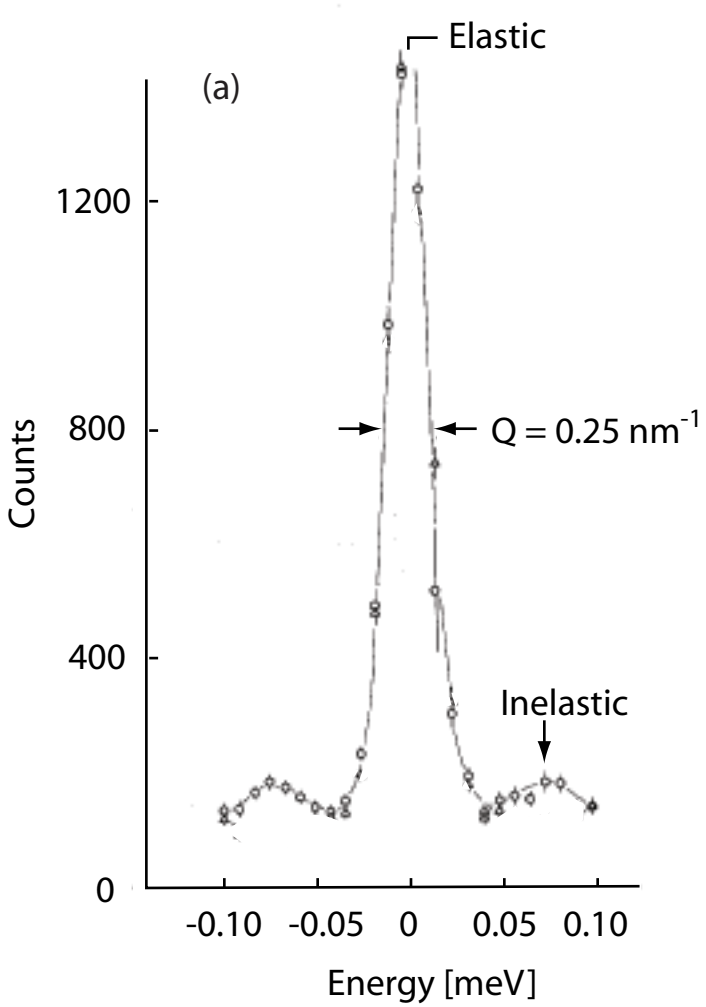
Elastic
(a)
1200
800
400
0
Counts
Q = 0.25 nm-1
Inelastic
-0.10
-0.05
0
0.05
0.10
Energy [meV]

Figure 11(a)

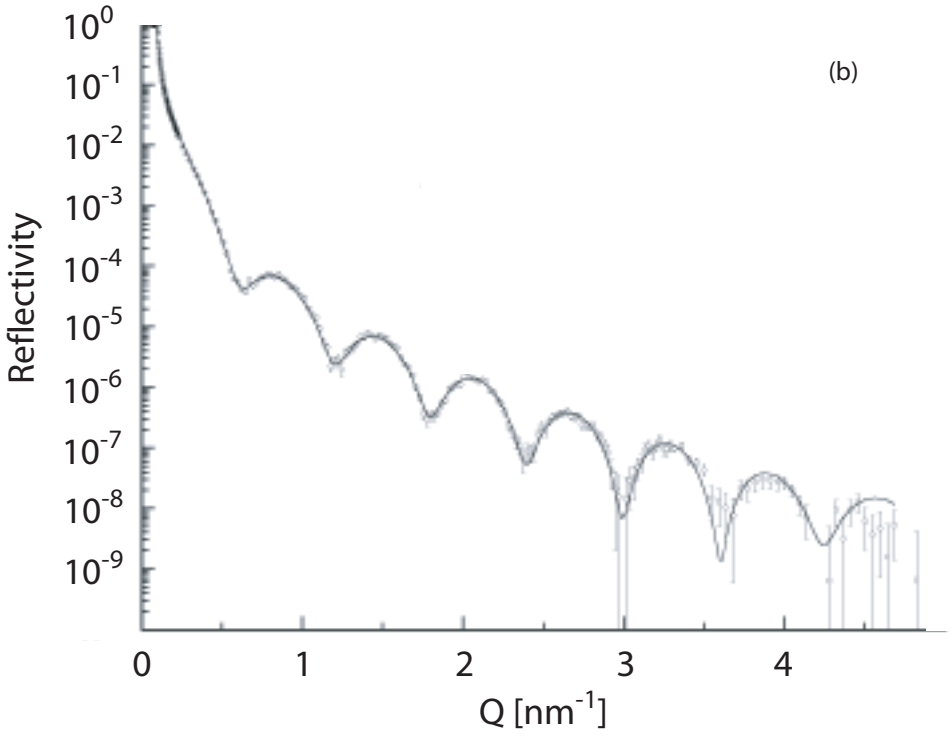
(b)
Reflectivity
10^{0}
10^{-1}
10^{-2}
10^{-3}
10^{-4}
10^{-5}
10^{-6}
10^{-7}
10^{-8}
10^{-9}
0
1
2
3
4
Q [nm^{-1}]

Figure 11(b)

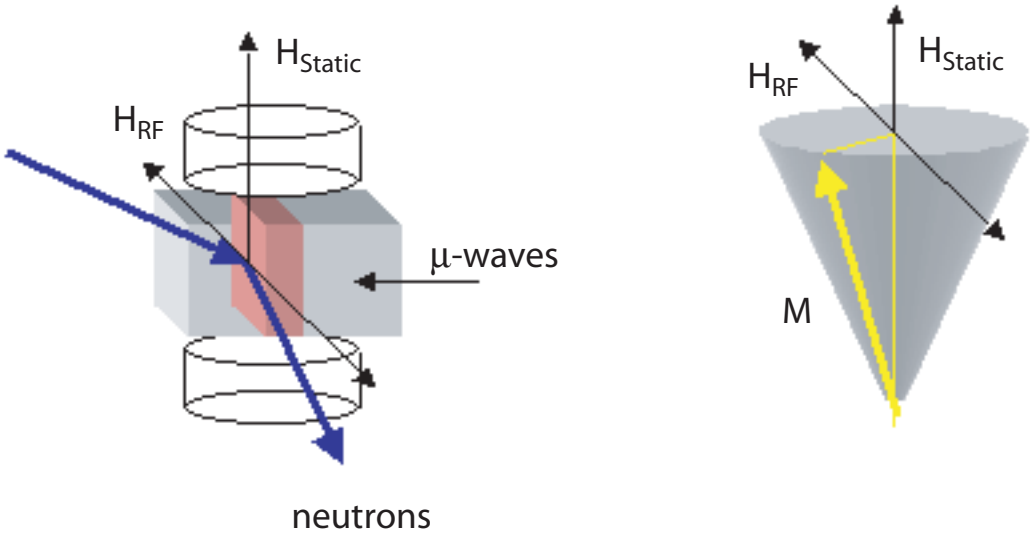

Figure 12

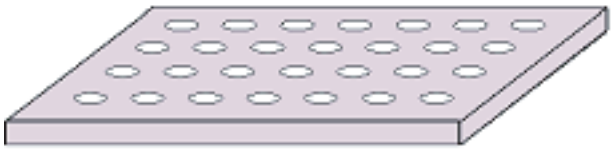

Alumina mask

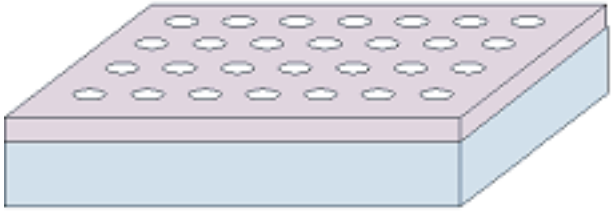

Mask application

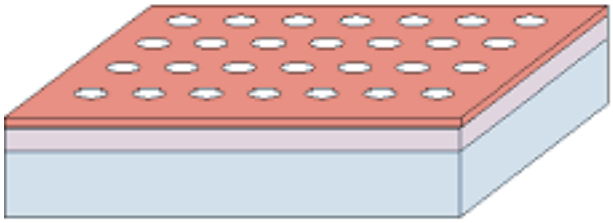

Deposition

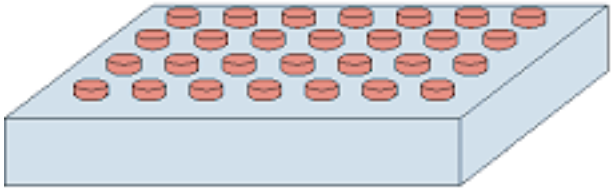

Lift-off

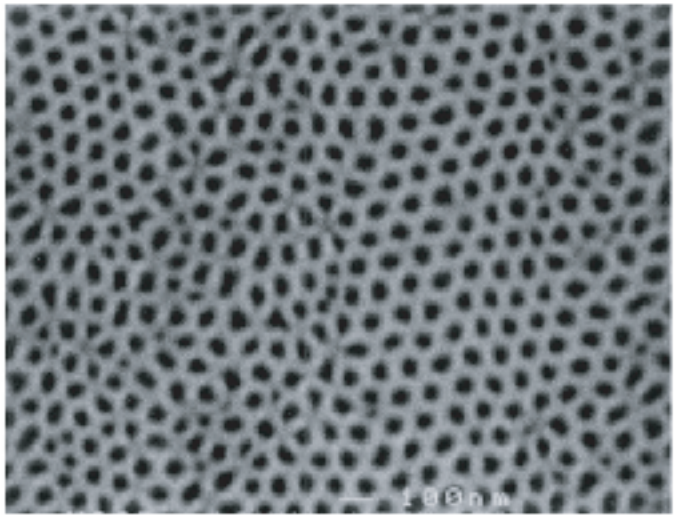

Alumina mask

60 nm

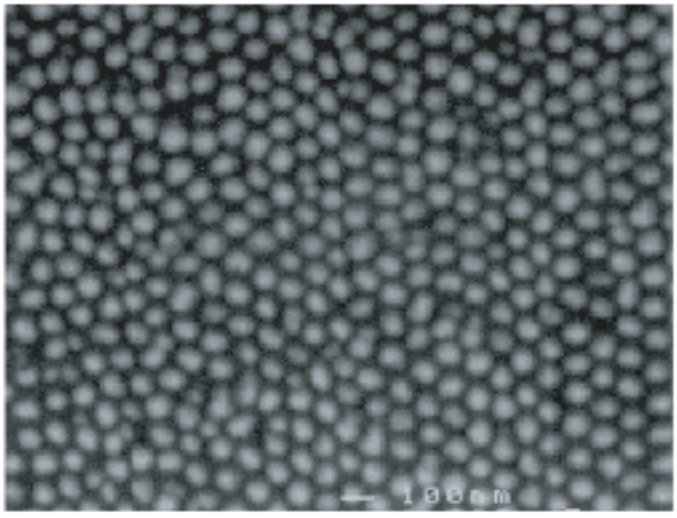

Nanodots

Figure 13

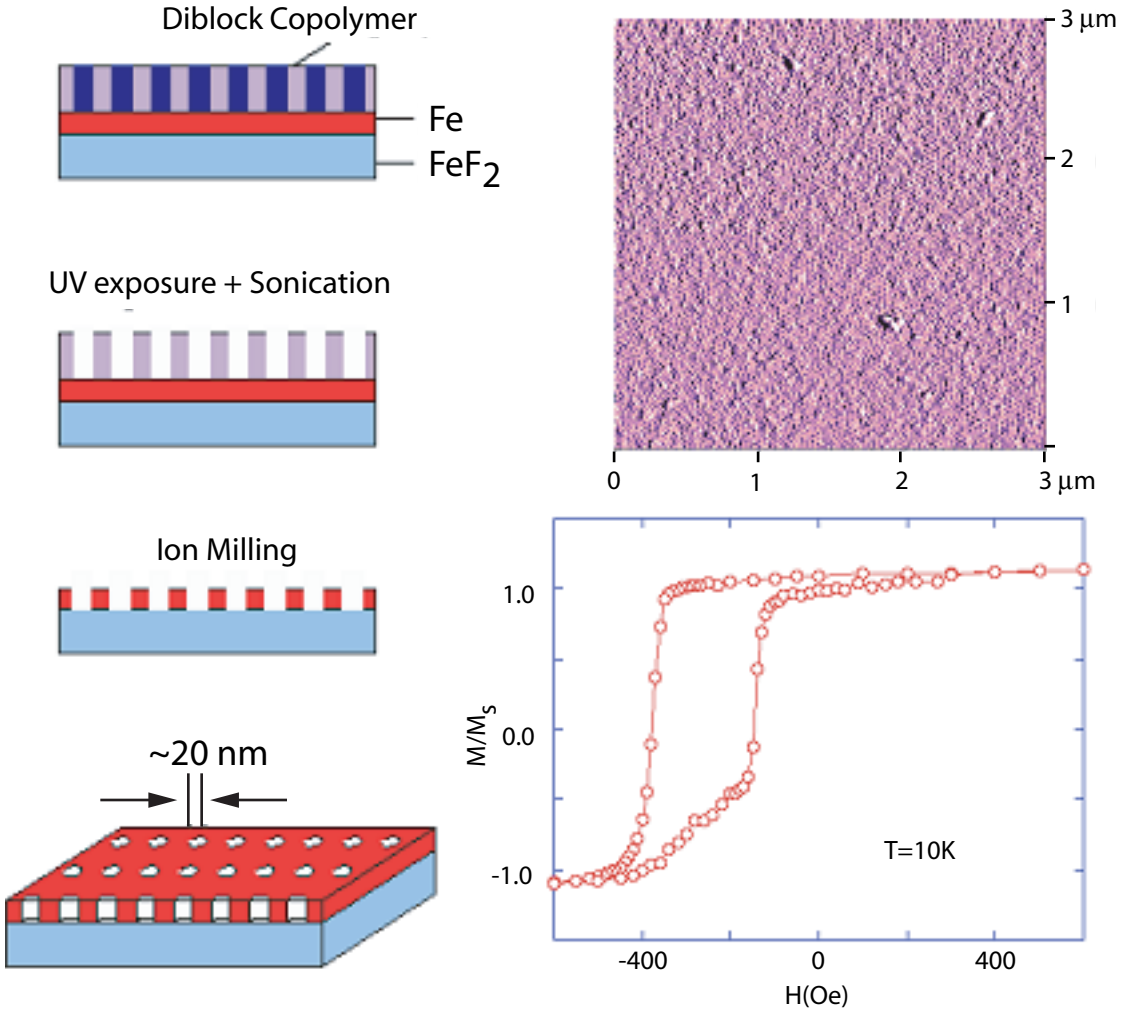
Diblock Copolymer
Fe
FeF_2
UV exposure + Sonication
Ion Milling
~20 nm
3 µm
2
1
0
1
2
3 µm
1.0
0.0
-1.0
M/M_s
T=10K
-400
0
400
H(Oe)

Figure 14

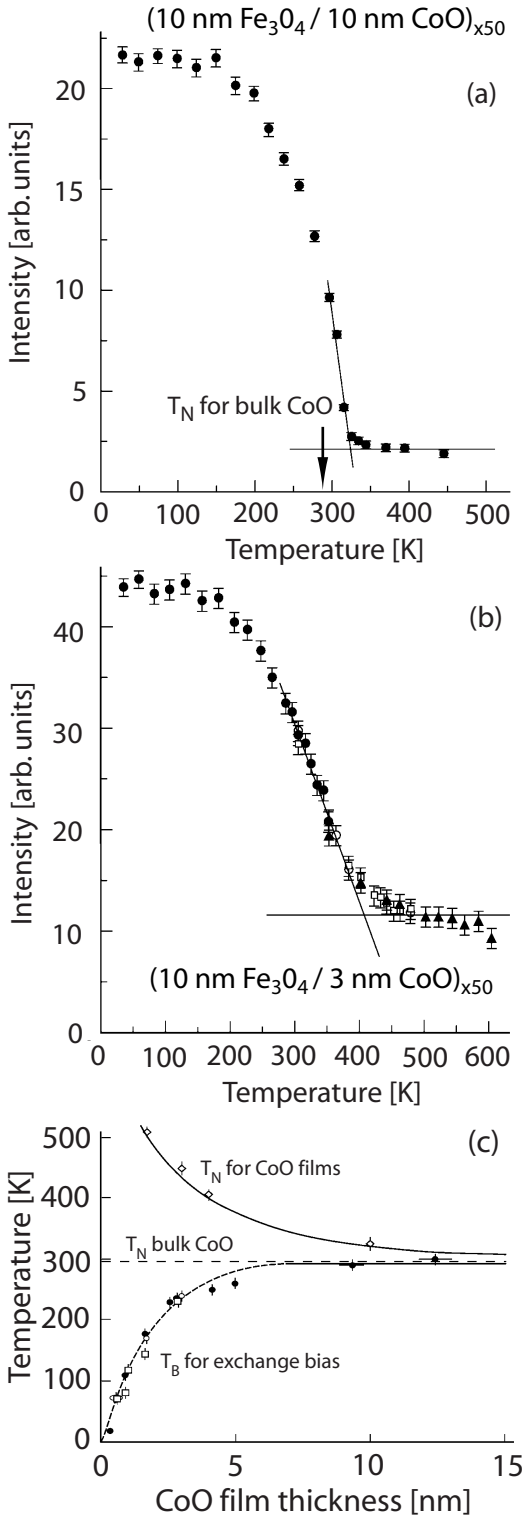
(10 nm Fe3O4 / 10 nm CoO)x50
(a)
Intensity [arb.units]
T_N for bulk CoO
Temperature [K]
(b)
Intensity [arb. units]
(10 nm Fe3O4 / 3 nm CoO)x50
Temperature [K]
(c)
T_N for CoO films
T_N bulk CoO
T_B for exchange bias
Temperature [K]
CoO film thickness [nm]

Figure 15

Model magnetization process for exchange-spring magnets

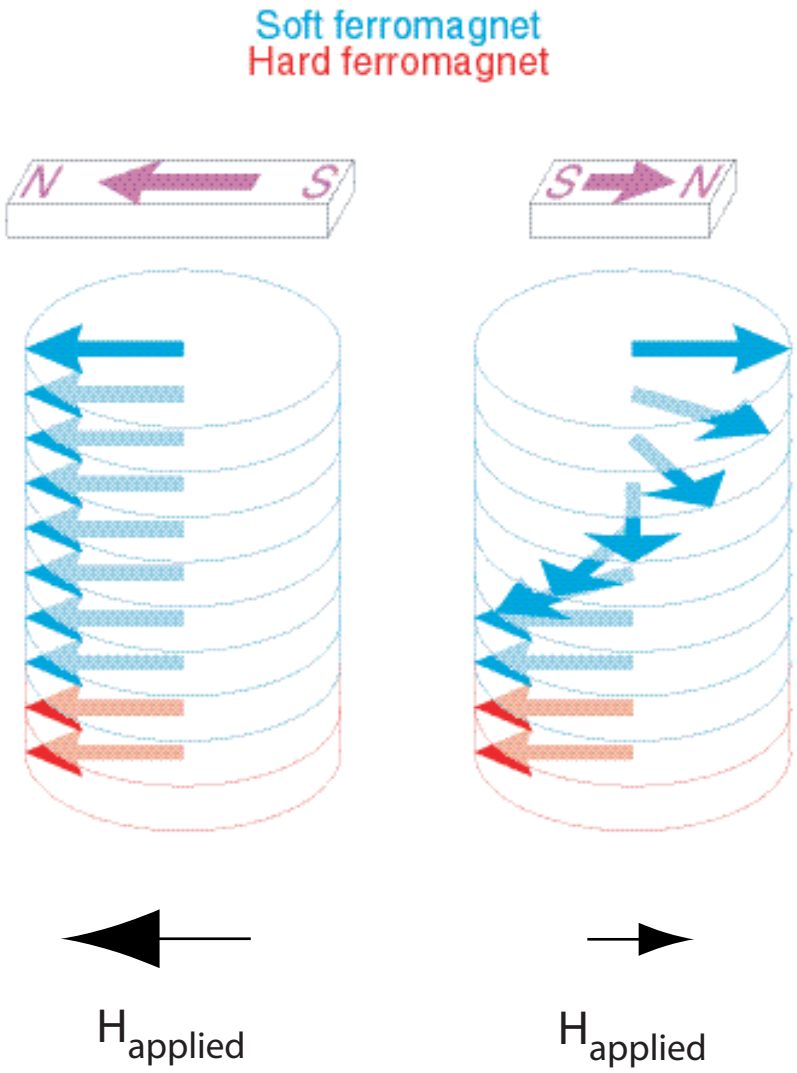

Figure 16

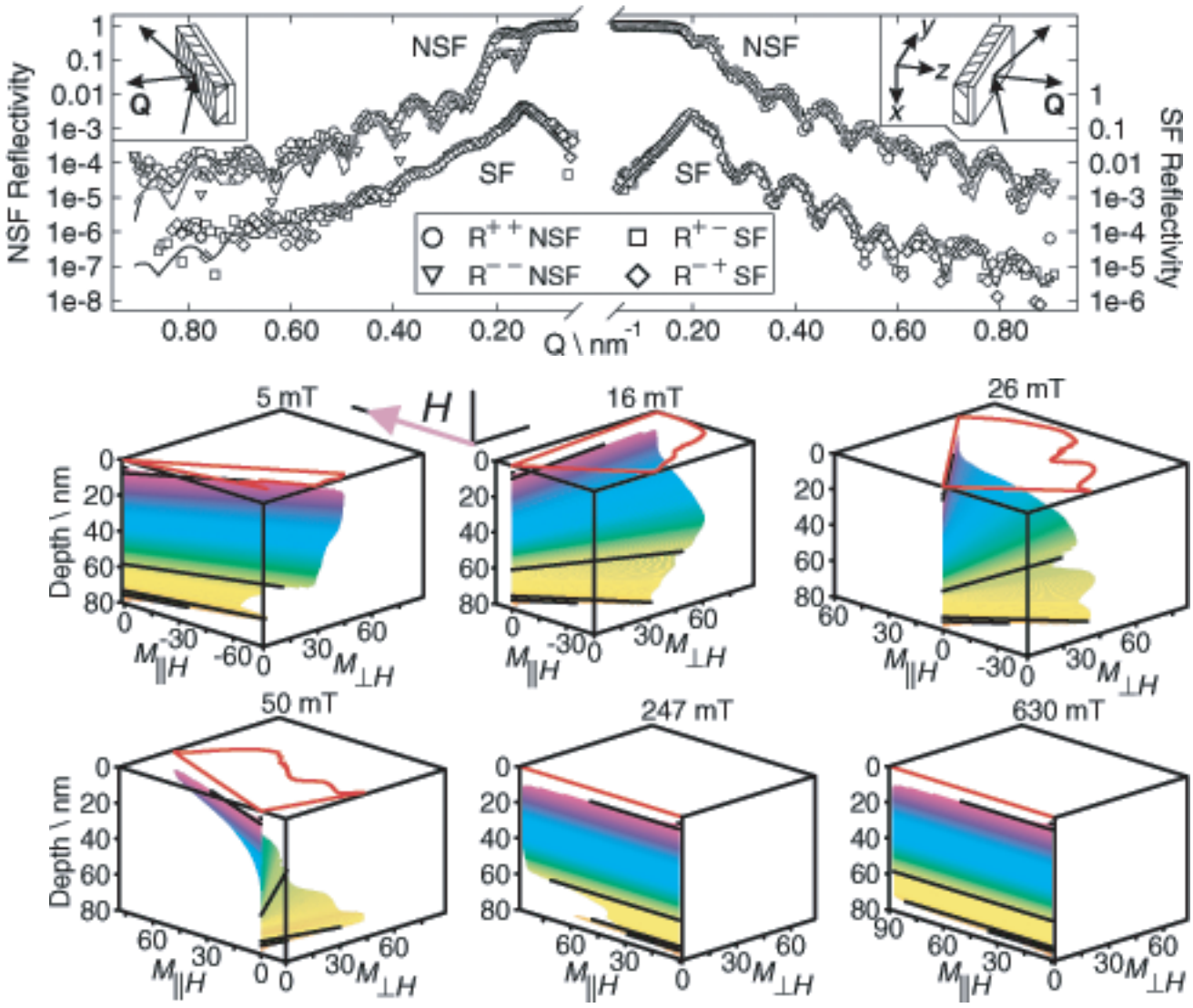
NSF Reflectivity
SF Reflectivity
NSF
SF
Q
y
z
x
R+ + NSF
R+ − SF
R− − NSF
R− + SF
Q \ nm-1
5 mT
16 mT
26 mT
50 mT
247 mT
630 mT
H
Depth \ nm
M||H
M⊥H

Figure 17

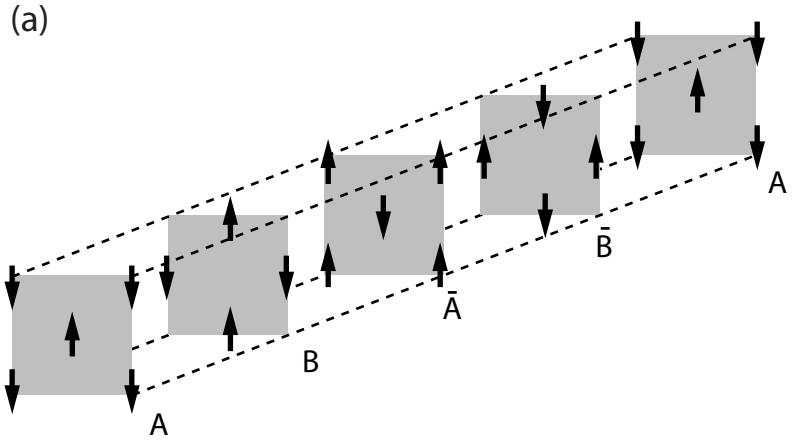

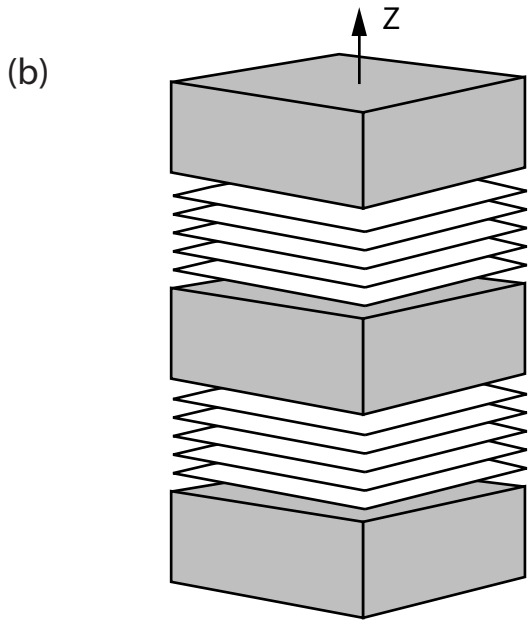

Figure 18

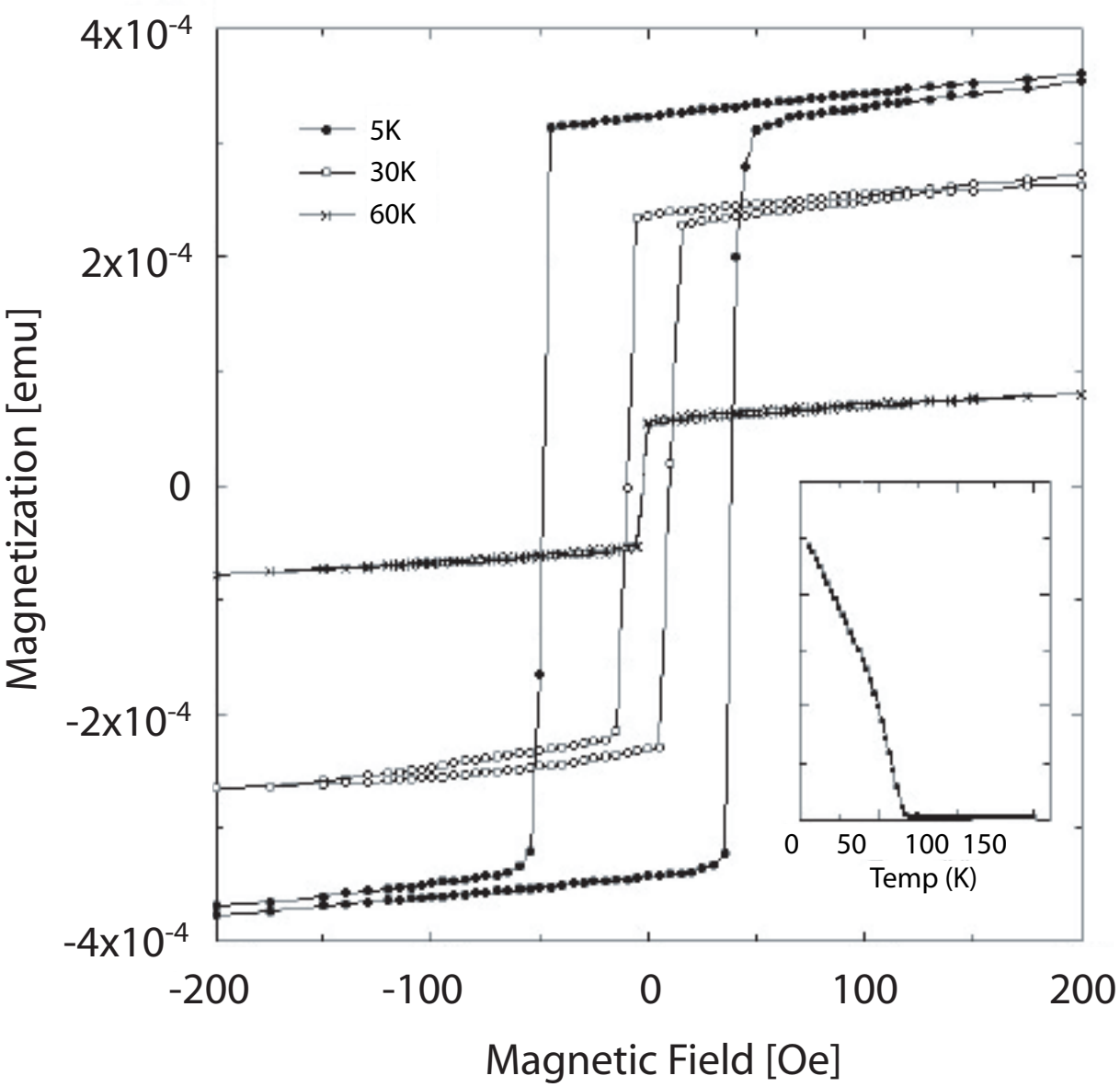
4x10-4
2x10-4
0
-2x10-4
-4x10-4
Magnetization [emu]
5K
30K
60K
-200
-100
0
100
200
Magnetic Field [Oe]
0
50
100
150
Temp (K)

Figure 19

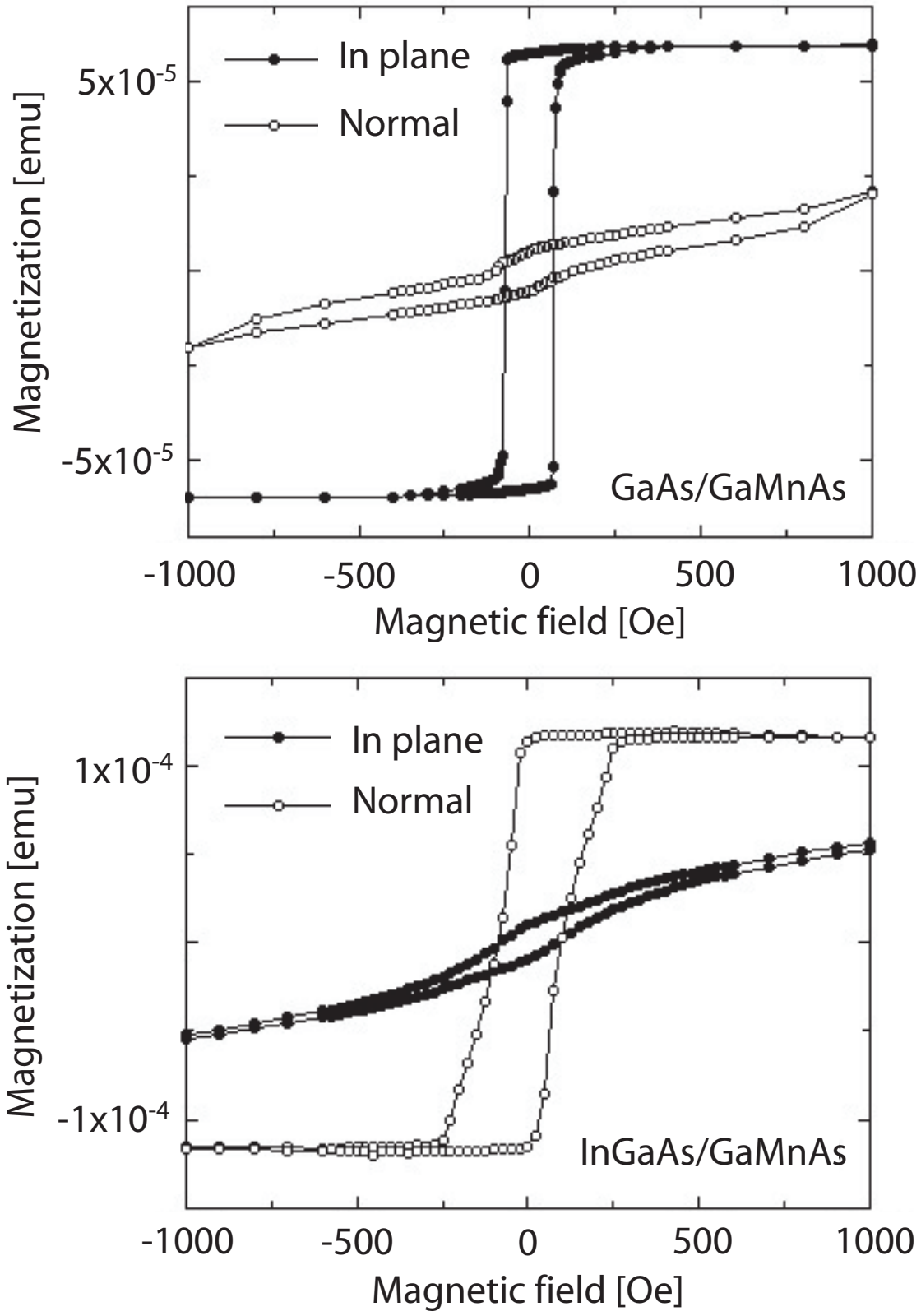
In plane
Normal
5x10-5
-5x10-5
Magnetization [emu]
GaAs/GaMnAs
-1000
-500
0
500
1000
Magnetic field [Oe]
In plane
Normal
1x10-4
-1x10-4
Magnetization [emu]
InGaAs/GaMnAs
-1000
-500
0
500
1000
Magnetic field [Oe]

Figure 20

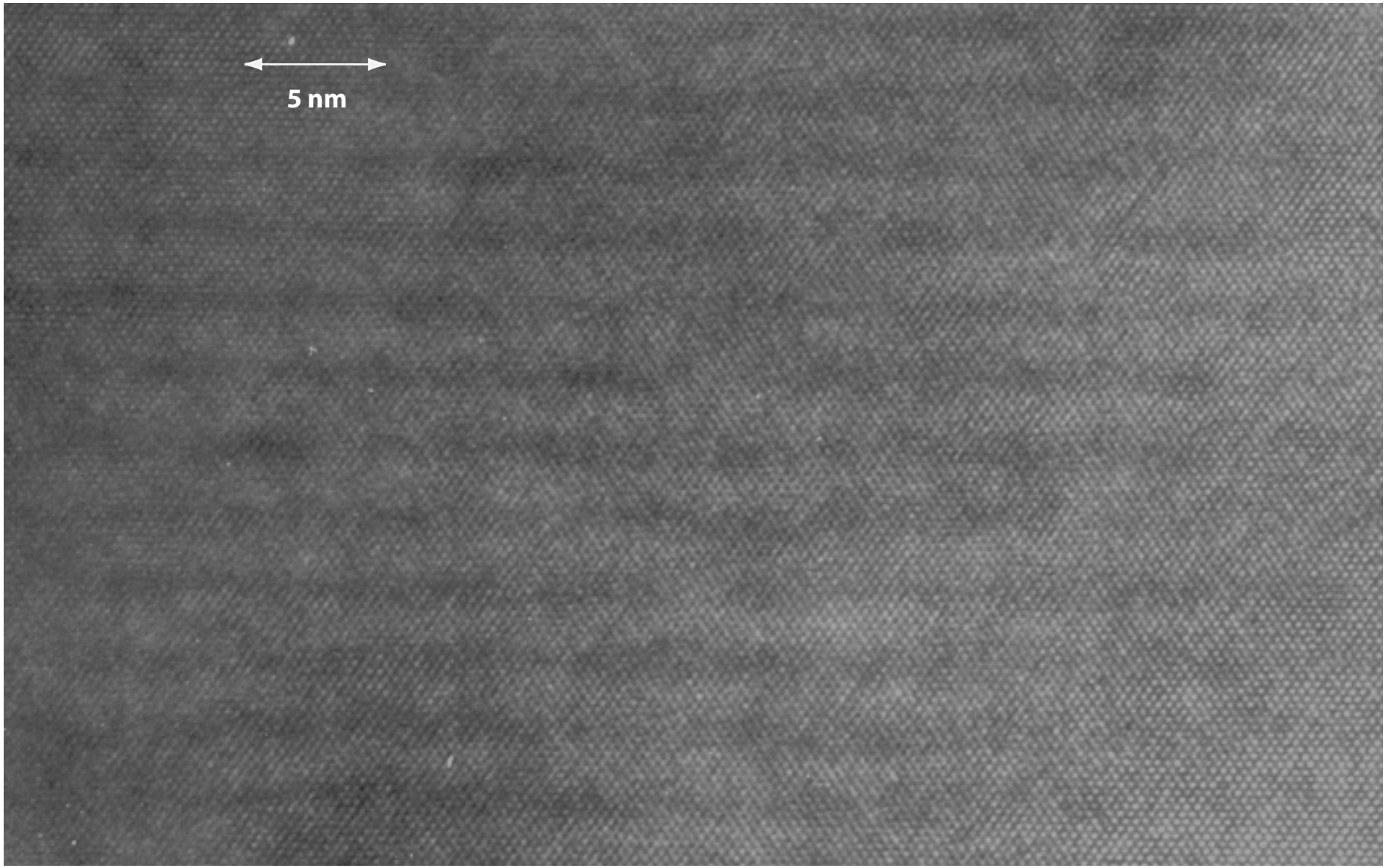

Figure 21

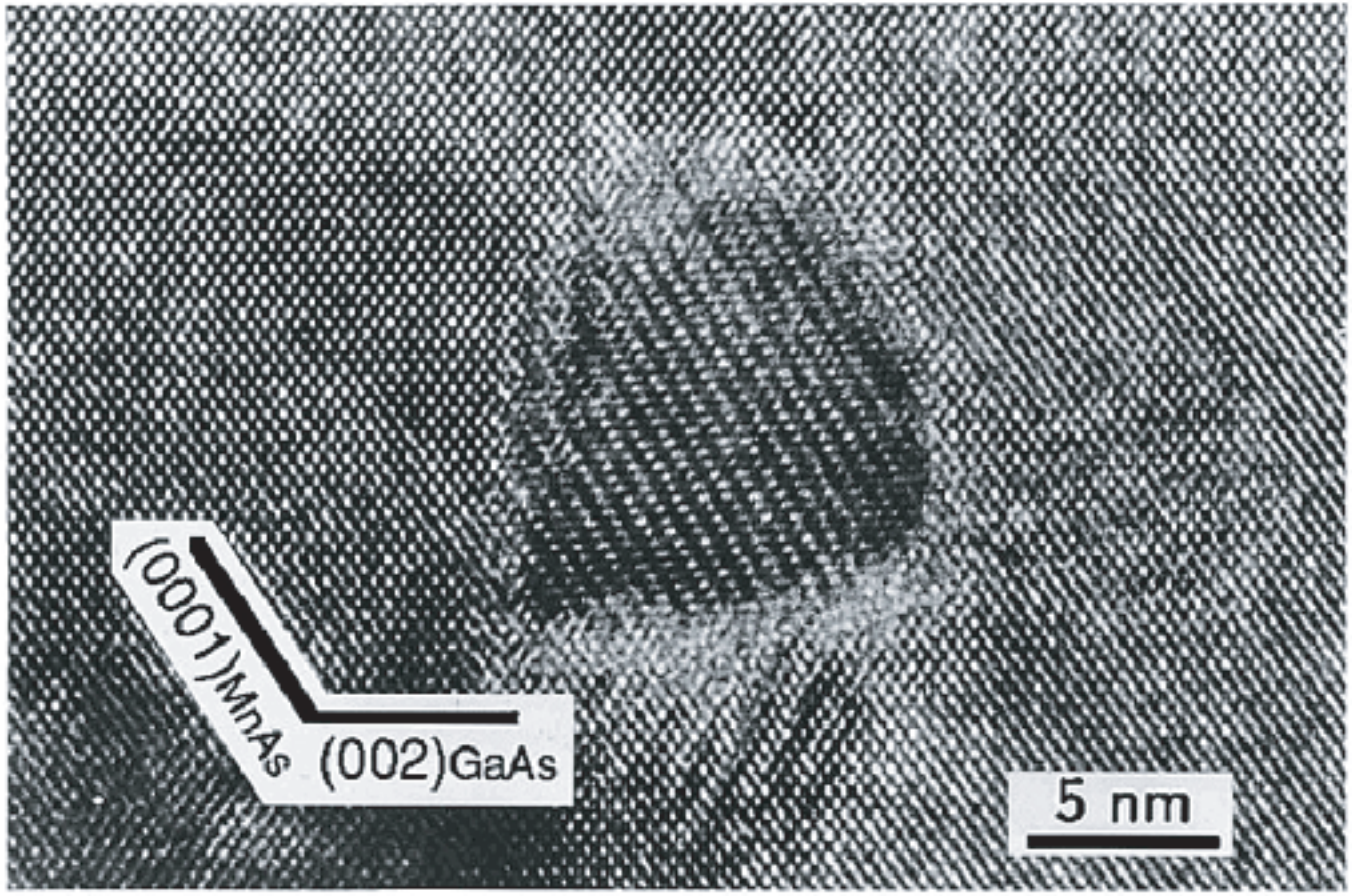

Figure 22

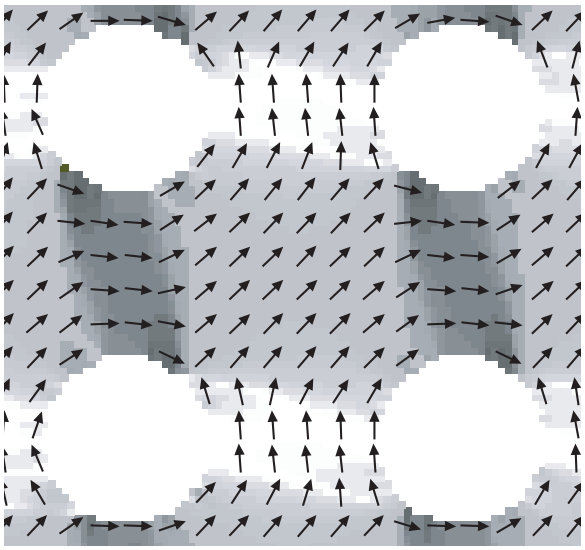

Figure 23

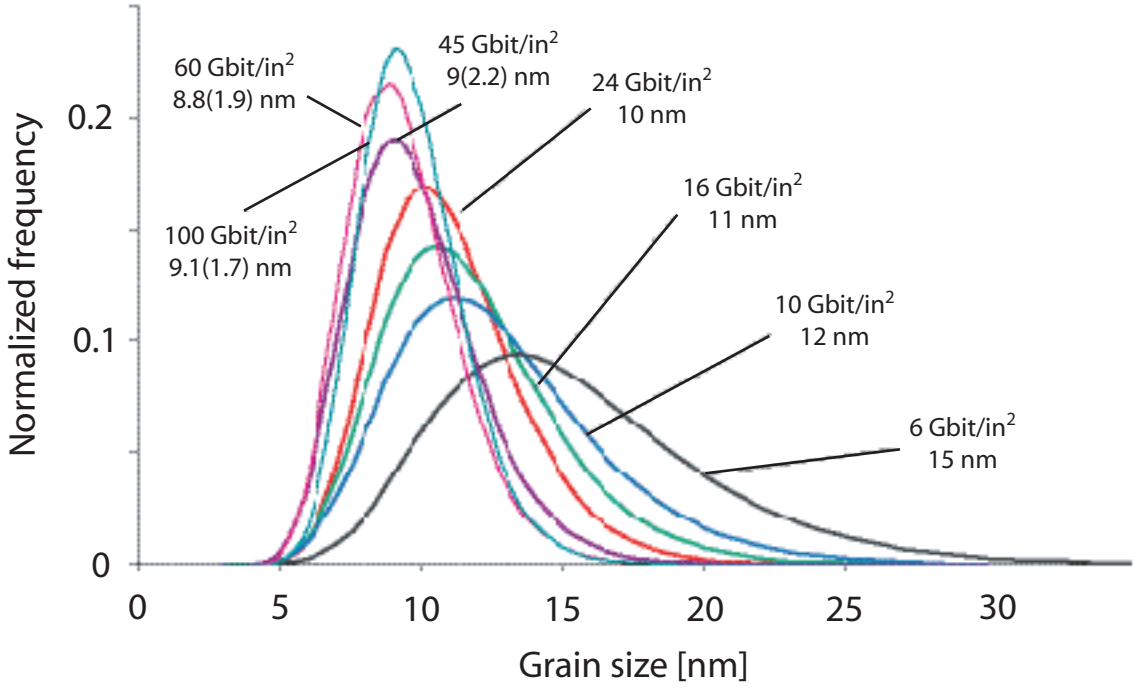
Normalized frequency
0.2
0.1
0
0
5
10
15
20
25
30
Grain size [nm]
60 Gbit/in2
8.8(1.9) nm
45 Gbit/in2
9(2.2) nm
24 Gbit/in2
10 nm
16 Gbit/in2
11 nm
10 Gbit/in2
12 nm
6 Gbit/in2
15 nm
100 Gbit/in2
9.1(1.7) nm

Figure 24

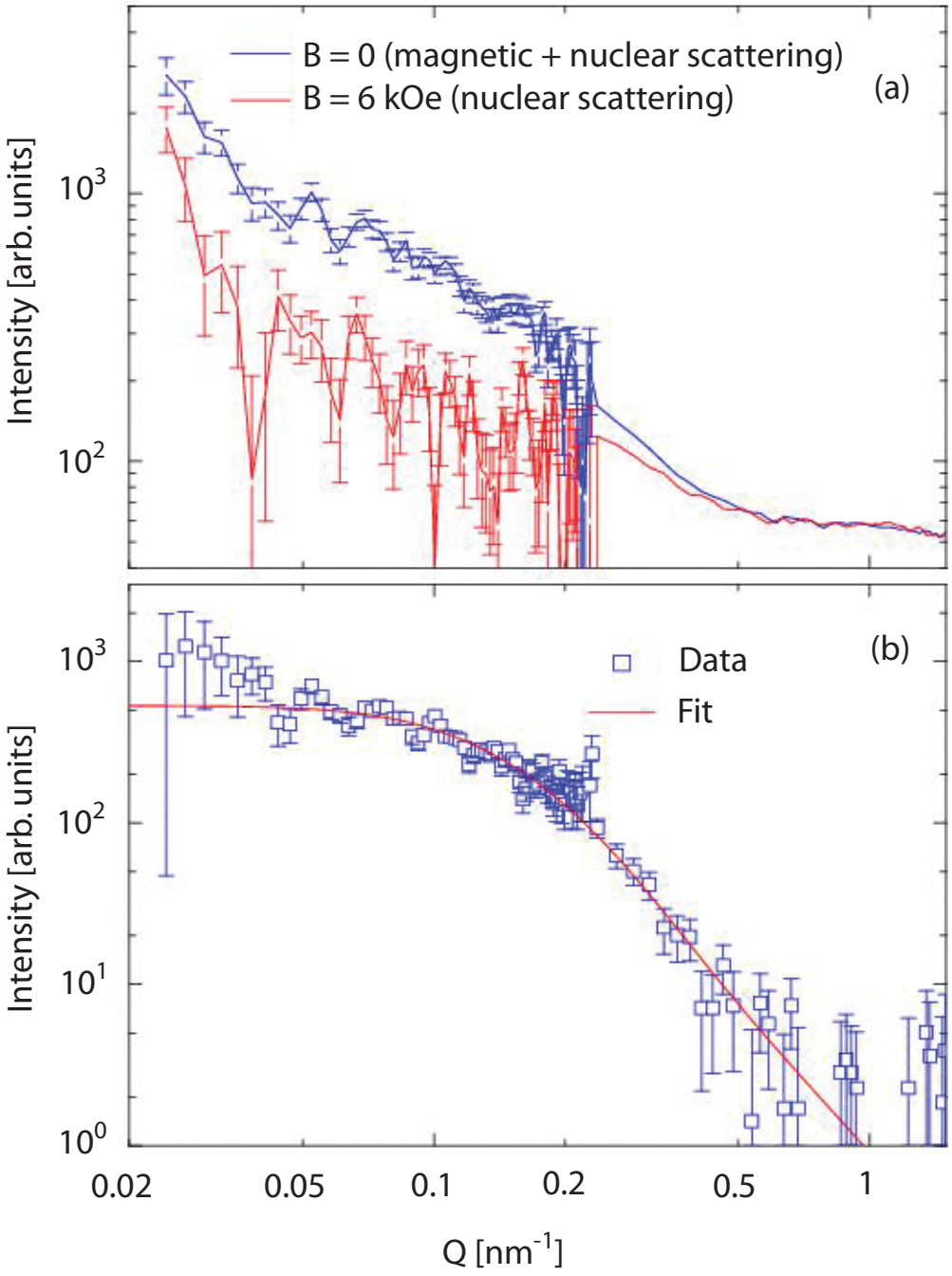
B = 0 (magnetic + nuclear scattering)
B = 6 kOe (nuclear scattering)
(a)
Intensity [arb. units]
10^3
10^2
Data
Fit
(b)
Intensity [arb. units]
10^3
10^2
10^1
10^0
0.02
0.05
0.1
0.2
0.5
1
Q [nm^-1]

Figure 25

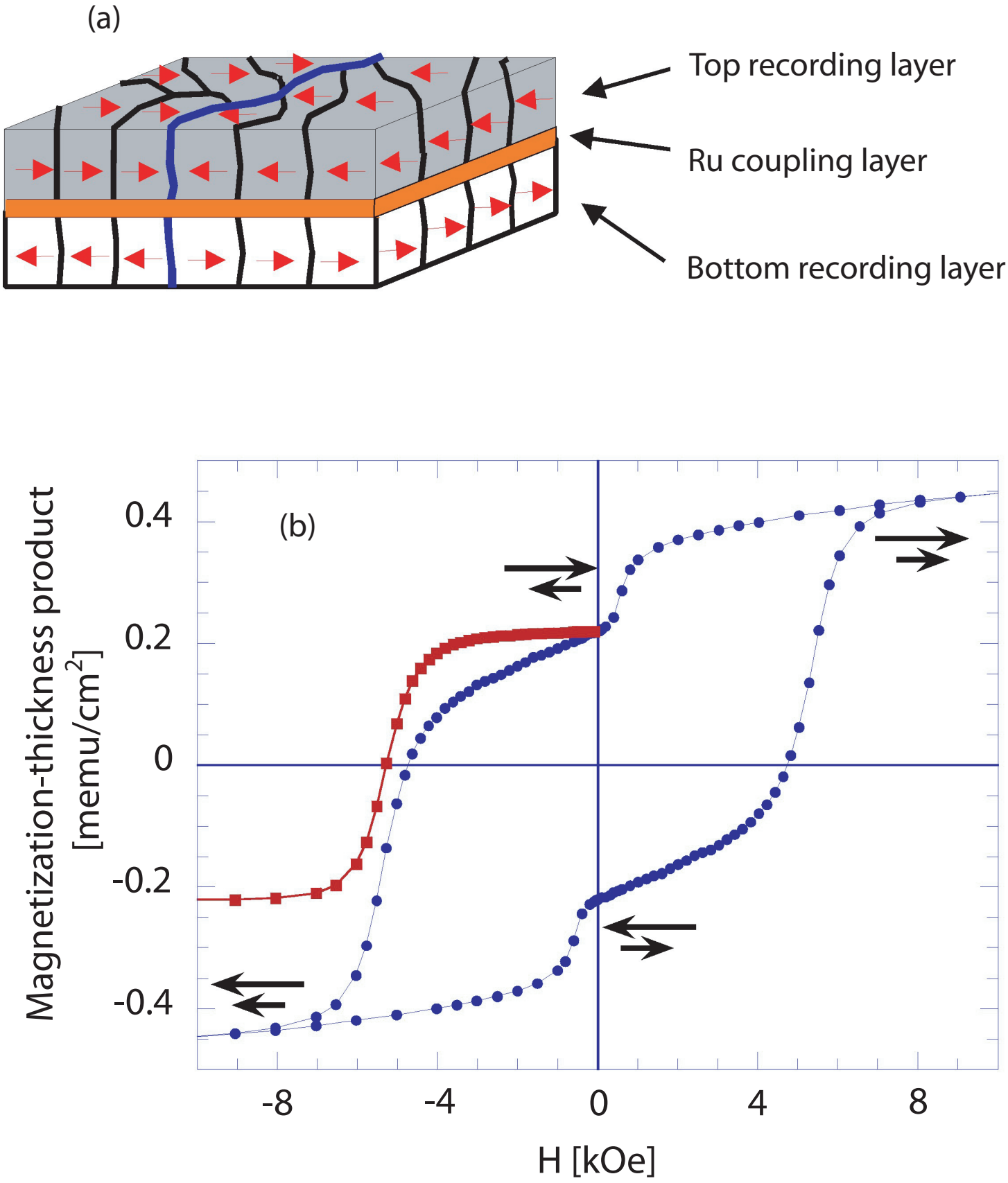
(a)
Top recording layer
Ru coupling layer
Bottom recording layer
(b)
Magnetization-thickness product
[memu/cm^2]
0.4
0.2
0
-0.2
-0.4
-8
-4
0
4
8
H [kOe]

Figure 26